Bipropellant Droplet Combustion in the Vicinity of the Critical Point

A Thesis in

Mechanical Engineering

by

Robert Stephen Lazar

Doctor of Philosophy

September, 1970

BIPROPELLANT DROPLET COMBUSTION IN THE VICINITY OF THE CRITICAL POINT

Robert Stephen Lazar

September 1970

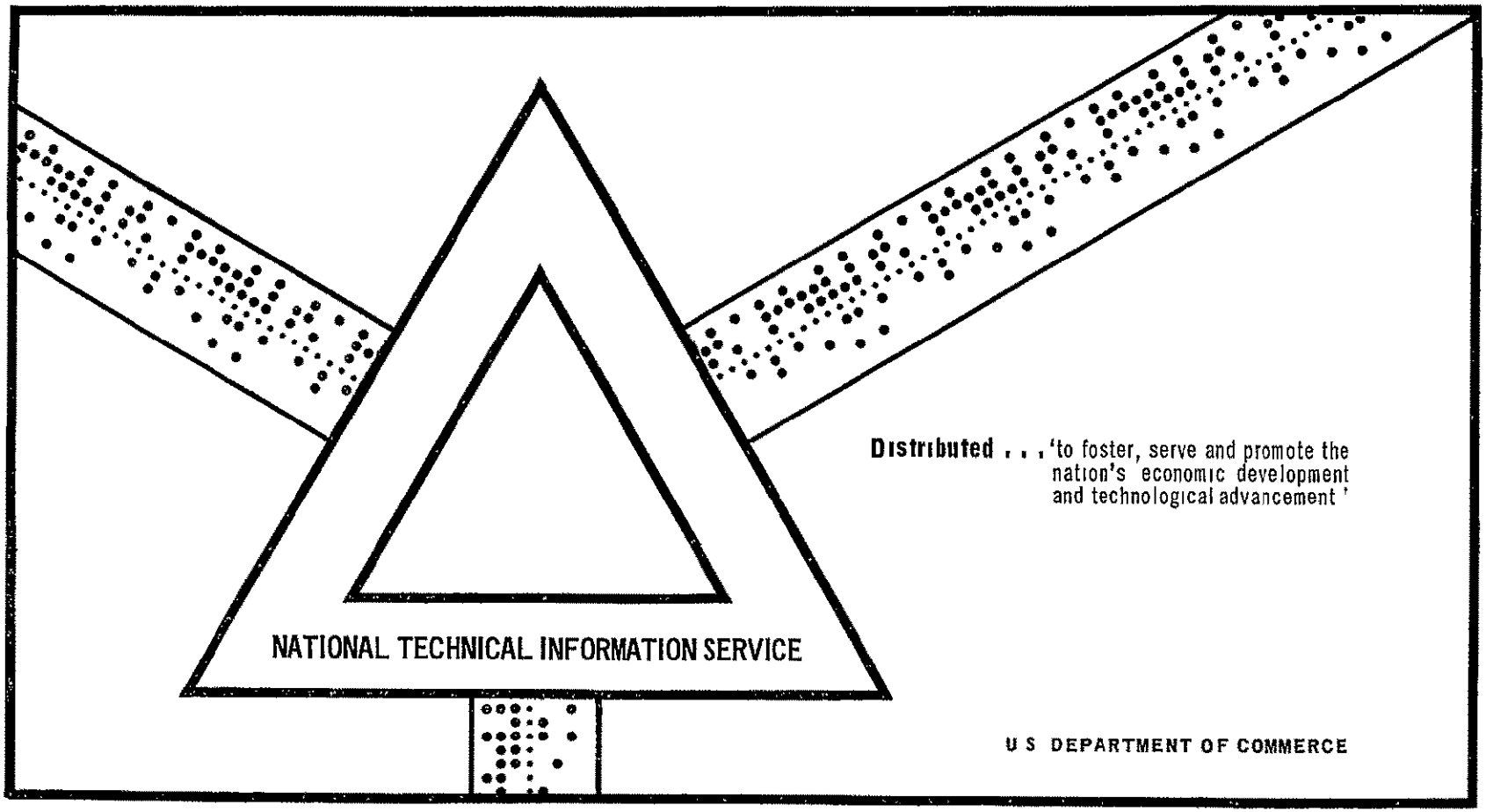

ABSTRACT

The characteristics of high pressure, bipropellant droplet combustion were examined both theoretically and experimentally

An existing low pressure, variable property, steady droplet burning theory was extended for application to high pressure combustion The extensions allowed for solubility of the ambient gases in the liquid phase and real gas effects at the droplet surface

Measurements were made of droplet burning rates in the combustion products of a flat flame burner at atmospheric pressure in order to serve as a baseline for the theory Various alcohols and paraffins were tested at ambient temperatures from 1660 to 2530°K and ambient oxygen concentrations in the range 0-40% by volume. The theory (when corrected for flame zone dissociation) gave an adequate prediction of the variation in burning rate with changes in the ambient temperature and oxygen concentration. However, the theory progressively over-estimated the burning rate as the fuel molecular weight increased, with errors as high as 50% for the heavier hydrocarbons This failure was attributed to gas phase fuel decomposition near the droplet surface.

Measurements were made of steady burning temperatures and the pressures required for the supercritical combustion of n octane and n decane droplets burning in air in a zero gravity apparatus. The measurements were made under zero gravity conditions in order to eliminate convection and to prevent the droplet from falling due to reduced surface tension near the critical point The measurements

were compared with theoretical results obtained from both the uncorrected low pressure theory and the corrected theory which allowed for high pressure effects and finite ambient gas solubility The high pressure theory was in reasonable agreement with the data, both with respect to steady burning temperatures and the pressures required for the onset of supercritical combustion The low pressure theory underestimated the pressures required for supercritical combustion by roughly a factor of two.

The concentration of ambient gases in the liquid phase were found to be quite high as the supercritical burning condition is approached (20-40% for paraffins heavier than n octane). The calculations also indicated conditions where water should condense on the droplet surface, both during heat up and steady burning, for the normal paraffin hydrocarbons.

The Pennsylvania State University

The Graduate School

Department of Mechanical Engineering

Bipropellant Droplet Combustion in the Vicinity of the Critical Point

A Thesis in

Mechanical Engineering

by

Robert Stephen Lazar

Submitted in Partial Fulfillment
of the Requirements
for the Degree of

Doctor of Philosophy

September, 1970

Date of Approval

July 28, 1970

Gerard M. Faeth, Associate Professor
of Mechanical Engineering
Thesis Advisor

July 29, 1970

Richard G. Cunningham, Professor and
Head of the Department of Mechanical
Engineering

ACKNOWLEDGMENTS

The author wishes to express his appreciation to his advisor, Professor Gerard M. Faeth, for his invaluable guidance and assistance throughout the investigation. The assistance and council of Professor Donald R. Olson is also appreciated.

The author also wishes to acknowledge the National Aeronautics and Space Administration for its financial support under Contract No. NGR-39-009-077. The invaluable suggestions of Dr. Richard J. Priem of the Lewis Research Center, who acted as contract monitor, is sincerely appreciated.

TABLE OF CONTENTS

TABLE OF CONTENTS (CONTINUED)

LIST OF TABLES

LIST OF FIGURES

LIST OF FIGURES (CONTINUED)

NOMENCLATURE

a, a'	Weighted specific heat constants, Equations (2.31, 2.39)
a^o	Parameter, Equation (2.58)
a^o_{ij}	Parameter, Equation (2.60)
a_d	Droplet absorptivity
A_i	Specific heat constant, Equation (2.25)
$\bar{A}$	Parameter, Equation (C.5)
b, b'	Weighted specific heat constants, Equations (2.32, 2.40)
b^o	Parameter, Equation (2.56)
b^o_i	Parameter, Equation (2.57)
B_i	Specific heat constant, Equation (2.25)
$\bar{B}$	Parameter, Equation (C.6)
C	Molar density
$\bar{C}$	Parameter, Equation (C.7)
C_p	Specific heat
C_1, ..., C_{22}	Constants in property equations, Appendix D
d_ℓ	Droplet diameter
D	Diffusion coefficient
$\bar{D}$	Parameter, Equation (C.8)
e_f	Emissivity
f	Fugacity
h	Enthalpy
$\bar{h}$	Partial molar enthalpy
$\bar{h}^o$	Partial molar enthalpy in the ideal state
H	Weighted heat of vaporization, Equation (2.21)

NOMENCLATURE (CONTINUED)

k_{ij}	Binary interaction parameters
K	Burning rate constant, Equation (4.3)
L	Heat of vaporization
M_i	Chemical symbol for species i
n	Total number of moles in the liquid phase
n_i	Number of moles of species i in the liquid phase
$\dot{n}$	Molar flow rate in the inner region
$\dot{n}_f$	Molar flow rate in the outer region
N_i	Molar flux of species i per unit area
N_L	Lewis Number ($N_L = \lambda/CDC_p$)
P	Pressure
Pr	Prandtl number ($Pr = C_p \sigma/\lambda$)
P_r	Reduced pressure ($P_r = P/P_c$)
P_{cij}	Parameter, Equation (2.61)
P_v	Vapor pressure
q	Parameter, Equation (2.41)
Q*	Standard heat of reaction at T*
Q_ℓ	Standard heat of reaction at T_ℓ
Q_R	Parameter, Equation (B.11)
$\dot{Q}_{Ra}$	Radiant heat flux
$\dot{Q}_T$	Total heat flux
r	Radial distance
R	Universal gas constant
Re	Reynolds number ($Re = \rho Vd/\sigma$)

NOMENCLATURE (CONTINUED)

s	Stephan-Boltzmann constant
t	Time
T	Temperature
T^*	Reference temperature
T_{fR}	Reduced temperature, Equation (D.16)
T_{cij}	Parameter, Equation (2.64)
v	Molar volume
$\bar{v}$	Partial molar volume
v_{cij}	Parameter, Equation (2.62)
V	Velocity
W	Molecular Weight
X	Mole fraction
Z	Compressibility factor
Z_{cij}	Parameter, Equation (2.63)
α	Stoichiometry parameter, Equation (2.14)
β	Parameter, Equation (2.42)
γ	Parameter, Equation (2.42)
δ	Mole flux fraction in the outer field
ε	Mole flux fraction in the inner field
ζ	Parameter, Equation (2.33)
η	Parameter, Equation (2.45)
λ	Thermal conductivity
μ	Parameter, Equation (B.10)
ν	Parameter, Equation (B 9)
ρ	Mass density

NOMENCLATURE (CONTINUED)

σ	Viscosity
ϕ	Parameter, Equation (2.33)
χ	Parameter, Equation (2.26)
ψ	Parameter, Equation (2.48)
ω	Acentric factor
Ω_{ai}	Dimensionless constant, Equation (2.59)
Ω_{bi}	Dimensionless constant, Equation (2.57)

Subscripts

A	Region A
B	Region B
c	Critical point
f	Flame surface
F	Fuel species
i	Species i
ℓ	Droplet surface
N	Species N
o	Oxygen species
p	Product species
∞	Ambient conditions
+	Outer side of a surface
-	Inner side of a surface

Superscripts

L	Liquid

NOMENCLATURE (CONTINUED)

V	Vapor
*	No convection effects

CHAPTER I

INTRODUCTION

1.1 General Statement of the Problem

The importance of studies on the evaporation and combustion characteristics of individual fuel droplets to the development of design procedures for bipropellant rocket engine combustion chambers was first demonstrated by Priem (1). Assuming that droplet vaporization was the rate controlling process in a combustion chamber, Priem calculated the chamber length necessary to complete the vaporization of a single droplet. Later, Priem and Heidmann (2) modified Priem's original analysis to model bipropellant spray combustion systems. The effects of propellants, spray conditions, engine design parameters and operating parameters on the vaporization of individual fuel droplets were correlated to predict combustor performance. Comparisons of their predictions with measured combustor performance provided good agreement at moderate pressures and established the utility of individual droplet studies.

Continued rocket engine development has lead to combustion chamber pressures which exceed the pressure levels considered by Priem and Heidmann. At high pressures, several of the assumptions made in the Priem and Heidmann model became inadequate giving rise to new problems in understanding droplet combustion characteristics.

With this in mind, the overall objective of the present investigation is to study the combustion characteristics of single

fuel droplets in an oxidizing atmosphere, at the high pressure levels encountered in rocket engine combustion chambers. The results of this study should have technical application in furthering the understanding and design capabilities of high pressure combustion systems.

1.2 Previous Related Studies

The vaporization and combustion of liquid fuel droplets are generally characterized by two distinct regimes during the life-time of the droplet The preheat and steady burning regimes. During the preheat period, a portion of the energy reaching the droplet surface goes into vaporizing the liquid while the excess goes into sensible heating of the droplet liquid. The increasing surface temperature during this period causes the mole fraction of the droplet vapor at the surface to increase, providing a greater potential for mass transfer and thus an increase in the vaporization rate. Eventually, all of the energy transferred to the droplet is required for the heat of vaporization and the droplet temperature remains constant at its so-called wet bulb temperature. This condition is characteristic of the steady burning regime.

The earliest droplet combustion studies concentrated on the steady burning period of the droplet. Various predictions of droplet burning rates have been derived from analysis of the steady burning period (3-5) and are in reasonable agreement with the results of experiments conducted at atmospheric pressure (4-7).

Typical among these, is the study by Godsave (4) in which the prediction of droplet burning rates is based upon a quasi-steady

analysis. In this analysis, steady state conditions are assumed for fixed droplet sizes. This requires that the temperature and concentration profiles in the gas phase adjust instantaneously to changes in the boundary conditions at the droplet surface. It also requires that the regression rate of the droplet surface (i.e., the radial interface velocity) be small compared to the velocity of the vapor leaving the liquid surface.

Godsave assumed that the rates of reaction at the flame zone are fast compared to the rates at which the reactants are transported to the reaction zone. The fuel and oxidizer are assumed to combine in stoichiometric proportions at the flame surface. The temperature dependence of the physical properties was neglected throughout Godsave's analysis, and constant average values were employed.

Goldsmith and Penner (8) presented a variable property model for the steady burning period of a fuel droplet in an oxidizing atmosphere which was an extension and generalization of the work of Godsave (4). The model differs from the work of Godsave, primarily through the use of integrated forms for the energy and continuity equations. This extension facilitates consideration of the temperature dependence of the fuel thermal conductivity and specific heat. While comparable predictions of droplet conditions can be obtained from a constant property solution, the results are strongly dependent upon a judicious choice of average values for the properties.

Expressing the fuel thermal conductivity and specific heat as a linear function of temperature, Goldsmith and Penner were able to provide a reasonable correlation of Godsave's experimental results.

They were also able to obtain explicit expressions for the temperature and location of the flame zone

Goldsmith (9) conducted experiments on fuel droplets under various ambient conditions in order to test the theory of Reference (8) He found that the theory resulted in extremely high computed flame temperatures owing to the neglect of dissociation effects at the flame surface in the theory. In spite of the high calculated flame temperatures, the theory provided reasonable agreement with the experimentally determined burning rates at various ambient oxygen concentrations for n heptane and ethyl alcohol droplets Although he also studied the effect of ambient temperature and pressure on the burning rate, he did not consider a sufficient range on these variables to provide a stringent test of the theory.

While there have been relatively few investigations of high pressure droplet combustion, there are two aspects of this problem that have received attention The first, discussed by Williams (10) and Brzustowski (11), is that at high pressures certain assumptions of the quasi steady analysis of transport rates to droplets become questionable. This includes both the neglect of the finite regression rate of the droplet surface and the transient adjustments of the boundary layer around the droplet to changing conditions at the droplet surface In attempting to determine the range of validity of the quasi steady analysis, both of these investigators point out that these two assumptions become questionable as the droplet liquid density approaches that of the gas mixture This situation could be expected to occur at high pressures.

The second aspect, which has been considered theoretically by Spalding (12), Wieber (13), Brzustowski (11), and Rosner (14), is the possibility that a burning droplet can approach or exceed its critical point. The droplet steady burning temperature increases with pressure and could reach the thermodynamic critical temperature of the droplet liquid if the pressure is sufficiently high Upon reaching its critical point, the droplet essentially becomes a puff of gas and the conventional low pressure models, which assume that droplet vaporization is the controlling combustion process, are no longer valid.

Wieber (13) computed droplet steady-state temperatures for vaporizing n heptane and oxygen droplets to determine if droplet temperatures could approach the critical temperature This analysis was based on a quasi steady, constant property treatment of the gas phase, neglecting ambient gas solubility and other high pressure corrections in the determination of phase equilibrium at the droplet surface.

Wieber's calculations indicated that n heptane droplets injected into a 5000°R atmosphere would require a total gas pressure of 1 78 to 2.30 times the critical pressure of n heptane for the droplet liquid to attain its critical temperature, depending on the value of the product of drop size and drop velocity. In contrast, he found that an oxygen droplet would reach its critical point when the total gas pressure equalled the critical pressure of oxygen

An examination of Wieber's calculations has revealed that an anomalously low value of the fuel thermal conductivity was used for n heptane. Calculations using a higher fuel thermal conductivity

in this low pressure theory would result in a lower predicted pressure for n heptane droplets to attain the critical point.

Recent investigations at the University of Wisconsin by Manrique (15) and by Savery and Borman (16) have shown that high pressure corrections cause significant changes in droplet equilibrium conditions during evaporation Manrique studied the vaporization of carbon dioxide droplets in a high pressure nitrogen atmosphere He considered both steady state and transient vaporization models which included non ideal effects associated with high pressure mixtures, ambient gas solubility in the liquid phase, variation of thermophysical properties in the boundary layer and the effects of total pressure on the vapor pressure and enthalpy of vaporization.

Manrique found that a droplet can each and exceed its thermodynamic critical temperature at supercritical pressures and high ambient temperature conditions. His results indicated that all of the non ideal effects, usually neglected in low pressure vaporization models, are important in the critical region

Comparisons with the low pressure models of droplet vaporization indicate that reasonable estimates of vaporization times over a wide range of temperatures and pressures can be obtained with the low pressure model provided the effects of ambient gas solubility and the effects of total pressure on the vapor pressure and enthalpy of vaporization are accounted for at high density conditions

Savery and Borman (16) measured histories of vaporizing n heptane and Freon-13 droplets suspended in a heated air stream. The

ambient conditions of their experiments included pressures from 1.5 to 100 atmospheres and temperatures between 100 and 300°F. Measured equilibrium temperatures and vaporization rates were compared with values predicted from a quasi steady theory uncorrected for high pressure properties as well as from a corrected version which included the effects of ambient gas solubility and other high pressure corrections to the thermodynamic properties. Some of the important conclusions of this study for high pressure vaporization are as follows:

1 At low ambient temperatures, the corrected theory gave good agreement with measured equilibrium temperatures and predicted vaporization rates to within $\pm$ 25% of the measured values. The uncorrected theory also gave good predictions of droplet equilibrium temperatures but underestimated the measured vaporization rates by 80%.

2. At moderate ambient gas temperatures and high pressures, predictions by the corrected and uncorrected theories were 10-15°F below the measured equilibrium temperatures. The mass transfer rates predicted by the corrected theory agreed to within 35% of the measured values at reduced pressures below 1 5 The predicted mass transfer rates were about 50% low at a reduced pressure of 1.75 and became progressively lower as the pressure increased. Errors in the mass transfer rates predicted by the uncorrected theory were generally twice as great as those obtained by the corrected theory.

1.3 Specific Statement of the Problem

The preceding discussion has indicated that several aspects of high pressure droplet combustion require further investigation.

The investigations at the University of Wisconsin (15, 16) have shown that high pressure effects cause an intrinsic change in the droplet evaporation mechanism and thus in the method of predicting the conditions required for the droplet to exceed the critical point during its lifetime. These results, therefore, have cast doubt on the validity of the calculations reported by Wieber (13) in which corrections for high pressure effects were neglected.

Since the Wisconsin studies considered only droplet vaporization in the absence of combustion, the case of high pressure droplet combustion requires examination in the light of these new findings. In particular, it would be useful to correct a simplified low pressure model of droplet combustion for these high pressure effects in order to examine droplet equilibrium conditions as well as the pressures required for supercritical combustion of hydrocarbon droplets.

Of the low pressure theories mentioned, the Goldsmith and Penner (8) model would be most suitable for extension in order to analyze high pressure combustion, since the variable property aspects of this theory eliminates the uncertainties arising from the selection of average properties. However, since this model has not received extensive experimental verification, it would be appropriate to provide a more stringent test of this theory.

With this in mind, the present investigation was undertaken with the following specific objectives

1. To provide a more stringent experimental test of the Goldsmith and Penner theory at low pressures.
2. To extend the Goldsmith and Penner theory in order to study the combustion characteristics of hydrocarbon droplets burning in an air environment in the vicinity of the critical point. Emphasis is placed on the conditions at the droplet surface (ambient gas solubility, etc) and the prediction of the pressures required for hydrocarbon droplets burning in air to reach a critical combustion condition.
3. To test the theoretical findings with experimental data for hydrocarbon droplets burning in a high pressure air environment.

The low pressure experiments in this investigation were conducted on a flat flame burner apparatus developed by Faeth (17). Test droplets were mounted on a probe and rapidly subjected to the combustion products of a flat flame burner in order to simulate a combustion chamber environment at atmospheric pressure. The burner provided ambient temperatures in the range 1660-2530°K and ambient oxygen concentrations in the range 0-40% at the droplet location. The fuels investigated on this apparatus included methyl, 1 butyl and 1 decyl alcohol as well as the paraffin hydrocarbons, n pentane, n heptane, iso octane, n decane, n tridecane and n hexadecane.

The high pressure experiments were conducted on the zero-gravity apparatus developed by Dominicis (18). The zero-gravity condition is required for suspended droplet experiments in the

vicinity of the critical point in order to prevent the droplet from falling due to reduced surface tension near the critical point. Test droplets were suspended in a high pressure reaction chamber and ignited once the chamber was placed in free-fall. Ambient pressures to 2000 psia could be obtained with this apparatus The droplets were suspended from a thermocouple junction enabling measurements of the droplet liquid temperature The fuels considered in this experiment were n octane and n decane.

CHAPTER II

THEORETICAL CONSIDERATIONS

2.1 General Model

The theoretical objective of this investigation was to extend low pressure theories of droplet combustion in order to analyze the characteristics of bipropellant droplet combustion at high ambient pressures. The first part of this chapter presents the development of the extended theory in terms of the boundary conditions at the droplet surface. The evaluation of the boundary conditions requires a consideration of the thermodynamics at the droplet interface. These considerations are presented in the last section of the chapter.

In order to concentrate on ambient gas solubility and high pressure effects at the droplet surface, the analysis was simplified to consider only steady state conditions All transient phenomena (finite radius regression rate, etc.) are neglected and the temperature and composition of the liquid phase are assumed to be uniform throughout the droplet. Under these conditions, the analysis is strictly valid only for a porous sphere fed continuously with a liquid fuel While this type of formulation has been shown (10) to give an adequate representation of low pressure droplet combustion, it can only be applied qualitatively to an actual high pressure combustion process. It was felt, however, that these other factors could be more adequately treated after the high pressure characteristics at the droplet surface had been examined with the present more simplified theory.

The gas phase was analyzed by extending the variable property, steady droplet burning solution of Goldsmith and Penner (8), since the property variations in this approach were particularly suitable for the conditions of the present study The extension included the effect of dissolved gas evaporation, separate determination of the concentrations of the various gas phase species and allowance for variable specific heats of all species For convenience in matching the gas phase solution with the phase equilibrium solution at the droplet surface, the analysis was cast on a molar basis

The model of the burning droplet is illustrated in Figure 1. Convection effects are neglected and the diffusion and heat transfer processes are assumed to be spherically symmetric. These assumptions are quite appropriate for the experiments conducted in the zero gravity apparatus due to the absence of gravitational effects and forced flow. For the low pressure experiments on the flat flame burner apparatus, the theory was corrected for convection effects with a multiplicative factor as discussed in a later chapter. Analysis of droplet combustion based on the assumption of spherical symmetry with a multiplicative correction for convection effects is an approach that has been demonstrated by many investigators (19-24) with good results.

Reaction is confined to a spherically symmetric, infinitely thin flame surface where fuel and oxidizer are assumed to combine in stoichiometric proportions. This assumption provides a useful limit when the reaction rates are fast in comparison to the diffusion rates Brzustowski (11) has shown that the accuracy of this assumption is directly proportional to the product of pressure and

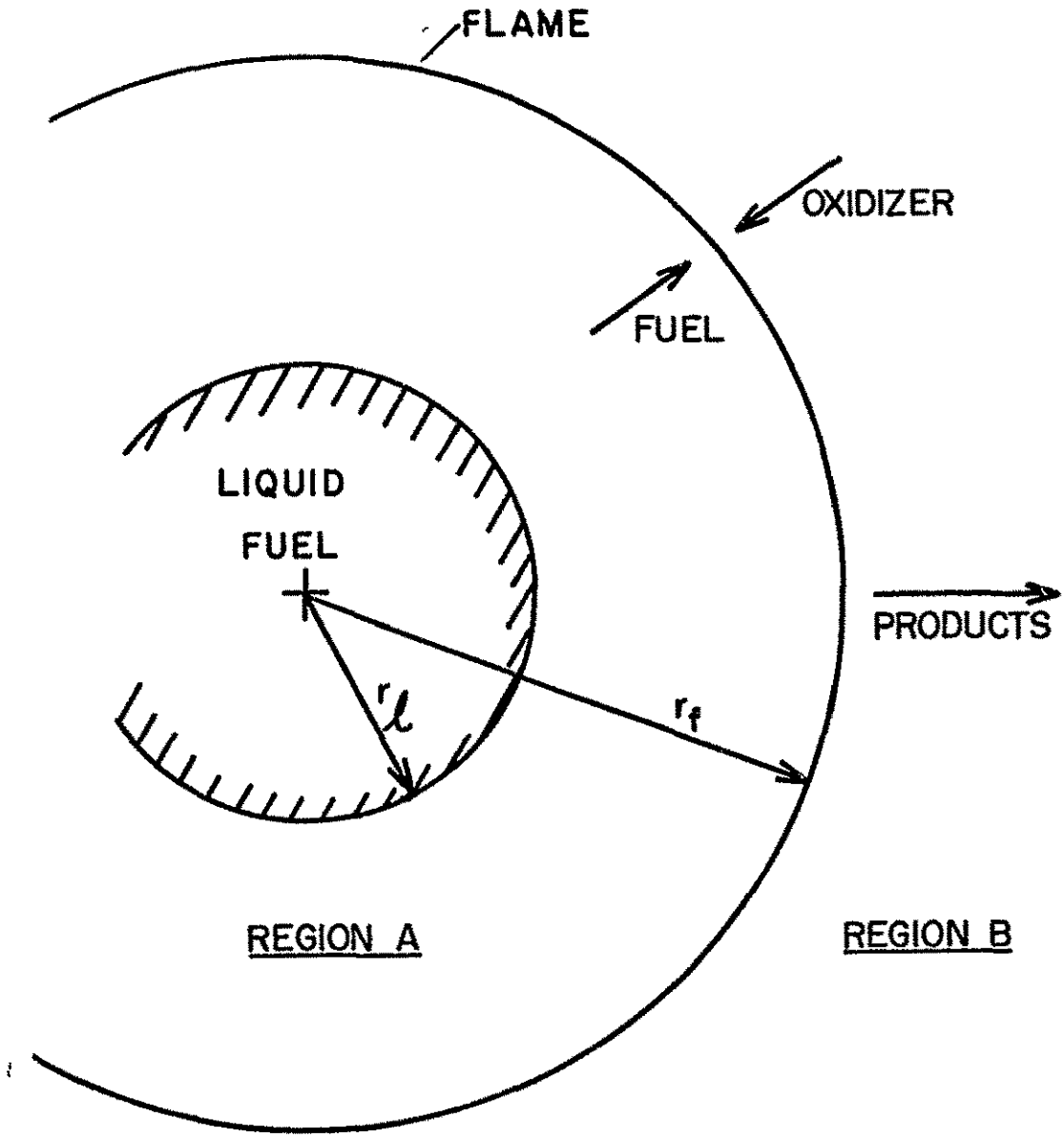

FIGURE 1 MODEL OF THE BURNING OF A FUEL DROPLET IN AN OXIDIZING ATMOSPHERE

droplet size. For the pressures and drop sizes considered in the present investigation, this product is above the lower limits determined by Brzustowski.

The total gas pressure is assumed to be constant throughout the boundary layer. A consideration of the momentum equation in Appendix A indicates that pressure changes across the boundary layer are small for the conditions of interest in the present study

Thermal radiation effects are neglected in the analysis, however, the influence of this assumption on the computed results is examined later. It is shown in Appendix A that radiant energy absorbed by the droplet represents a small fraction of the energy required to vaporize the droplet at moderate pressures This finding is in agreement with the results of several studies on droplet combustion (4, 5, 7, 25) at low pressures. At higher pressures, the calculations in Appendix A indicate that radiant energy from the flame can contribute a significant fraction of the heat required to vaporize the droplet However, a study by Brzustowski and Natarajan (26) on the combustion of aniline droplets at high pressures compared results allowing for radiation from the flame with those obtained when radiation was neglected. The results indicated that the increase in droplet burning rates due to radiation from the flame were on the order of 10% for pressures as high as 48 atmospheres. The apparent disagreement between the calculations in Appendix A and the results of Reference (26) is probably due to the effects of natural convection in the experiments of Brzustowski and Natarajan. The increase in the total heat flux to the droplet

due to natural convection has the tendency of reducing the fraction of the radiant heat flux to the total heat flux and thus the results would be less sensitive to radiation effects Due to the absence of natural convection in the zero gravity apparatus, the effects of radiation on the steady droplet burning rates can be expected to be somewhat greater. However, the effect on steady droplet burning temperatures can not be determined a priori. Therefore, the effects of radiation on computed steady burning temperatures are examined in Chapter 6.

For multicomponent mixtures, it was assumed that the binary diffusivities of all species were the same, although different values could be employed inside (Region A) and outside (Region B) the flame. The equality of binary diffusivities in multicomponent mixtures is a common assumptions (19, 27) employed in the analysis of diffusional processes for droplet combustion. Thermal diffusion is not considered in the gas phase analysis. The calculations in Reference (28) indicate that the mass flux due to thermal diffusion is less than 20% of the concentration flux for the gas phase surrounding an evaporating iso octane droplet. On this basis, and considering the lack of accurate thermal diffusion measurements, treatment of this complicated phenomena does not appear to be warrented.

Compressibility effects are neglected in the boundary layer and the ideal gas equation is employed to compute the molar density in the gas phase Due to the high temperature of most of the gas phase for burning droplets, compressibility effects are small except

near the droplet surface. The fact that the droplet approaches a critical mixing point due to its solubility, as opposed to a critical point for a pure liquid-vapor system, reduces the errors introduced by this assumption even at the droplet surface. Available experimental evidence (29) shows that transport properties are not appreciably analomous near a critical mixing point, unlike the case of a pure liquid-vapor critical point. The effect of uncertainties in the property values employed in the calculations on the final results are examined in Chapter VI.

2.2 Governing Equations

Under the assumptions of the preceding section, the governing equations for the spherical shells defined by Region A and Region B in Figure 1 are obtained from the general equations of conservation of mass, energy and species for multicomponent systems presented by Bird, Stewart, and Lightfoot (30). Employing spherical symmetry, these equations are

$$\frac{d}{dr}\left(r^2 N_i\right) = 0 \quad , \qquad i=1, \quad , N \tag{2.1}$$

$$\frac{d}{dr}\left[r^2 \sum_{i=1}^{N} N_i h_i - r^2 \lambda \frac{dT}{dr}\right] = 0 \tag{2 2}$$

$$N_i = -C\mathcal{D} \frac{dX_i}{dr} + X_i \sum_{J=1}^{N} N_J \quad , \qquad i=1, \quad , N \tag{2.3}$$

where N_i is the molar flux per unit area of species i. For convenience, the fuel (which is absent in the outer field) is taken to be component 1 and the oxidizer (which is absent in the inner field) is taken to be component N.

The overall molar burning rate, n, can be shown to be a constant by multiplying Equation (2 1) by 4π, summing over all species and integrating to obtain.

$$n = 4\pi r_\ell^2 \left(\sum_{i=1}^{N-1} N_i \right)_\ell , \quad \text{a constant} \tag{2.4}$$

The mole flux fraction of species i in Region A is defined as

$$\varepsilon_i \equiv \frac{N_i}{\sum_{i=1}^{N-1} N_i} \tag{2 5}$$

The equation of conservation of energy for Region A can be expressed in terms of the mole flux fractions and the molar burning rate by introducing Equations (2.4) and (2.5) into Equation (2.2) Applying the resulting expression to the spherical shell between r_ℓ and r for $r < r_f$, the following expression is obtained.

$$\dot{n} \sum_{i=1}^{N-1} \varepsilon_i h_i - 4\pi r^2 \lambda_A \frac{dT}{dr} = \left[\dot{n} \sum_{i=1}^{N-1} \varepsilon_i h_i - 4\pi r^2 \lambda \frac{dT}{dr} \right]_{\ell+} \tag{2 6}$$

The right hand side of Equation (2.6) can be evaluated further through a consideration of conservation of energy at the droplet interface Under the steady burning assumption, all of the energy reaching the droplet goes into the heat of vaporization of the evaporating material. This is expressed as

$$4\pi r_{\ell}^{2}\,\lambda\left(\frac{dT}{dr}\right)_{\ell+} = n\sum_{i=1}^{N-1}\varepsilon_{i}L_{i} \tag{2.7}$$

Introducing this condition into Equation (2 6), the steady burning equation of conservation of energy for Region A becomes.

$$\dot{n}\sum_{i=1}^{N-1}\varepsilon_{i}\,(h - h_{\ell} + L)_{i} = 4\pi r^{2}\,\lambda_{A}\frac{dT}{dr} \tag{2.8}$$

The steady burning equation of conservation of species for Region A can be expressed in terms of $\dot{n}$ and ε_i by introducing Equations (2.4) and (2.5) into Equation (2.3) The result is

$$\dot{n}\,(X_{i} - \varepsilon_{i}) = 4\pi r^{2}\,(CD)_{A}\frac{dX_{i}}{dr}\quad,\qquad i=1,\ \ldots,\ N-1 \tag{2 9}$$

The boundary conditions on Equations (2.8) and (2.9) are as follows

$$\begin{aligned} &r = r_{\ell},\quad T = T_{\ell},\quad X_{i} = X_{i\ell}\qquad (i=1,\ \ldots,\ N-1)\\ &r = r_{f},\quad T = T_{f},\quad X_{1} = 0,\quad X_{i} = X_{if}\qquad (i=2,\ \ldots,\ N-1) \end{aligned} \tag{2.10}$$

Equation (2.1) along with Equation (2.5) yields the result that the mole flux fractions, ε_i, are constant throughout the inner field. Two limits may be established for the mole flux fractions. For a porous sphere experiment, with pure fuel introduced at the center of the sphere, $\varepsilon_1 = 1$ and the remainder are all zero In this case, although there are dissolved gases in the liquid phase, the net flux of each dissolved gas inside the reaction zone is zero since only fuel is entering the system (in this case L must also include any liquid phase enthalpy change of the fuel). The second

limit is more appropriate to steady droplet combustion, where the temperature and composition are uniform throughout the liquid phase. In this case, the dissolved gas evaporates along with the fuel, in order to maintain constant liquid phase composition. Conservation of mass applied at the droplet surface provides the relations·

$$\frac{dn_i}{dt} = -4\pi r_\ell^2 N_{i\ell} \quad , \qquad i=1, \ldots, N-1$$

and

$$\frac{dn}{dt} = -4\pi r_\ell^2 \sum_{i=1}^{N-1} N_{i\ell} \tag{2.11}$$

where n_i represents the number of moles of species i in the liquid phase and n represents the total number of moles in the liquid phase. By definition, the mole fraction of species i in the liquid phase, $X_{i\ell-}$, is the ratio of n_i to n. When differentiated with respect to time, this becomes:

$$\frac{dX_{i\ell-}}{dt} = \frac{1}{n^2}\left(n\frac{dn_i}{dt} - n_i\frac{dn}{dt}\right)$$

Since the composition is assumed uniform and constant in the liquid phase, the mole fractions must remain constant with time. Setting the derivative of $X_{i\ell-}$ equal to zero in the above expression yields.

$$X_{i\ell-} = \frac{dn_i}{dt}\Big/\frac{dn}{dt} \tag{2.12}$$

Substitution of Equations (2.11) and (2 12) into the defining equation for the mole flux fraction, Equation (2 5), reveals that for steady state combustion with a uniform liquid phase composition, the mole flux fractions, ε_i, are equal to the liquid phase mole fractions, i.e.

$$\varepsilon_i = X_{il-} \quad , \qquad i=1, \ldots, N-1 \tag{2.13}$$

In order to evaluate the mole flux fractions in Region B, the flame surface must be considered. Denoting the chemical symbol of species i as M_i, the stoichiometry of the reaction was taken as follows.

$$M_1 \rightarrow \sum_{i=2}^{N} \alpha_i M_i \tag{2.14}$$

With this formulation, α_N, the number of moles of oxygen produced (or consumed) per mole of fuel at the flame surface will be negative for stoichiometric combustion of a hydrocarbon fuel. In the outer region, fuel is absent and the total mole flux of each component results from both diffusion from the inner region and production (or consumption) at the flame surface. An expression of this condition is:

$$N_{if+} = N_{if-} + \alpha_i N_{if-} \quad , \qquad i=2, \ldots, N \tag{2.15}$$

Since the quantity $r^2 N_i$ is a constant in both regions A and B, as obtained from Equation (2.1), the mole flux fractions in the outer region can be expressed in terms of the inner field mole flux fractions through the application of Equation (2.15). The outer

field mole flux fractions, designated as δ_i, become.

$$\delta_i = \left(\varepsilon_i + \varepsilon_1\alpha_i\right) \Big/ \sum_{j=2}^{N} \left(\varepsilon_j + \varepsilon_1\alpha_j\right) \quad , \qquad i=2, \ldots, N \tag{2.16}$$

The total molar flux in the outer region, n_f, can be obtained by summing Equation (2 1) over all species, multiplying by 4π and integrating. The result is

$$\dot{n}_f = 4\pi r_f^2 \sum_{j=2}^{N} N_{if} \quad , \qquad \text{a constant} \tag{2.17}$$

Combining Equations (2 4), (2.15) and (2.17) yields an expression for the relationship between $\dot{n}$ and $\dot{n}_f$. That expression is

$$\frac{\dot{n}_f}{\dot{n}} = \sum_{i=2}^{N} \varepsilon_i + \varepsilon_1\alpha_i \tag{2.18}$$

The conservation of energy equation, Equation (2.2), can be written for the outer region in terms of δ_i and $\dot{n}_f$ as

$$\frac{d}{dr}\left[\dot{n}_f \sum_{i=2}^{N} \delta_i h_i - 4\pi r^2 \lambda \frac{dT}{dr}\right] = 0 \tag{2.19}$$

Applying conservation of energy across the flame service

$$\left[n \sum_{i=1}^{N-1} \varepsilon_i h_i - 4\pi r^2 \lambda \frac{dT}{dr}\right]_{f-} = \left[\dot{n}_f \sum_{i=1}^{N-1} \delta_i h_i - 4\pi r^2 \lambda \frac{dT}{dr}\right]_{f+}$$

The left hand side of this equation is constant throughout Region A and can be evaluated at the droplet surface. With this condition, Equation (2.19) can be integrated to provide the steady burning

equation of conservation of energy for Region B This equation is:

$$\dot{n}\left\{\sum_{i=2}^{N}\left(\varepsilon_i + \varepsilon_1\alpha_i\right)\left(h - h_\ell\right)_i - \varepsilon_1 Q_\ell + H\right\} = 4\pi r^2 \lambda_B \frac{dT}{dr} \qquad (2.20)$$

where

$$H = \sum_{i=1}^{N-1} \varepsilon_i L_i \qquad (2.21)$$

The quantity, Q_ℓ, is the heat of reaction at T_ℓ for gaseous reactants and products, i. e.

$$Q_\ell = h_{1\ell} - \sum_{i=2}^{N} \alpha_i h_{i\ell} \qquad (2.22)$$

The steady burning equation of conservation of species for Region B is obtained by substituting for δ_i and $\dot{n}_f$ into Equation (2.3). This equation is:

$$\dot{n}\left(X_i - \delta_i\right)\sum_{j=2}^{N}\left(\varepsilon_j + \varepsilon_1\alpha_j\right) = 4\pi r^2 (CD)_B \frac{dX_i}{dr} \quad , \quad i=2, \ldots, N \qquad (2.23)$$

The boundary conditions on Equations (2.20) and (2.23) are as follows

$$\begin{aligned} &r = r_f; \quad T = T_f, \quad X_i = X_{if} \quad (i=2, \ldots, N-1) \\ &r = \infty, \quad T = T_\infty, \quad X_i = X_{i\infty} \quad (i=2, \ldots, N) \end{aligned} \qquad (2\ 24)$$

The steady burning equations of conservation of species and energy, Equations (2 8), (2.9), (2.20), and (2.23), and the boundary conditions, Equations (2 10) and (2.24), can be integrated upon

substitution of relationships for the physical properties contained in these equations

The following relations were assumed for the specific heat and thermal conductivity.

$$C_{pi} = A_i + B_1 T \quad , \qquad i=1, \ldots, N$$

$$\lambda = \lambda_\ell \, (T/T_\ell) \tag{2.25}$$

The linear increase in specific heat with temperature is particularly useful in providing for the temperature variation of the specific heat of the heavier hydrocarbons. The quantity

$$\chi = \lambda/(CD) \tag{2.26}$$

is only a weak function of temperature and composition and was assumed to have a constant average value in each field.

The following section of this chapter discusses the solution of the steady burning equations using the property variations given by Equations (2.25) and (2.26) Since fuel is absent in the outer region and B_i in Equation (2.25) is small for the remaining species, the solution for the case of zero B_1 for the non-fuel species provides a useful approximation. However, since the solution for finite B_1 does not reduce conveniently to the case of zero B_1 for the non-fuel species, the latter solution is presented in Section 2.4 of this chapter Two additional solutions to the steady burning equations are considered for completeness and are presented in Appendix B The first corresponds to the conditions given by Goldsmith and Penner (8) in which only the fuel

specific heat was allowed to vary with temperature and only binary mixtures were considered in the gas phase. Although the analysis presented in Reference (8) is on a mass basis, a molar basis was used in Appendix B for convenience in matching the gas phase solution with the phase equilibrium solution at the droplet surface. In the second solution, the temperature dependence was neglected for all properties and the solution corresponds to the usual low pressure, constant property model of droplet combustion.

2.3 Gas Phase Solution (Finite B_1)

Under the assumption that compressibility effects are small in the gas phase, the ideal gas relationships are employed to evaluate the enthalpy difference terms appearing in the steady burning equations for conservation of energy. With the use of Equation (2.25), the enthalpy difference becomes

$$(h - h_\ell)_i = \int_{T_\ell}^{T} (A_1 + B_i T)\, dT = A_i(T - T_\ell) + \frac{B_i}{2}(T^2 - T_\ell^2) \qquad (2.27)$$

An expression for the fuel mole fraction at the droplet surface is obtained by introducing Equations (2.26) and (2.27) into Equation (2.8), eliminating spatial derivatives between Equations (2.8) and (2.9), and integrating. The solution was found to have three branches which are as follows

$$\frac{X_{1\ell}}{\varepsilon_1} = 1 - \exp\left\{\frac{2\chi_A}{\phi}\left[\tan^{-1}\left(\frac{a + b\, t_\ell}{\phi}\right) - \tan^{-1}\left(\frac{a + b\, T_f}{\phi}\right)\right]\right\}, \qquad (2.28)$$

$$\phi^2 > 0$$

$$\frac{X_{1\ell}}{\varepsilon_1} = 1 - \exp\left\{\frac{2\chi_A b\ (T_\ell - T_f)}{(a + b\ T_\ell)(a + b\ T_f)}\right\}, \qquad \phi^2 = 0 \tag{2.29}$$

$$\frac{X_{1\ell}}{\varepsilon_1} = 1 - \left\{\frac{(a + b\ T_f + \zeta)(a + b\ T_\ell - \zeta)}{(a + b\ T_f - \zeta)(a + b\ T_\ell + \zeta)}\right\}^{\chi_A/\zeta}, \qquad \zeta^2 > 0 \tag{2.30}$$

where

$$a = \sum_{i=1}^{N-1} \varepsilon_i A_i \tag{2.31}$$

$$b = \sum_{i=1}^{N-1} \varepsilon_i B_i \tag{2.32}$$

and

$$\zeta^2 = -\phi^2 = a^2 - 2b\ (H - aT_\ell - \frac{b}{2} T_\ell^2) \tag{2.33}$$

The concentration of any species at the droplet surface can be determined in terms of the fuel mole fraction at the droplet surface and concentrations at the flame. Dividing Equation (2.9) for species i by Equation (2.9) for the fuel, eliminating spatial derivatives and integrating yields:

$$\frac{X_{i\ell} - \varepsilon_i}{X_{if} - \varepsilon_i} = \frac{\varepsilon_1 - X_{1\ell}}{\varepsilon_1} \tag{2.34}$$

In order to determine conditions at the flame surface, the outer region must be considered. Eliminating spatial derivatives between Equation (2.23) for species i and the oxidant, species N,

and integrating yields an expression for the species concentrations at the flame surface in terms of the ambient concentrations.

$$\frac{X_{1f} - \delta_i}{X_{1\infty} - \delta_1} = \frac{\delta_N}{\delta_N - X_{N\infty}} \tag{2.35}$$

An expression for the combustion temperature was determined by substituting Equations (2.26) and (2.27) into Equation (2.20), eliminating spatial derivatives between Equations (2.20) and (2.23) for the oxidant species and integrating through the outer region. As before, there are three branches to the solution. They are:

$$\ln\left(\frac{\delta_N}{\delta_N - X_{N\infty}}\right) = \frac{2\chi_B}{\beta}\left\{\tan^{-1}\left(\frac{a' + b' T_f}{\beta}\right) - \tan^{-1}\left(\frac{a' + b' T_\infty}{\beta}\right)\right\},$$

$$\beta^2 > 0 \tag{2.36}$$

$$\frac{\delta_N}{\delta_N - X_{N\infty}} = \left[\frac{(a' + b' T_\infty + \gamma)(a' + b' T_f - \gamma)}{(a' + b' T_\infty - \gamma)(a' + b' T_f + \gamma)}\right]^{\chi_B/\gamma}, \quad \gamma^2 > 0 \tag{2.37}$$

$$\ln\left(\frac{\delta_N}{\delta_N - X_{N\infty}}\right) = 2\chi_B\left[\frac{b'(T_f - T_\infty)}{(a' + b' T_f)(a' + b' T)}\right], \quad \gamma^2 = 0 \tag{2.38}$$

where

$$a' = \sum_{i=2}^{N} \delta_1 A_i \tag{2.39}$$

$$b' = \sum_{1=2}^{N} \delta_1 B_1 \tag{2.40}$$

$$q = (h - \varepsilon_1 Q_\ell) \Big/ \sum_{1=2}^{N} (\varepsilon_i + \varepsilon_1 \alpha_i) \qquad (2\ 41)$$

and

$$\gamma^2 = -\beta^2 = a'^2 - 2b' \left(q - a' T_\ell - \frac{b'}{2} T_\ell^2\right) \qquad (2.42)$$

An expression for the flame radius, r_f, is obtained by substituting Equations (2.25) and (2.27) into Equation (2 20), applying the boundary conditions, Equation (2.24), and integrating. The reulst is.

$$\frac{1}{r_f} = \frac{4\pi\lambda_{B\ell}}{\dot{n}_f T_\ell b'} \left\{ \ln \left[\frac{q + a' (T_\infty - T_\ell) + \frac{b'}{2} (T_\infty^2 - T_\ell^2)}{q + a' (T_f - T_\ell) + \frac{b'}{2} (T_f^2 - T_\ell^2)} \right] + \eta \right\} \qquad (2\ 43)$$

where η is given by.

$$\eta = \frac{2a'}{\beta} \left\{ \tan^{-1} \left(\frac{a' + b' T_f}{\beta} \right) - \tan^{-1} \left(\frac{a' + b' T_\infty}{\beta} \right) \right\}, \quad \beta^2 > 0 \qquad (2.44)$$

or

$$\eta = \ln \left[\frac{(a' + b' T_\infty + \gamma)(a' + b' T_f - \gamma)}{(a' + b' T_\infty - \gamma)(a' + b' T_f + \gamma)} \right]^{a'/\gamma}, \quad \gamma^2 > 0 \qquad (2.45)$$

or

$$\eta = \frac{2a' b' (T_f - T_\infty)}{(a' + b' T_f)(a' + b' T_\infty)}, \quad \gamma^2 = 0 \qquad (2\ 46)$$

The burning rate, $\dot{n}$, is determined by applying Equations (2.25) and (2.27) and the boundary conditions, Equation (2.10) to Equation

(2.8). Upon integration, the result is:

$$\frac{n\, T_\ell\, b}{4\pi r_\ell\, \lambda_{A\ell}} \left(1 - \frac{r_\ell}{r_f}\right) = \ln\left\{1 + \left[a(T_f - T_\ell) + \frac{b}{2}\left(T_f^2 - T_\ell^2\right)\right]\Big/ H\right\} + \psi \tag{2.47}$$

where ψ is given by:

$$\psi = -\frac{2a}{\phi}\left\{\tan^{-1}\left(\frac{a + b\, T_f}{\phi}\right) - \tan^{-1}\left(\frac{a + b\, T_\ell}{\phi}\right)\right\}, \qquad \phi^2 > 0 \tag{2.48}$$

or

$$\psi = \ln\left[\frac{(a + b\, T_f + \zeta)(a + b\, T_\ell - \zeta)}{(a + b\, T_f - \zeta)(a + b\, T_\ell + \zeta)}\right]^{a/\zeta}, \qquad \zeta^2 > 0 \tag{2.49}$$

or

$$\psi = -\frac{2ab\,(T_f - T_\ell)}{(a + b\, T_f)(a + b\, T_\ell)}, \qquad \zeta^2 = 0 \tag{2.50}$$

Equations (2.28) to (2.42) are sufficient to determine steady droplet burning conditions. For given values of T_∞ and the $X_{i\infty}$, the liquid temperature can be varied by trial and error until the droplet surface concentrations given by these equations agree with phase equilibrium calculations at the droplet surface for the same liquid temperature.

2.4 Gas Phase Solution ($B_i = 0$)

If B_i is set equal to zero in Equation (2.25) when solving the outer field, steady burning conservation of energy equation,

Equation (2.20), only the expressions for the combustion temperature and the flame radius will differ from the equations presented in the preceding section. The most significant difference, is the absence of three separate branches to the solutions. The simple form of the resulting expressions reduces computational efforts. Proceeding as before, this approximation results in the following expressions for the combustion temperature and flame radius.

$$\frac{q + a' (T_f - T_\ell)}{q + a' (T_\infty - T_\ell)} = \left(\frac{\delta_N}{\delta_N^i - X_{N\infty}} \right)^{a'/\chi_B} \tag{2.51}$$

and

$$\frac{1}{r_f} = \frac{4\pi\lambda_{B\ell}}{\dot{n}_f \, a'^2 \, T_\ell} \left\{ a' (T_\infty - T_f) - (q - a' T_\ell) \ln \left[\frac{q + a' (T_\infty - T_\ell)}{q + a' (T_f - T_\ell)} \right] \right\} \tag{2.52}$$

where the terms in these two equations were defined in the preceding section.

2.5 Surface Equilibrium Considerations

The determination of steady state conditions requires that the solutions of the preceding sections be matched with the boundary conditions at the droplet surface. The evaluation of these boundary conditions requires a consideration of the thermodynamics of phase equilibrium at the vapor-liquid interface of the droplet.

At low pressures, it is usually a good approximation to neglect solubility effects, ($\varepsilon_1 = 1$) and take the fuel mole fraction

at the droplet surface, $X_{1\ell}$, as the vapor pressure of the pure fuel at the liquid temperature divided by the total pressure. The heat of vaporization, L, is also taken to be that of the pure fuel for saturation conditions at the liquid temperature.

These approximations, although perfectly adequate at low pressures, become less realistic at higher pressures and in the critical region, they become extremely questionable

A vapor phase and a liquid phase are in equilibrium when both are at the same temperature and pressure and when the fugacity (or chemical potential) of any component in the vapor phase is equal to that in the liquid phase, i e.,

$$\left.\begin{aligned} T &= \text{constant} \\ P &= \text{constant} \\ f_i^V &= f_i^L \quad , \quad i=1, \ldots, N \end{aligned}\right\} \tag{2.53}$$

The fugacity of a component in a mixture is related to the volumetric properties of the mixture through the relation:

$$RT \ln (f_i/X_i P) = \int_0^P (\bar{v}_i - RT/P)dP \tag{2.54}$$

Several methods for computing component fugacities were evaluated for use in determining phase equilibrium conditions at high pressures. Most of the methods are discussed by Reid and Sherwood (31). In addition, liquid and vapor phase component fugacities were computed from Equation (2.54) by employing the equation

of state of Redlich and Kwong (32). The modified mixing rules given by Prausnitz and Chueh (33) were used in applying the equation to mixtures.

Evaluation of the various methods was accomplished by comparing the calculated phase-behavior with experimental data for binary mixtures of a paraffinhydrocarbon with carbon dioxide or nitrogen. On this basis, the equation of state method with the Redlich and Kwong equation was found to be the most satisfactory for the present study.

The Redlich and Kwong equation of state is of the form

$$P = \frac{RT}{v - b^\circ} - \frac{a^\circ}{T^{0.5}\, v(v + b^\circ)} \tag{2.55}$$

The mixing rules of Prausnitz and Chueh (33) were used to apply Equation (2.55) to mixtures. For a mixture of N components,

$$b^\circ = \sum_{i=1}^{N} X_i b_i^\circ \tag{2.56}$$

where

$$b_i^\circ = \frac{\Omega_{bi}\, RT_{ci}}{P_{ci}} \tag{2.57}$$

and

$$a^\circ = \sum_{i=1}^{N} \sum_{j=1}^{N} X_i X_j\, a^\circ_{ij} \tag{2.58}$$

where

$$a^\circ_{ii} = \frac{\Omega_{ai}\, R^2\, T_{ci}^{2.5}}{P_{ci}} \tag{2.59}$$

$$a^{\circ}_{ij} = \frac{(\Omega_{ai} + \Omega_{aj})\ R^2\ T_{cij}^{2.5}}{2\ P_{cij}} \tag{2.60}$$

$$P_{cij} = \frac{Z_{cij}\ R\ T_{cij}}{v_{cij}} \tag{2.61}$$

$$v_{cij} = (v_{ci} + v_{cj})/2 \tag{2.62}$$

$$z_{cij} = 0.291 - 0.04\ (\omega_i + \omega_j) \tag{2.63}$$

$$T_{cij} = \sqrt{T_{ci}\ T_{cj}}\ \ (1 - k_{ij}) \tag{2.64}$$

Component fugacities were determined by substituting Equation (2.55) and the mixing rules, Equations (2.56) to (2.64), into Equation (2.54) and integrating. The results are presented in Appendix C along with the equations used to compute the enthalpy of vaporization of a component in a mixture from the equation of state and mixing rules given above.

Fuel, carbon dioxide, water vapor and nitrogen components were considered in the present investigation. The pure component constants, P_c, T_c, v_c and ω, where ω is the acentric factor, were obtained from References (31) and (33). These constants are given in Appendix C for the components considered in the high pressure region.

The dimensionless constants Ω_a and Ω_b in the mixing rules were obtained by setting the first and second isothermal derivatives

of pressure with respect to volume equal to zero at the critical point They are 0 4278 and 0.0867 respectively For temperatures remote from the critical region, it is more appropriate to obtain these constants by fitting the equation to the volumetric data of the saturated liquid and vapor as discussed by Prausnitz and Chueh (33). However, when this is done, it was found that the equality of component fugacities in both phases could not be satisfied in the vicinity of the critical region. Therefore, the universal values given above were used in the calculations in order to provide a consistant solution over the entire range of temperature

The binary constant, k_{ij}, in Equation (2 64) is characteristic of the i-j interaction for each binary pair present in the system This constant varies between zero and one and increases with increasing molecular weight of the hydrocarbon component in systems containing hydrocarbons with nitrogen and carbon dioxide. The constant must be obtained from some experimental information about the binary interaction Reference (33) tabulates this information for n paraffin hydrocarbons up to n pentane with carbon dioxide and up to n butane with nitrogen. Additional values were obtained by fitting the equation of state to experimental phase equilibrium data for n pentane-carbon dioxide (34), n hexane-nitrogen (35), n heptane-nitrogen (36) and n decane-nitrogen (37). The remaining values with respect to carbon dioxide and nitrogen were obtained by interpolation.

Since methods for accurately treating polar compounds in high pressure equilibrium calculations have not been developed, results

involving water in the system are considered to be more tentative. For the heavier hydrocarbons, temperatures exceed a reduced critical temperature of 0.95 for water, as the critical region is approached. Prausnitz, et al (38) suggest that polar contributions are small at these temperatures so that the present treatment might be adequate under these conditions The binary interaction parameters for the water-n paraffin systems were obtained by matching with data in the literature, References (39) and (40), and interpolating for intermediate paraffins. The sensitivity of the final calculations to these values of the interaction parameter is discussed in Chapter VI The numerical values of the binary interaction parameters employed in the calculations are given in Appendix C

The general characteristics of phase equilibrium behavior are best illustrated through the use of a fugacity-composition diagram. Such a diagram is shown in Figure 2 for the n decane-nitrogen system. The curves shown were computed by the methods discussed above. The diagram shows the calculated fugacity of n decane plotted against the mole fraction of n decane for three different temperatures at a total pressure of 41.5 atmospheres This pressure is twice the critical pressure of pure n decane. The fugacity of nitrogen is also shown plotted for the lowest temperature.

At a temperature of 550°K, a liquid and vapor phase coexist and the equilibrium criterion, given by Equations (2.53), are depicted graphically on the diagram by the broken lines which determine the mole fractions of n decane in the vapor (X_1^V) and liquid (X_1^L) phases. At a temperature of 611°K, the fugacity-mole

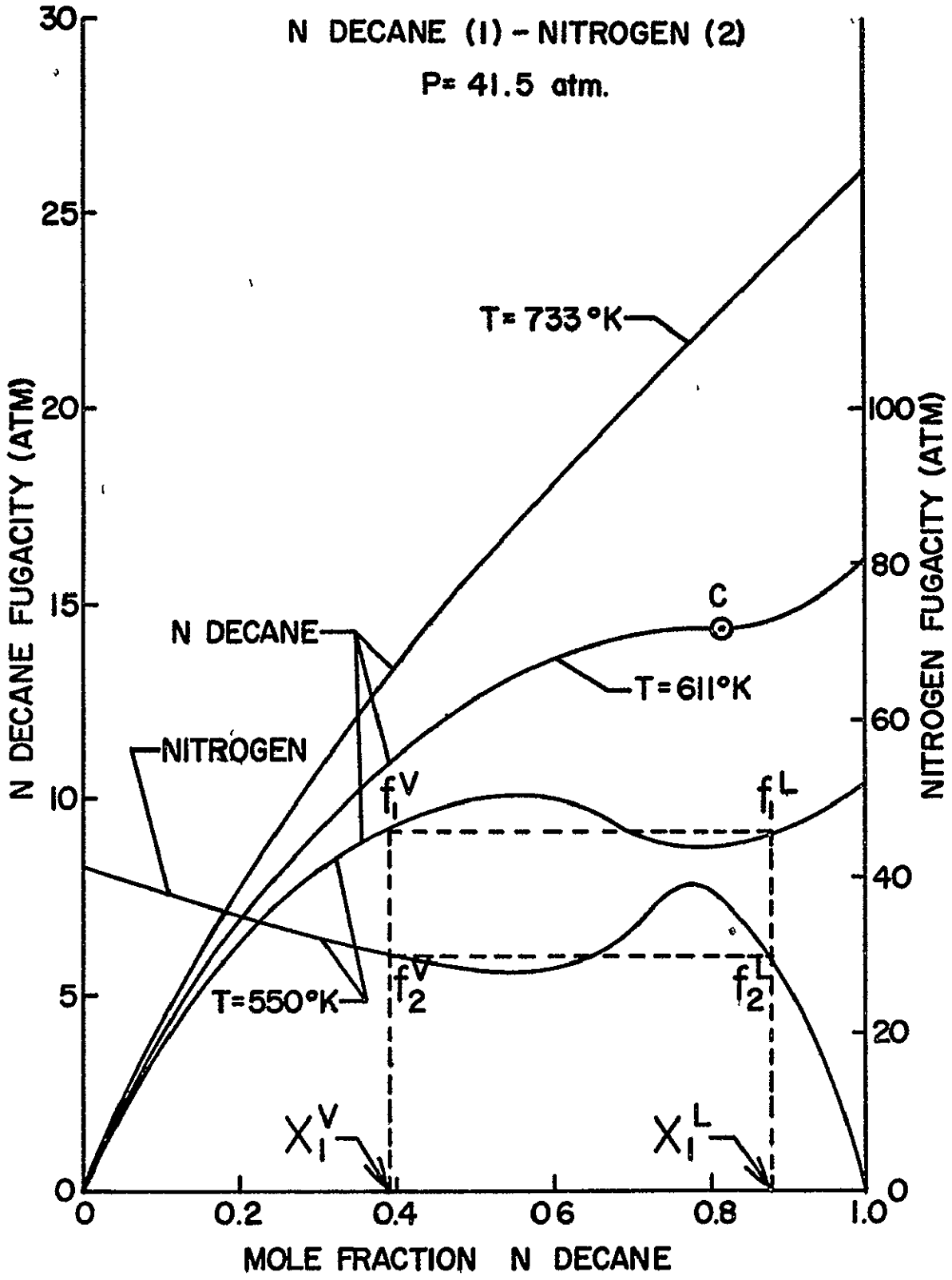

FIGURE 2 FUGACITY-COMPOSITION DIAGRAM FOR THE N DECANE-NITROGEN SYSTEM AT CONSTANT PRESSURE

fraction curve for n decane exhibits a point of inflection as shown at point C. Although the nitrogen fugacity curve was not shown for this temperature to avoid overcrowding the diagram, it can be shown, as discussed by Lewis and Randall (41), that for a binary mixture the slope of the curve for one component is entirely determined by the slope of the curve for the other component and the composition of the mixture If at any composition, one of the curves has a maximum, the other curve will have a minimum at the same composition. Thus, the nitrogen fugacity curve would also exhibit a point of inflection at the composition of point C Application of the equilibrium criterion, Equations (2.53), would therefore show that the liquid and vapor phase compositions are identical at the temperature, pressure and composition for point C.

This behavior is closely analogous to the phenomenon of the critical point for the case of a pure substance and therefore, the state at point C is known as the critical mixing point. The determination of the point C for different pressures would determine the locus of critical mixing states for this set of components.

Finally, at temperatures greater than the critical mixing temperature, only a single phase exists which consists of a mixture of the two components. Application of Equations (2.53) to the fugacity-mole fraction curves at 733°K shown in Figure 2 reveal this behavior which is analogous to the supercritical behavior of a pure substance.

It follows from the above discussion, that under the assumption of thermodynamic equilibrium at the droplet surface, a droplet can

reach a supercritical state only when the temperature exceeds the critical mixing temperature for the total pressure of the system For the fuels considered in this study, these states occurred at pressures greater than the critical pressure of the pure fuel and at temperatures which were less than the critical temperature of the pure fuel.

In order to establish confidence in the phase equilibrium calculations at high pressures, comparisons were made with experimental data in the literature. A comparison with the experimental data of Poston, et al. (35) for the n hexane-nitrogen system (which shows behavior near a critical mixing point) and of Azarnoosh, et al. (37) for the n decane-nitrogen system is shown in Figure 3 The predictions are in reasonably good agreement with the data over the range of temperatures and pressures available for comparison. Similar agreement was obtained in comparisons with the n pentane-carbon dioxide data of Poettmann, et al. (34) shown in Figure 4. This data also exhibits behavior in the vicinity of the critical mixing points for the two isotherms shown

The calculation procedures enable the construction of phase equilibrium diagrams which represent the locus of equilibrium states for a system of components. Figure 5 shows a calculated phase equilibrium diagram for the n decane-nitrogen system. In the diagram, equilibrium temperature is plotted against the mole fraction of n decane Curves are shown for several different reduced pressures, where the reduced pressure is defined here as the system pressure divided by the critical pressure of the pure fuel (i.e , $P_r = P/P_c$).

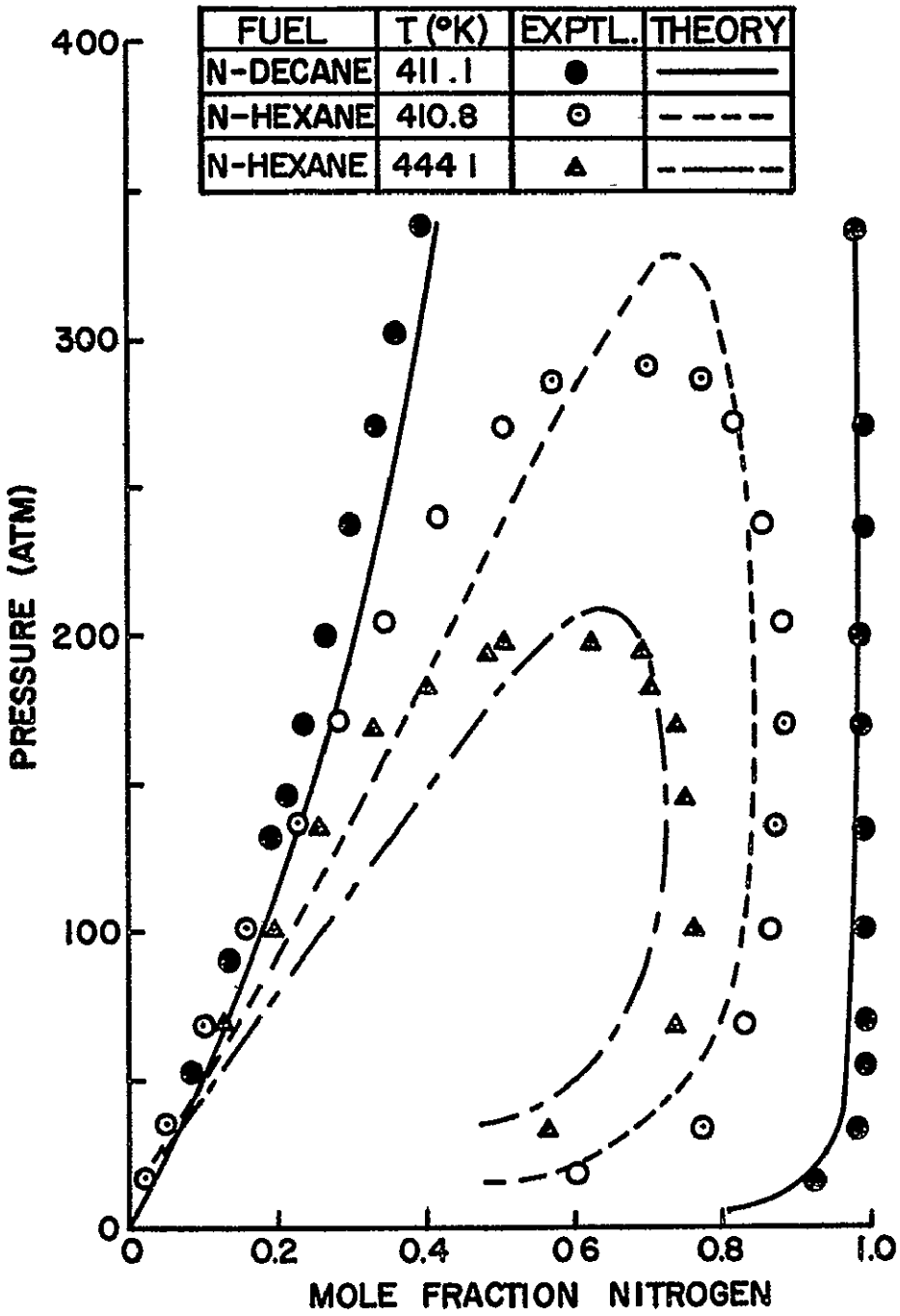

FIGURE 3 COMPARISON BETWEEN COMPUTED AND EXPERIMENTAL HIGH PRESSURE PHASE EQUILIBRIA, N HEXANE-NITROGEN DATA, REFERENCE (35), N DECANE-NITROGEN DATA, REFERENCE (37)

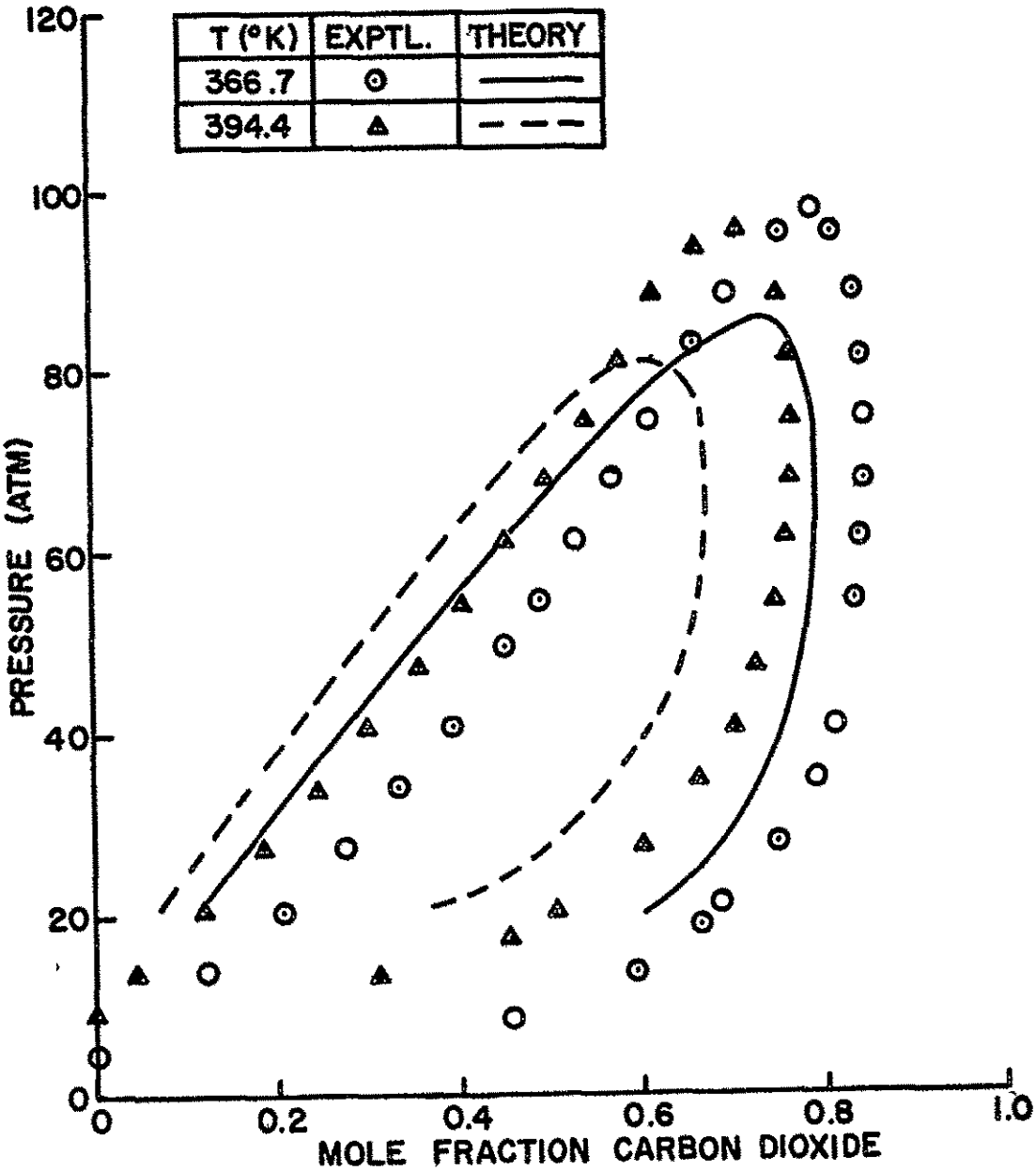

FIGURE 4 COMPARISON OF COMPUTED AND EXPERIMENTAL HIGH PRESSURE PHASE EQUILIBRIA, N PENTANE-CARBON DIOXIDE DATA, REFERENCE (34)

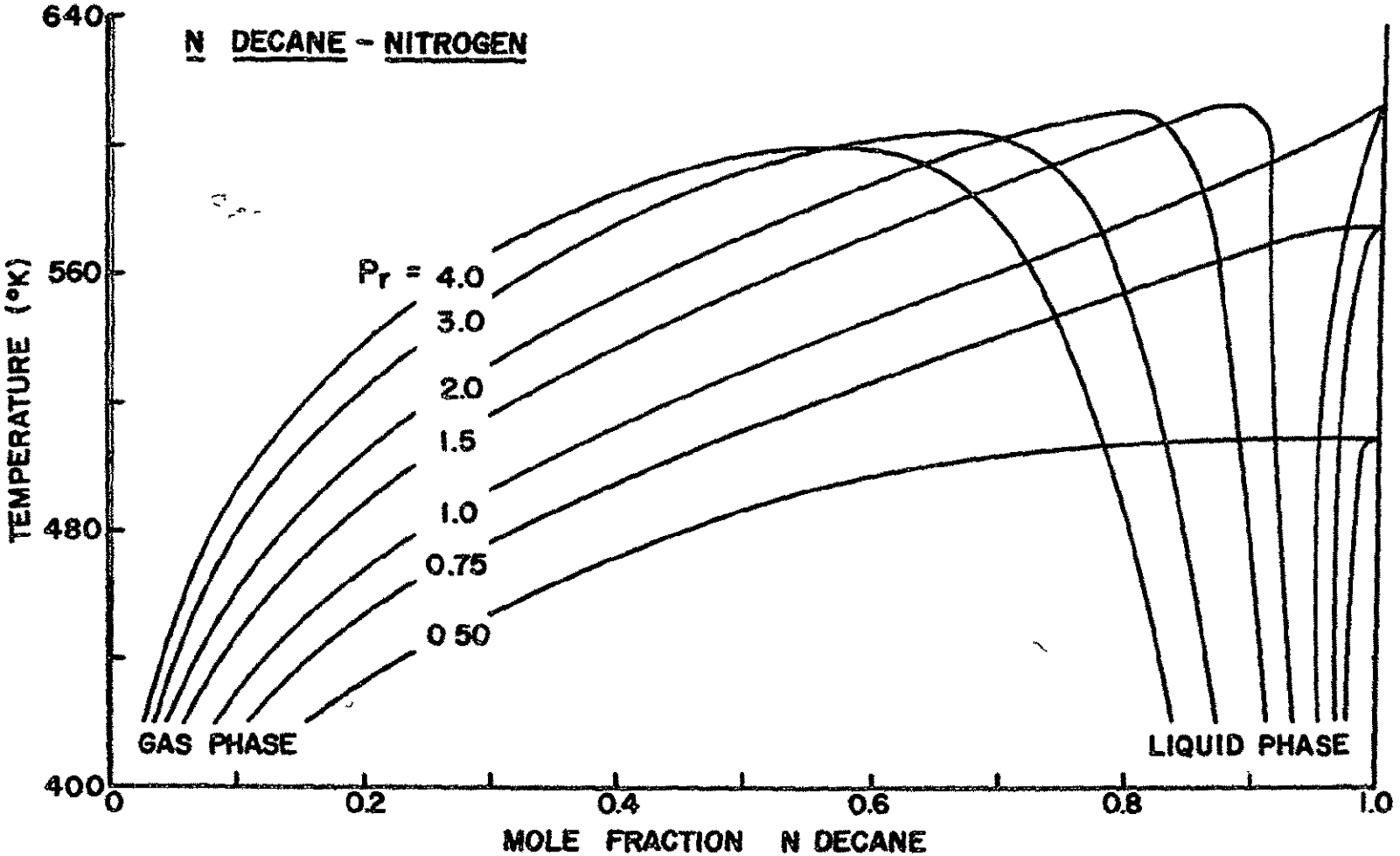

FIGURE 5 PHASE EQUILIBRIUM CALCULATIONS FOR THE N DECANE-NITROGEN SYSTEM AT VARIOUS TEMPERATURES AND PRESSURES

The liquid and gas phase compositions become identical at either the boiling point of the pure fuel ($P_r < 1$) or at the critical mixing point ($P_r > 1$), which is located at the maximum temperature of each curve for $P_r > 1$. For pressures greater than the critical pressure of the pure fuel, the concentration of nitrogen in the liquid phase increases at higher liquid temperatures for a fixed total pressure Thus, at high pressures where the droplet steady state temperature may become high, the amount of nitrogen dissolved in the liquid phase can become appreciable.

With calculational procedures established for the high pressure behavior at the droplet surface, it is useful to compare these calculations with the low pressure approximations discussed at the beginning of this section. The two methods of computing the fuel mole fraction at the droplet surface are compared with the experimental data of Poston, et al (35) for the n hexane-nitrogen system at 410.8°K in Figure 6 At low pressures, both methods provide a reasonable approximation of the data. As the pressure is increased, however, the n hexane mole fraction computed from the vapor pressure of pure n hexane considerably underestimates the experimental value, while the high pressure method provides a reasonably good prediction. At the computed critical mixing point, shown as Point C in Figure 6, the low pressure approximation exhibits a very large error.

Figure 7 shows the effect of pressure on the calculated heat of vaporization of n hexane in an equilibrium mixture of n hexane and nitrogen. Heats of vaporization, computed from the Redlich and Kwong equation by the methods given in Appendix C, are shown

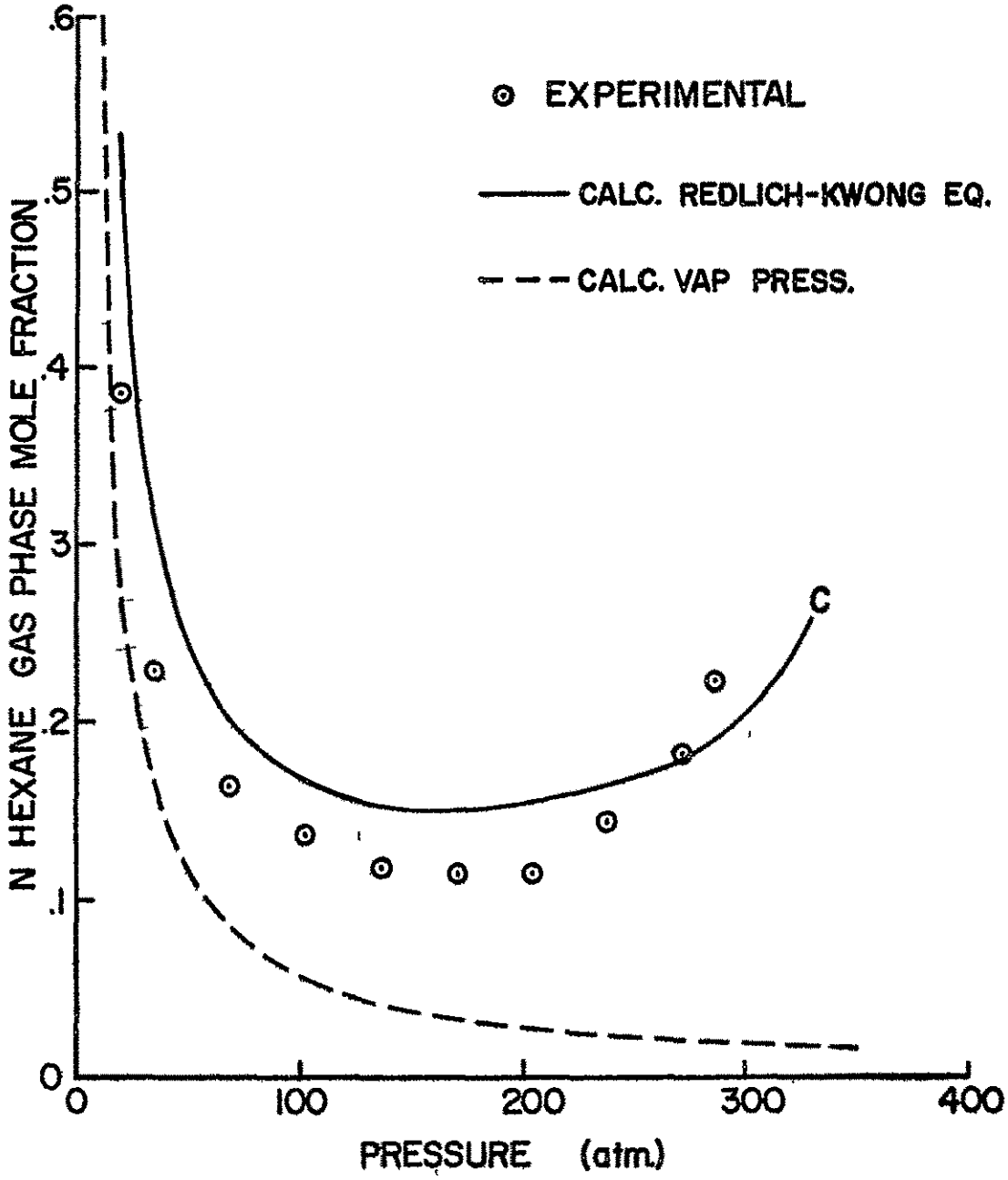

FIGURE 6 COMPARISON OF CALCULATED N HEXANE GAS PHASE MOLE FRACTIONS IN THE N HEXANE-NITROGEN SYSTEM WITH THE EXPERIMENTAL DATA OF POSTON AND MCKETTA (35) at 410.8K

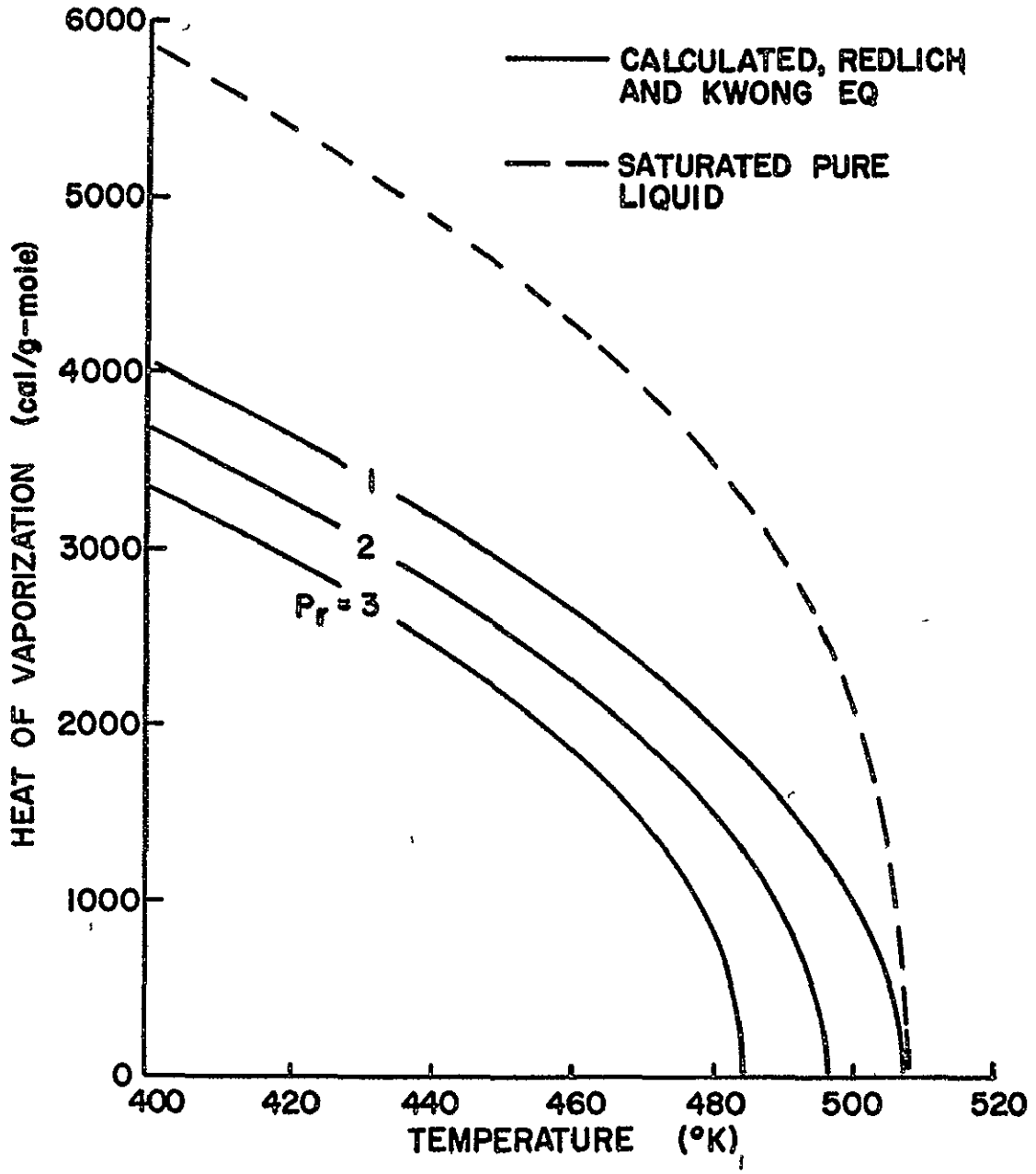

FIGURE 7 EFFECT OF PRESSURE ON THE HEAT OF VAPORIZATION OF N HEXANE IN AN EQUILIBRIUM MIXTURE OF N HEXANE AND NITROGEN

for reduced pressures of 1, 2 and 3 These curves show that the heat of vaporization, which is the isothermal difference in the partial molal enthalpies of n hexane in the vapor and liquid phases, becomes equal to zero at the critical mixing points since the temperature, pressure and composition are identical in both phases for these states These curves are compared with the low pressure approximation in which the heat of vaporization is taken to be that of the pure fuel for saturated conditions at the liquid temperature These values, which are independent of pressure, were computed from the Watson correlation discussed by Reid and Sherwood (31). For this approximation, the heat of vaporization becomes equal to zero only at the critical temperature of the pure fuel (T_c = 507 3°K for n hexane) This figure illustrates that even at subcritical temperatures, the difference in enthalpy across the interface may vanish at sufficiently high pressures.

CHAPTER III

FLAT FLAME BURNER APPARATUS

3.1 Test Facility

In order to provide a more stringent test of the Goldsmith and Penner (8) theory, an experimental apparatus was required which allowed the measurement of burning rates for liquid fuel droplets under various ambient conditions. The flat flame burner apparatus developed by Faeth (17) was used for these experiments. The test droplets were mounted on a probe and rapidly subjected to the combustion products of a flat flame burner in order to simulate a combustion chamber environment.

A schematic diagram of the flat flame burner apparatus is shown in Figure 8. The burner was mounted on rails so that it could be rapidly moved under the droplet location with a solenoid valve actuated pneumatic cylinder The time between the droplet first entering the burner flame and the burner coming to rest in the test position (illustrated in Figure 8) was measured with a high speed motion picture camera and found to be on the order of 10 ms

The flat flame burner was similar to the one described by Friedman and Macek (42). A porous bronze disk, 5 cm in diameter, was used for the burner face The lower surface of the porous disc was cooled at a series of points by contact with a water cooled copper block. The heat loss from the burner flame to the face of the burner was determined by measuring the temperature rise and

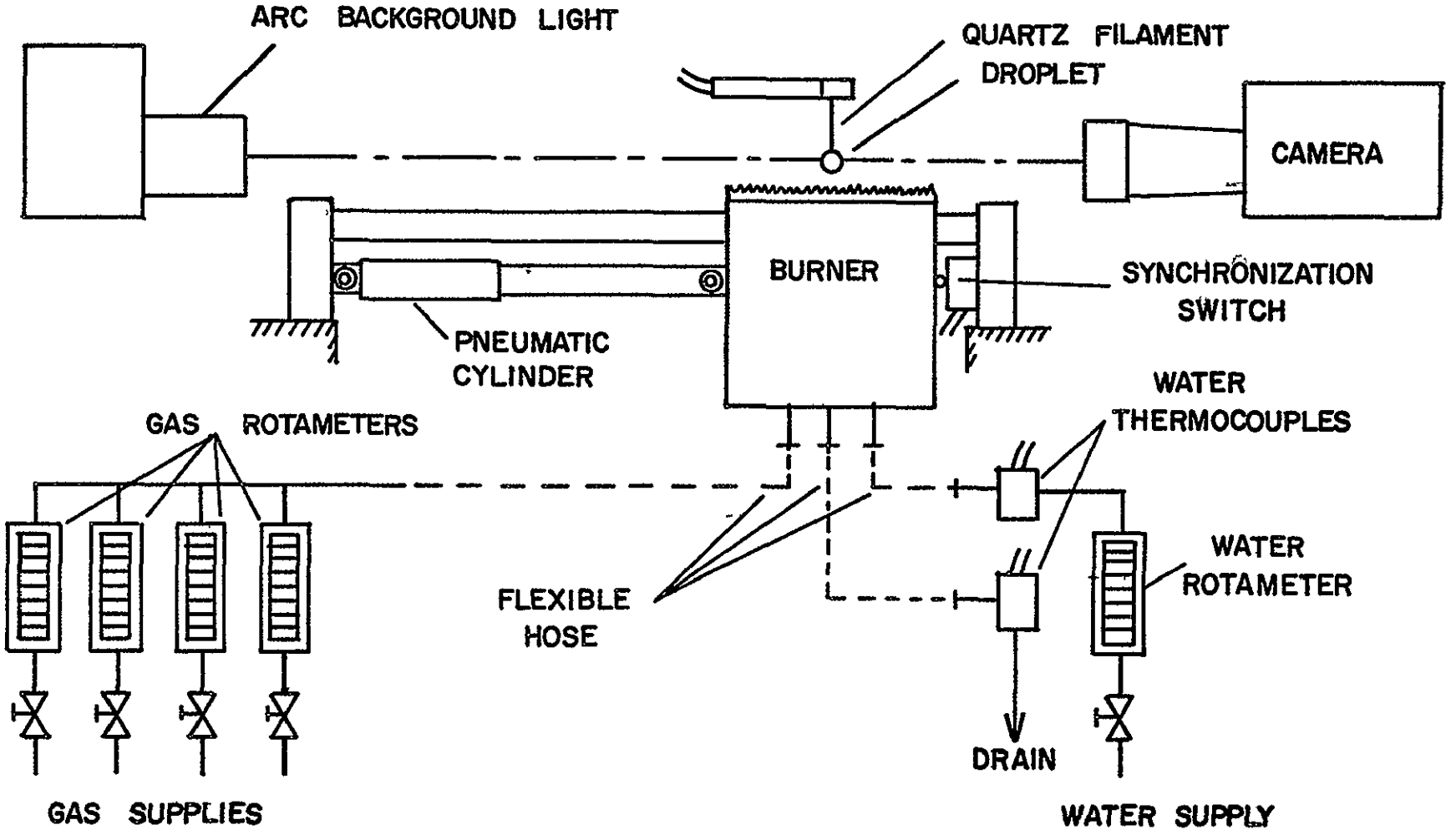

FIGURE 8 SCHEMATIC DIAGRAM OF THE FLAT FLAME BURNER APPARATUS

flow rate of the burner cooling water The water thermocouples and rotameter shown in Figure 8 were used for this purpose

The burner was operated with various mixtures of carbon monoxide, hydrogen, oxygen and nitrogen (commercial grade) at atmospheric pressure to provide ambient oxygen concentrations in the range of 0-40% by volume and ambient temperatures in the range of 1660-2530°K. The flow rate of the gases was measured with rotameters which were calibrated with a wet test meter

The test droplet was mounted on a quartz filament having a diameter of approximately 100μ. The bottom end of the probe was slightly enlarged to aid in supporting the droplet. In the test position the droplet was 1 cm. above the center of the burner face

The temperature and composition of the burned gas flowing around the droplet was determined from theoretical calculations allowing for all relevant dissociation reactions and heat loss to the burner. The thermochemical properties for these calculations were taken from the JANAF Tables (43)

The gas velocity at the droplet location was calculated from the mass flux into the burner and the known properties of the burned gas. This procedure is adequate since the test position is well within the potential core of the jet leaving the burner. Table 1 summarizes the computed properties of the gas stream at the droplet location for the test conditions employed in the present study. The ambient oxygen mole fraction, $X_{N\infty}$, shown in the table is an effective value based on the concentrations of possible oxidizing species (O_2, O, NO).

TABLE 1

PROPERTIES OF THE AMBIENT GAS FOR VARIOUS TEST CONDITIONS

$X_{N\infty}$	T_∞ (°K)	V_∞ (cm/sec)	PRODUCT MOLE FRACTION							
			CO	CO_2	H_2	H_2O	NO	N_2	O	O_2
050	2530	62.5	.099	415	0	0	.009	.430	.004	043
154	2530	62.5	.058	439	0	0	.014	.339	.007	.143
.254	2530	62 5	.041	.423	0	0	017	.270	.009	.240
.346	2530	62 5	.033	402	0	0	.016	208	.011	.330
415	2530	62.5	.022	381	0	0	.015	172	.009	.401
0	2350	46.7	.288	427	0	0	0	285	0	0
0	2220	46.7	251	374	0	0	0	.375	0	0
0	2060	46 7	.371	429	029	171	0	0	0	0
0	1830	46.7	294	.353	.029	134	0	.190	0	0
0	1660	46.7	245	.296	026	109	0	.324	0	0

Droplet diameters were measured from shadowgraphs recorded by a 16 mm cine camera operating at speeds on the order of 100 pictures per second. A mercury arc lamp was used to provide the background light Timing marks were placed on the edge of the film by an internal timing light powered by a 100 cps pulse generator to allow time correlation of the film

A cycling timer was used to control the operation of the solenoid valve and motion picture camera.

3 2 Operation of the Apparatus

Before conducting the experiments on the apparatus, the burner was calibrated to determine the gas flow rates required to give the test conditions shown in Table 1 Photographs of wires of a known diameter were also taken with the wire occupying the location of the droplet in the test position in order to provide a calibration for the droplet diameter measurements

The preliminary setup for a series of tests at a given test condition involved focussing of the camera, pressurizing the supply tank to operate the pneumatic cylinder and regulating the cooling water supply and burner gases. After igniting the gas mixture from the burner, the flame was allowed to stabilize for a sufficient period of time.

The droplet was then mounted on the quartz filament with a hyperdermic syringe and the cycling timer was actuated At the beginning of the timer cycle, the electrically driven motion picture camera was started. Once the camera reached operating speed, the

solenoid valve was actuated and the pneumatic cylinder forced the burner into the test position below the droplet The burner remained in this position for approximately 2 seconds allowing the liquid fuel droplet to ignite and burn in the hot burner gases. The solenoid was then de-energized allowing the burner to return to its original position and the camera power was turned off to complete the test cycle

For additional tests at the same ambient conditions, a new droplet was mounted on the probe and the cycle was repeated For a different test condition, the gas flow rates were adjusted and the flame allowed to stabilize before beginning a new test cycle.

Since the droplets were usually elliptical in shape, a correction suggested by Kobayasi (6) was used to determine an equivalent diameter for a sphere having the same volume as the elliptical droplet A Vanguard Motion Analyzer was used to analyze the films

CHAPTER IV

LOW PRESSURE BASELINE RESULTS

4.1 Steady Droplet Burning Rates

Experimental measurements of steady droplet burning rates were obtained from the flat flame burner apparatus described in the preceding chapter in order to provide a more stringent test of the Goldsmith and Penner (8) theory. The droplet fuels considered in the study included methyl, 1 butyl and 1 decyl alcohol as well as the paraffin hydrocarbons, n pentane, n heptane, iso octane, n decane, n tridecane and n hexadecane. The test droplets were burned at atmospheric pressure in the combustion products of a flat flame burner to provide ambient temperatures in the range 1660 to 2530°K and ambient oxygen concentrations of 0 to 40% by volume at the droplet location. The measured burning rates were compared with values predicted by the Goldsmith and Penner theory for the conditions of the experiments.

The Goldsmith and Penner analysis presented in Appendix B is limited to the case of no relative motion between the droplet and its surroundings For the conditions of the experiments, however, the flow of the product gas past the droplet gave Reynolds numbers (based on the droplet diameter and ambient gas properties) in the range of 1.3 to 2.2. Therefore, it was necessary to correct the theory for the influence of convection prior to comparison with the experimental results

For steady droplet evaporation or burning at the wet bulb state, numerous investigators (19-24) have suggested a convection correlation of the following form

$$\frac{\dot{n}}{\dot{n}^*} = 1 + \text{function (Re, Pr, Sc)} \qquad (4.1)$$

where n^* is the molar burning rate at no flow. Fendel, et al. (22, 23) have demonstrated the validity of this general form for incipient convection, constant properties and chemical reaction limited to a flame surface. Although there is no theoretical justification for Equation (4.1) for larger Reynolds numbers, this type of correlation has proven reasonably successful as pointed out by Rosner (24)

While there is general agreement that transport rates can be corrected for convection by an equation of the form of Equation (4 1), there is less agreement concerning the details of the correlation, particularly for Reynolds numbers less than ten which is the range of interest in the present investigation.

Prompted by this difficulty in the convection correlation for Reynolds numbers of order unity, Fendell (23) and Rosner (24) have suggested some general forms that are asymptotically correct for $\mathrm{Re\ Pr} \ll 1$ and $\mathrm{Re} > 10$ Adopting the form suggested by Rosner (24) and fitting the correlation to the data of Yuge (44), Frossling (21) and Allender (45) at $\mathrm{Re} = 100$ and $\mathrm{Pr} = .715$, yields the following expression.

$$\frac{\dot{n}}{\dot{n}^*} = 1 + 0.278\ \mathrm{Re}^{1/2}\ \mathrm{Pr}^{1/3} \left[1 + 1\ 237\ \mathrm{Re}^{-1}\ \mathrm{Pr}^{-4/3}\right]^{-1/2} \qquad (4.2)$$

Equation (4.2) asymptotically approaches the correlation of Fendell, et al. (22, 23) and Acrivos and Tylor (46) for Re Pr << 1 The equation is also in good agreement with Yuge's low Reynolds number data in the range 3 5 < Re < 10 as well as the results of References (21), (44) and (45).

Equation (4.2) was employed to correct the molar burning rate for no flow given in Appendix B for comparison with the experimental results of the flat flame burner apparatus. The properties in the correlation were taken to be those of the ambient product gases as suggested by Combs (47) since this method eliminates the difficulties in defining unambiguous mean properties.

For the test conditions of the experiments, the correction was on the order of 20%. Table 2 lists the values of the correction term computed from Equation (4.2) for the test conditions. The Reynolds numbers and Prandtl numbers are also listed. The correlations used for the ambient gas properties required for the computation of the Reynolds and Prandtl numbers are given in Appendix D.

The molar burning rate for no flow was computed from the equations given in Appendix B. The expression for the fuel mole fraction at the droplet surface was solved simultaneously with the vapor pressure equation to determine the droplet steady burning temperature. Computations were also made by approximating the steady burning temperature with the boiling temperature of the fuel since this approximation was used by Goldsmith and Penner and shown by Williams (10) to be adequate for conditions remote from the critical.

TABLE 2

CONVECTION CORRECTION FOR VARIOUS TEST CONDITIONS

$X_{o\infty}$	T_∞(°K)	Re	Pr	$\dot{n}/\dot{n}^*$
0 050	2530	1.549	0.662	1.195
0 154	2530	1 552	0.647	1.193
0.254	2530	1 528	0.641	1.189
0.346	2530	1.504	0.635	1.185
0.415	2530	1.483	0.643	1.185
0	2350	1 330	0 684	1.177
0	2220	1.434	0 686	1.189
0	2060	1.554	0 581	1.178
0	1830	1.865	0.591	1.208
0	1660	2.174	0.606	1 239

Since the differences between the two methods never exceeded 3% for the present test conditions, only the results obtained with the computed steady burning temperature are reported. The gas and liquid phase properties employed in the calculations are given in Appendix D.

A convenient way of representing steady burning rate data involves the use of the burning rate constant which is defined as

$$K = - \frac{d\, d_\ell^2}{dt} \qquad (4\ 3)$$

The molar burning rate expressed in terms of the liquid phase molar density and droplet diameter is

$$\dot{n} = - \frac{d}{dt} \left(\frac{\pi}{6} d_\ell^3 \, C_\ell \right) \qquad (4.4)$$

Differentiating Equation (4.4) for constant liquid molar density and combining with Equation (4 3) yields the following expression for the burning rate constant

$$K = \frac{2n}{\pi r_\ell C_\ell} \qquad (4.5)$$

where $\dot{n}$ is the molar burning rate corrected for convection effects with Equation (4.2).

The molar burning rate, derived for no flow, is a function of the droplet radius and the ratio of the droplet radius to flame radius As pointed out by Goldsmith and Penner (8), this radius ratio is a constant for fixed values of the physiochemical parameters and therefore the burning rate for no flow is a linear function of the

droplet radius during steady burning. Thus, in the absence of convective flow, the burning rate constant, K, is independent of the droplet radius and the square of the droplet diameter is a linear function of time as seen by an examination of Equations (4.3) and (4 5) When the convection correction is included, however, K becomes dependent on d_ℓ through the Reynolds number. However, for the present test conditions, the dependence is small for the Reynolds number range considered and the square of the droplet diameter remains approximately linear with time.

The measured burning rate constant was obtained from the experimental variation of diameter squared with time. A typical diameter squared plot is shown in Figure 9 The slope was measured at a fixed average diameter of 1100μ in order to eliminate variations due to the influence of convection. For the droplet sizes tested, this diameter was sufficiently removed from the heat up period to provide a good estimation of the steady burning rate.

The burning rate constants reported here are average values obtained from four separate tests Typically, the values from the individual tests were within 3% of the average.

4.2 Effect of Ambient Temperature

The first series of tests considered the influence of ambient temperature on high temperature droplet evaporation. For these tests, the ambient oxygen concentration was less than one percent, through dissociation. The ambient gas velocity was also maintained essentially

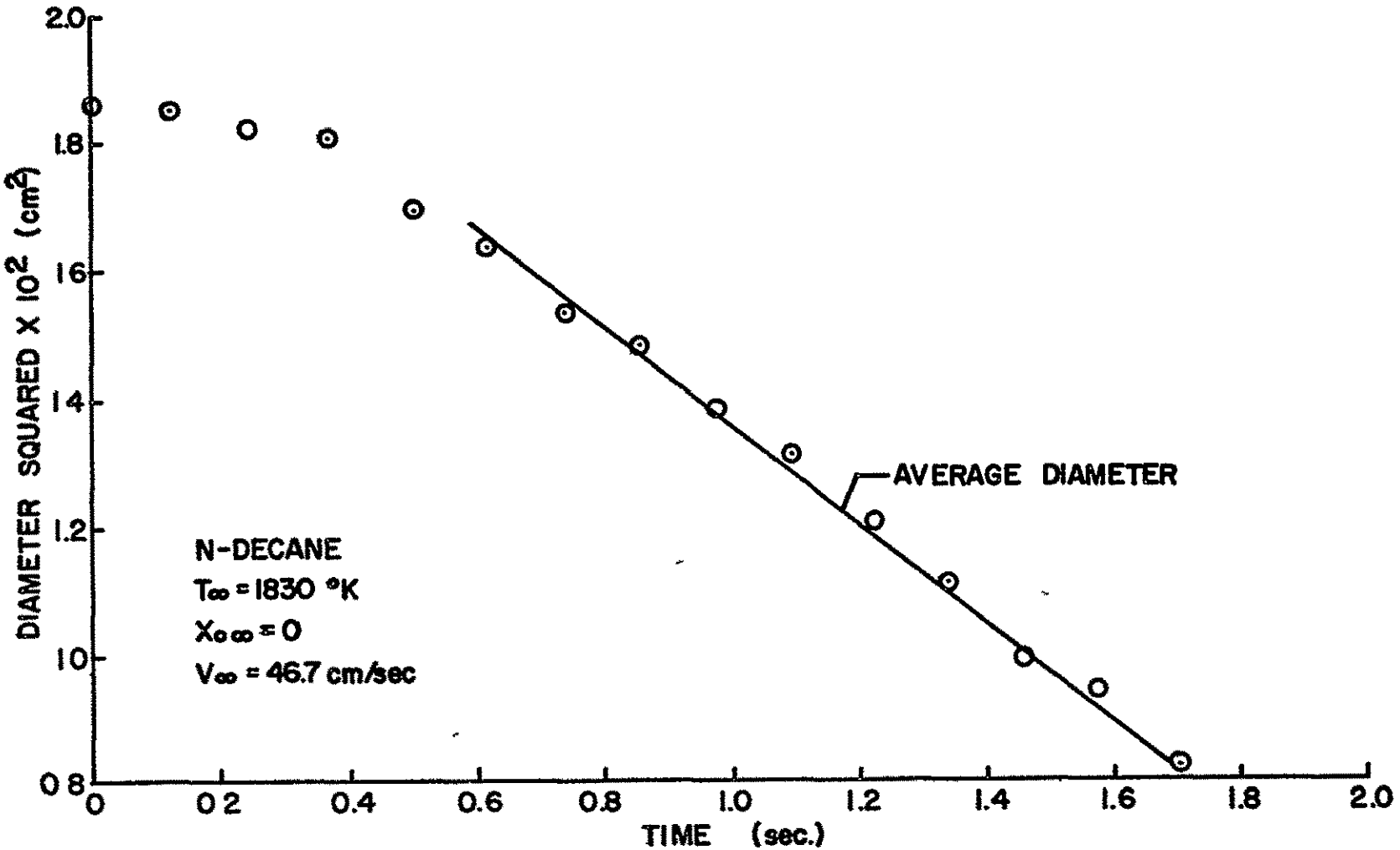

FIGURE 9 A TYPICAL DIAMETER SQUARED PLOT

constant at 46.7 cm/sec. The experimental results for methanol, n pentane and n decane are compared with the theoretical predictions in Figure 10.

The theory provides a reasonable prediction of the variation of the evaporation rate with ambient temperature The discrepancy between theory and experiment is greatest for n decane, reaching about 26% at the highest temperature tested

4.3 Effect of Ambient Oxygen Concentration

In the second series of tests, the ambient oxygen concentration was varied while the ambient temperature and velocity were maintained relatively constant at 2530°K and 62.5 cm/sec respectively

Two approaches were taken with regard to the chemical energy release in the reaction zone. In the first, dissociation was neglected and the standard heat of reaction was employed in the calculations. In the second approach, the heat of reaction was corrected for the effect of dissociation at the flame. This was accomplished by separately determining the chemical energy release, allowing for dissociation, for the combustion of a stoichiometric mixture of fuel and oxygen at various temperatures. The results were correlated with temperature by a least squares polynomial and employed in the theoretical solution to determine the correct flame temperature and chemical energy release by iteration.

The use of the standard heat of reaction resulted in absurdly high flame temperatures, confirming the observations of Goldsmith (9). Table 3 compares the flame temperatures computed by the two methods

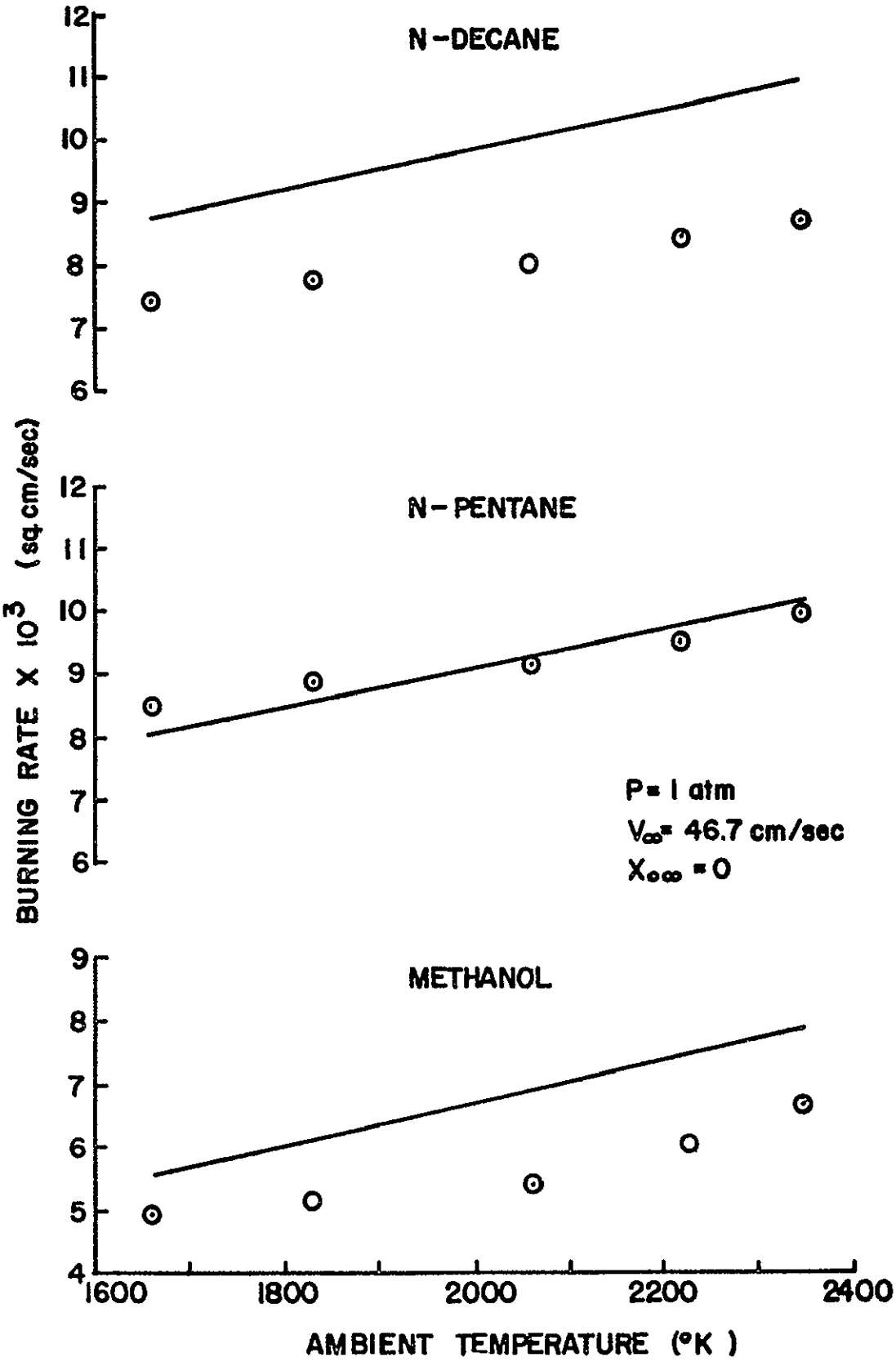

FIGURE 10 METHANOL, N PENTANE AND N DECANE EVAPORATION AT VARIOUS AMBIENT TEMPERATURES, $d_{\ell\ avg}$ = 1100μ

TABLE 3

COMPUTED FLAME TEMPERATURES DURING STEADY BURNING

FUEL	HEAT OF REACTION	FLAME TEMPERATURE (°K)		
		$X_{O\infty} = 0.050$	$X_{O\infty} = 0.254$	$X_{O\infty} = 0.415$
METHANOL	STANDARD	2920	4100	4700
	CORRECTED	2760	2950	3040
N PENTANE	STANDARD	2980	4560	5530
	CORRECTED	2820	3160	3210
N DECANE	STANDARD	2980	4550	5520
	CORRECTED	2820	3170	3220

for a variety of fuels and ambient oxygen mole fractions The flame temperatures obtained with the corrected heat of reaction were all on the order of 3000°K for the present test conditions

Computed burning rate constants for these two methods are compared with the experimental data in Figures 11, 12, and 13 for menthanol, n pentane and n decane respectively. The curves constructed with the corrected heat of reaction show better agreement with the variation in the burning rate with ambient oxygen concentration.

4 4 Effect of Molecular Weight

The results shown in the previous two sections indicate an apparently random shifting of the theoretical curves above and below the experimental results for the different fuel types This behavior was examined in a more systematic way by comparing the theory and measurements for a wider range of fuel types. Figure 14 shows this comparison for 1-alcohols ranging from methanol to decyl alcohol. Figure 15 shows a similar comparison for normal paraffin fuels ranging from n pentane to n hexadecane. These tests were conducted for three different ambient oxygen concentrations while maintaining a constant ambient gas temperature and velocity of 2530°K and 62.5 cm/sec respectively

The theoretical curves were computed with the corrected heat of reaction since this approach gave the best representation of the effect of varying oxygen concentration For both the alcohols and paraffins, the trend of the theory with respect to fuel molecular weight is not in good agreement with the experimental results The theory increasingly overestimates the burning rate of the heavier

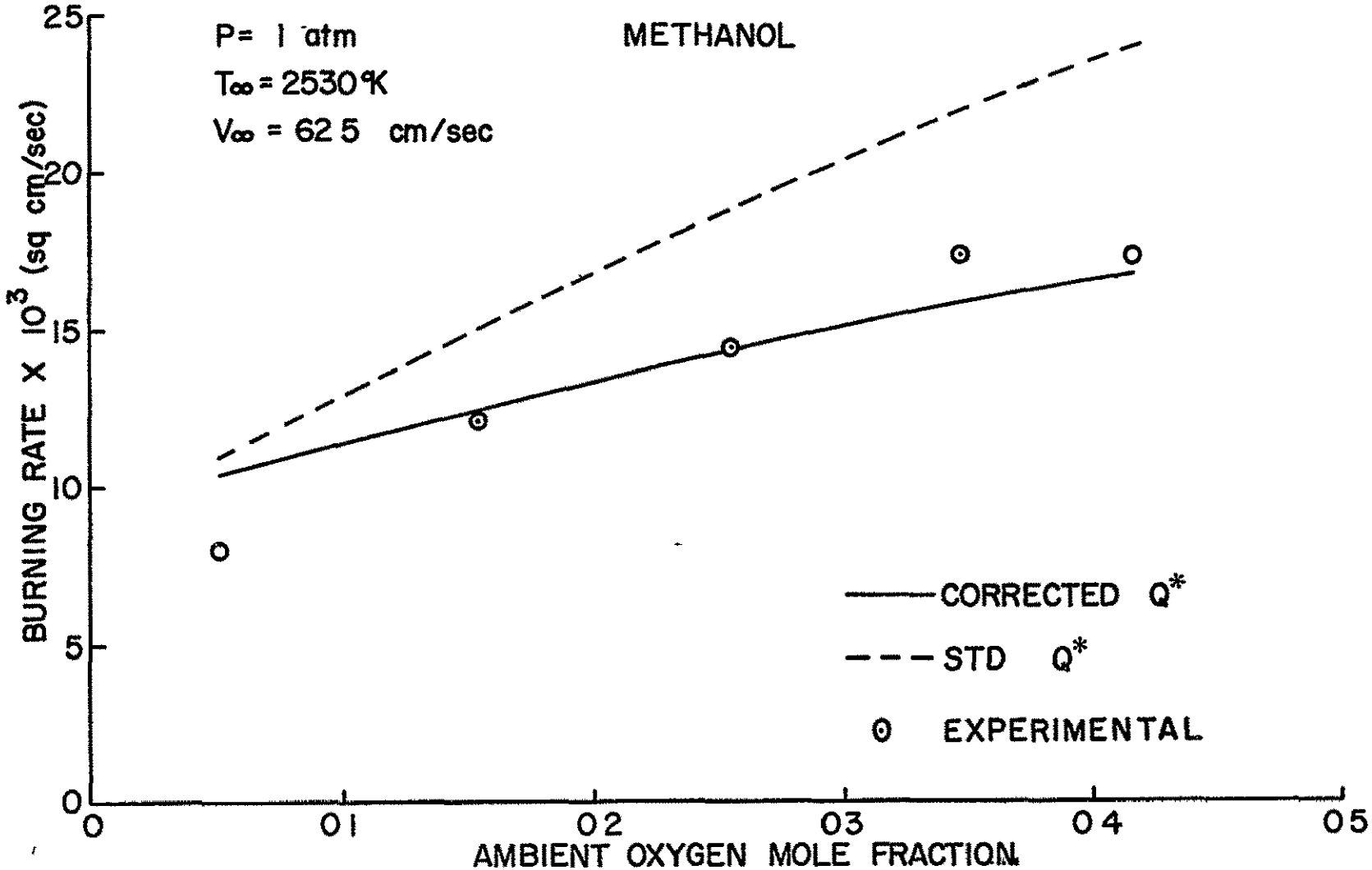

FIGURE 11 METHANOL BURNING RATES AT VARIOUS AMBIENT OXYGEN CONCENTRATIONS, $d_{\ell\ avg}$ = 1100μ

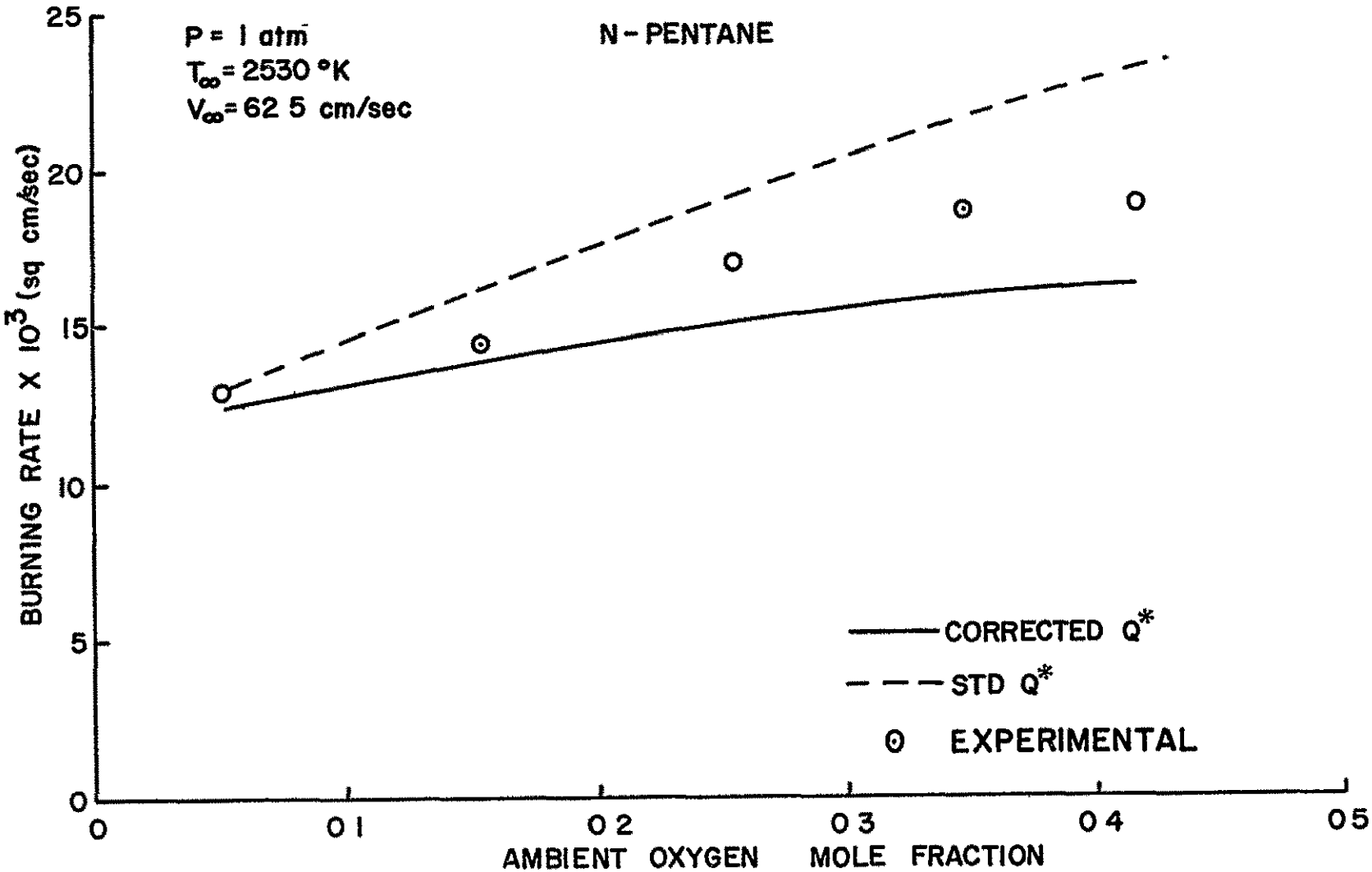

FIGURE 12 N PENTANE BURNING RATES AT VARIOUS AMBIENT OXYGEN CONCENTRATIONS, $d_{\ell\ avg}$ = 1100μ

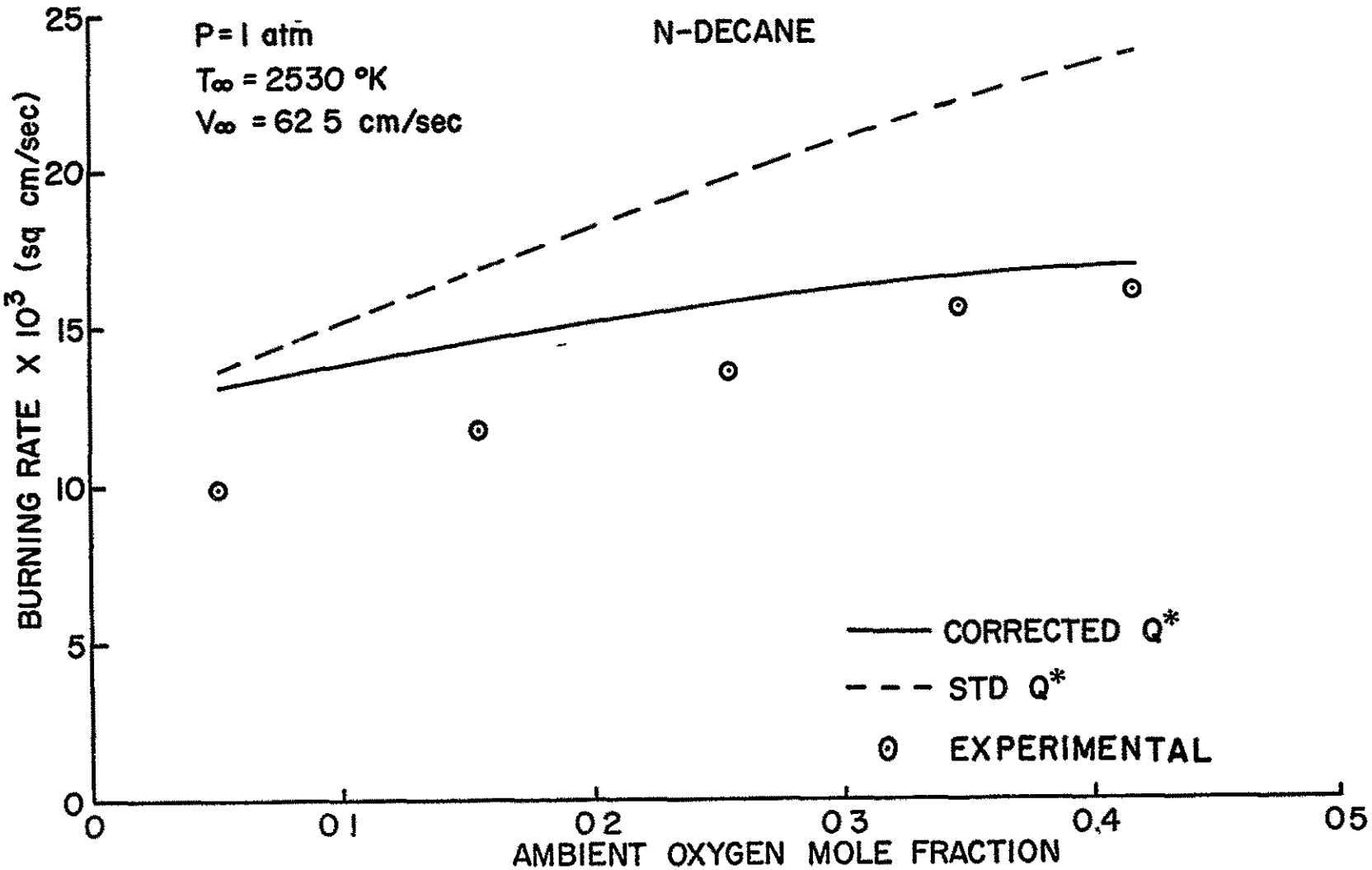

FIGURE 13 N DECANE BURNING RATES AT VARIOUS AMBIENT OXYGEN CONCENTRATIONS, $d_{\ell\ avg} = 1100\mu$

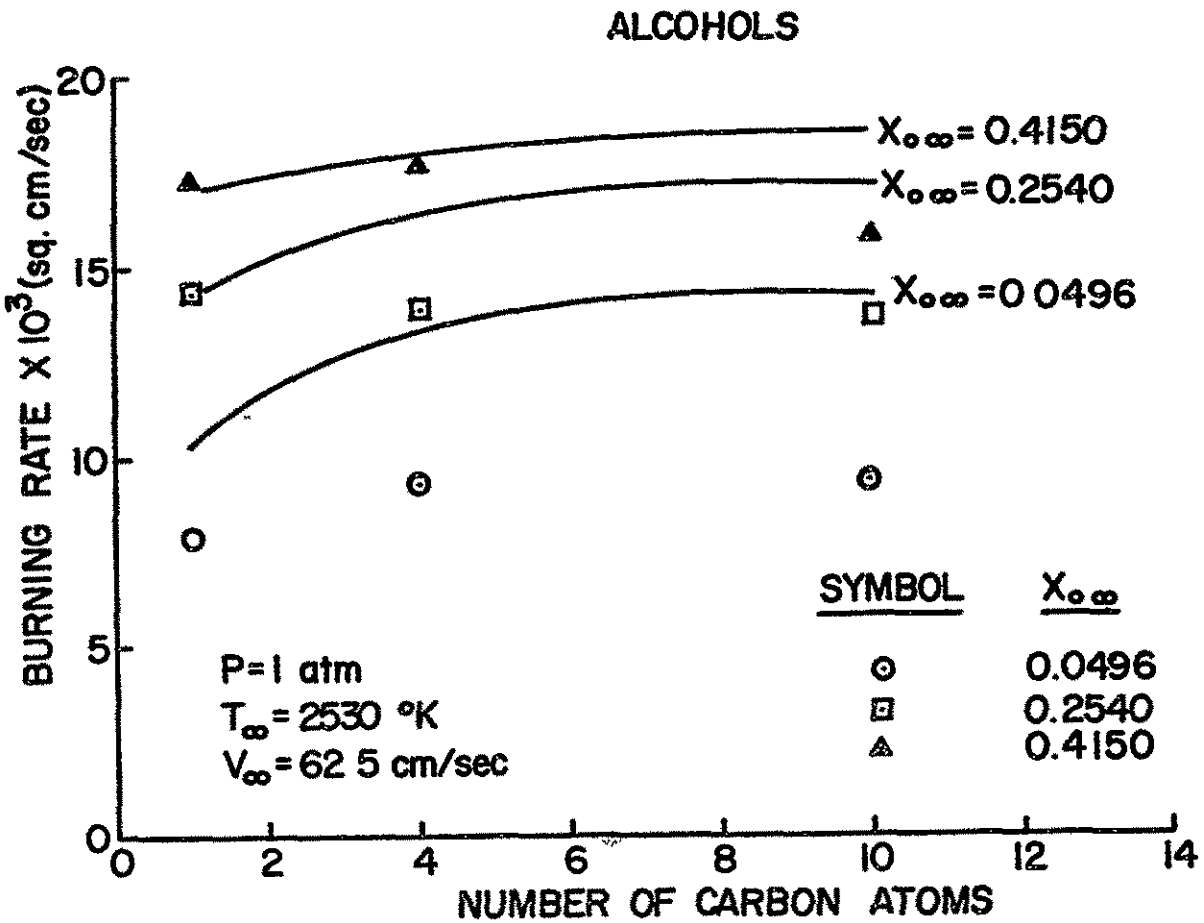

FIGURE 14 THEORETICAL AND EXPERIMENTAL BURNING RATES FOR VARIOUS ALCOHOLS, $d_{\ell\ avg}$ = 1100μ

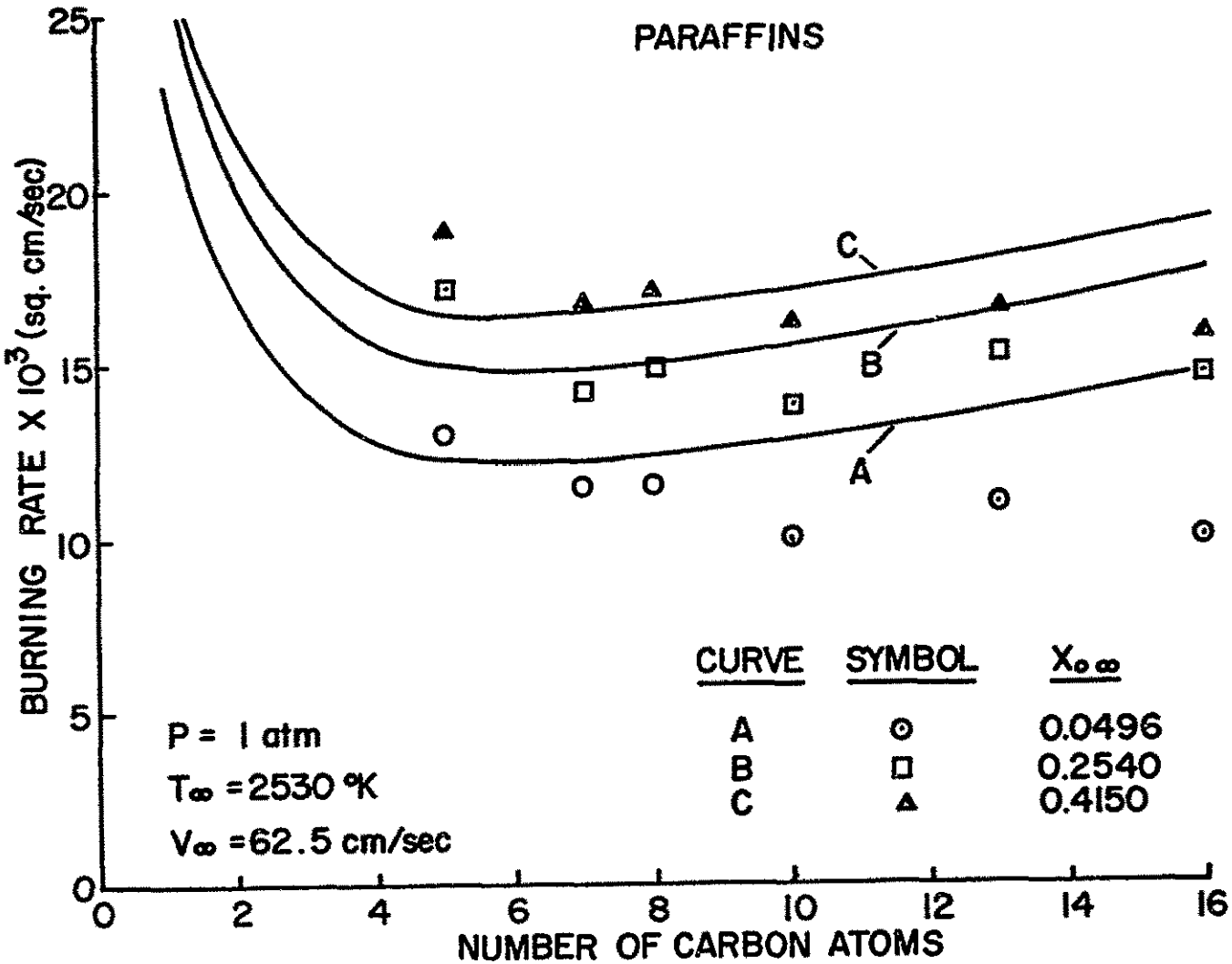

FIGURE 15 THEORETICAL AND EXPERIMENTAL BURNING RATES FOR VARIOUS PARAFFINS, $d_{\ell\ avg}$ = 1100μ

hydrocarbons with a maximum error of nearly 50% for n hexadecane at low ambient oxygen concentrations.

4.5 Discussion of Baseline Results

These experiments have provided a fairly stringent test of the Goldsmith and Penner (8) variable property model. When corrected for the effects of dissociation at the flame zone, the model provides a reasonable prediction of the trend of the burning rate with ambient temperature and ambient oxygen concentration However, the failure of the theory to give the correct trend of the burning rate with increasing fuel molecular weight raises questions which warrant further considerations

The trend of the present experimental data with increasing fuel molecular weight appears to be in general agreement with the findings of other investigators. Aldred and Williams (48) investigated the combustion of normal alkanes for a wide range of molecular weights in motionless air and oxygen at room temperature. Although the experimental conditions differ from the present test conditions, they also observed a reduction in burning rate with increasing fuel molecular weight. Hottel, et al. (5) also observed the same behavior during an investigation of the burning rate of heavier paraffins (n hexadecane and eicosane) in a furnace operating at temperatures on the order of 1000°C. Thus, the experimental trend of decreasing burning rate with increasing fuel molecular weight, for paraffins heavier than n pentane, appears to be quite firmly established and not simply a characteristic of the present experimental apparatus.

The evaluation of physical properties has a considerable influence on the predicted burning rate trend with molecular weight Sioui and Roblee (49) empirically fitted the data of several investigators to a constant property theoretical burning rate equation by adjusting the properties to give the correct trend Even in the present variable property solution, which has considerably less latitude for arbitrary property adjustment, the correct trend can be predicted by adjusting the liquid density and heat of vaporization. The burning rate increase with molecular weight in the present theory is primarily due to a reduction of these two properties at the higher steady burning liquid temperatures of the heavier hydrocarbons Evaluating these properties at 25°C for all fuels eliminates the increasing trend (e.g at $X_{o\infty} = 0.050$, the computed burning rate becomes 0122 and .0105 cm^2/sec for n pentane and n hexadecane as compared to the present values of 0123 and .0148 cm^2/sec). However, this is hardly more than empirical fitting since the use of the correct steady burning temperature is more realistic.

The method of property selection in the convection correction also effects the predicted influence of molecular weight on the burning rate. The use of approach conditions in the present calculations tends to minimize the discrepancy between theory and experiment. The use of mean film properties, as suggested by Eisenklam, et al. (20), would cause the predicted burning rate to increase even more rapidly with increasing fuel molecular weight

The relaxation of temperature gradients within the droplet provide a possible source of error since a uniform temperature was assumed during steady burning in the theory. The results of several investigators (17, 50, 51) indicate that temperatures near the center of the drop are still increasing during most of the so-called steady burning period The uniform temperature assumption neglects the sensible energy input to the droplet during this relaxation process and results in an overestimation of the energy available for vaporization of the droplet liquid. This leads to a corresponding overestimate of the burning rate Since the heat of vaporization of the hydrocarbon fuels at temperatures close to the boiling temperature decrease with increasing molecular weight, this effect becomes more significant for the heavier molecules

Faeth (17) computed droplet life histories and compared results allowing for temperature gradients within the drop with those obtained under the assumption of a uniform droplet temperature at each instant of time Although the study was conducted for monopropellants, the energy and mass fluxes at the droplet surface were similar to those of the present study The results show that the apparent steady burning rate is reduced when allowance is made for the continued relaxation of internal temperatures For materials having volatilities comparable to the heavier hydrocarbons, differences on the order of 5% were found for the two cases Therefore, although this effect probably influences the present results, it is not large enough to entirely explain the discrepancies

Decomposition of the fuel molecule could be a contributing factor which was neglected in the theory Griswold (52) points out that hydrocarbon decomposition reactions are approximately first order and the rates of these reactions increase rapidly with increasing temperature. For first order reactions, Benson (53) has shown that liquid and gas phase reaction rates are approximately the same at a given temperature and therefore, gas phase reaction rates given in Reference (52) may be employed to estimate the role of decomposition in both liquid and gas phases. In general, estimated reaction times for one percent decomposition in the liquid phase were found to be more than three orders of magnitude greater than the time available during a droplet lifetime. Therefore, for the present experiments, decomposition in the liquid phase was engligible

In contrast to liquid phase reactions, gas phase decomposition in the region between the droplet surface and the oxidation zone was found to be possible since higher temperatures are encountered. Due to the great complexities involved, details of hydrocarbon decomposition and carbon formation are not fully understood However, it is generally agreed that unsaturated hydrocarbons and radicals are initially formed by thermal cracking and dehydrogenation In the later stages, very large polymeric molecules are formed by radical recombination and with increasing molecular weight and continued dehydrogenation, approach the properties of carbon (54-55) Recent studies of sampled diffusion flames (56-57) have confirmed the presence of significant amounts of unsaturated hydrocarbons on the fuel side of the flame

The initial formation of unsaturated hydrocarbons involves endothermic steps which would alter the temperature distribution in the gas phase, tending to reduce the evaporation rate of the droplet. At a given temperature, decomposition rates are larger for the heavier hydrocarbons (52) and therefore, the occurrence of significant decomposition effects would explain the observed trend of the burning rate with molecular weight. However, in the absence of detailed mechanisms, the contribution of decomposition effects to the discrepancies observed in this study can only be conjectured.

The results of this baseline study indicate that the Goldsmith and Penner (8) model can be reasonably applied over a wide range of test conditions for the lighter hydrocarbons. The use of this model for heavy molecular weight fuels should be avoided until the failure with molecular weight is suitably resolved

CHAPTER V

ZERO GRAVITY APPARATUS

5 1 Test Facility

The high pressure experiments required an apparatus in which a suspended droplet could be ignited and burned in a high pressure air environment while providing a means of observing combustion and measuring the droplet temperature variation. It was also required that the experiments be conducted under zero gravity conditions in order to prevent the droplet falling from its support due to reduced surface tension near the critical point The zero gravity apparatus developed by Dominicis (18) was used for these experiments

A sketch of the overall test facility is shown in Figure 16 The experimental apparatus was enclosed in a chamber which could be dropped through a free fall distance of 16 feet This distance provided a test time of approximately one second under zero gravity conditions. The chamber dropped into a tub filled with Resilite, a foam plastic, which absorbed the shock of the fall The chamber was held in place prior to testing by a sliding pin mechanism. The pin was removed by a solenoid actuated penumatic cylinder to begin the free fall period

The free fall chamber, shown in Figure 17, consisted of an aluminum shell with two doors along its length in order to gain access to the internal components. The chamber housed the high pressure droplet chamber, high speed camera, background light and associated instrumentation.

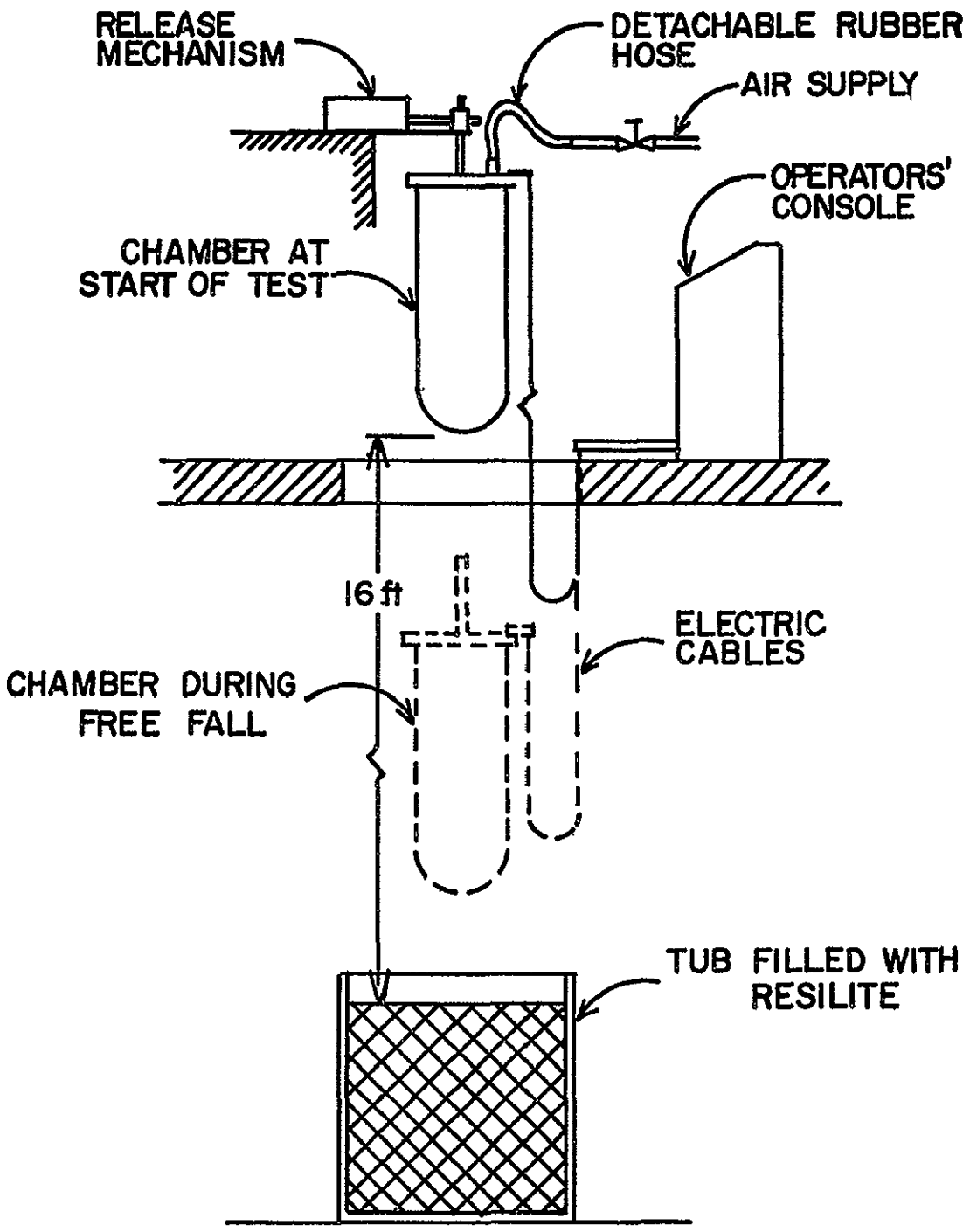

FIGURE 16 SKETCH OF THE ZERO GRAVITY TEST FACILITY

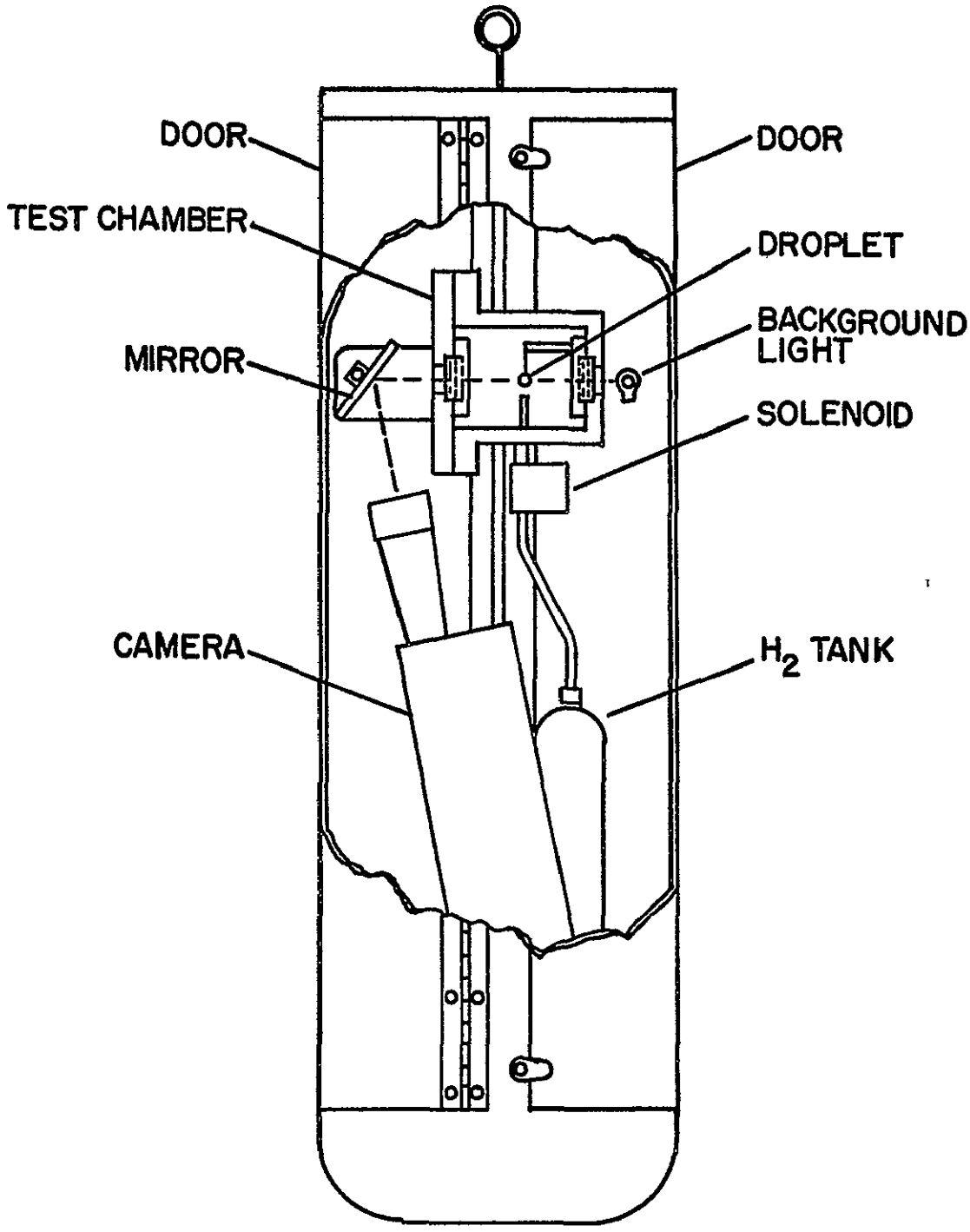

FIGURE 17 SKETCH OF THE FREE FALL CHAMBER

The high pressure (up to 2000 psia) droplet reaction chamber is shown schematically in Figure 18. The stainless steel chamber was cylindrical in shape and had an internal volume of approximately 26 cubic inches. The interior of the chamber was accessible through a removable end plate provided with an "O" ring seal A small quartz window was built into the end plate to permit photographing of the combustion process. A second quartz window was built into the closed end of the chamber to allow for background lighting

The droplet was suspended on the junction of a chromel-alumel thermocouple Following a procedure first used by Hall (50), the thermocouple wires were protected with small quartz tubes in order to reduce heat transfer along the wires from the flame surrounding the droplet The tubes were adjusted to extend through the flame zone without touching the droplet surface. Thermocouple wires of various sizes were used in the experiments in order to illustrate the relative errors resulting from conduction along the wires The bulk of the tests were conducted with .002 inch O.D. wires since this size was the smallest that could be used reliably throughout the test range A few tests were conducted with 001 and .003 inch O.D. wires also, although testing with the smaller size was problematical. It was difficult to construct .001 inch O D. thermocouples which had a bead large enough to support a droplet. In addition, this size rarely could survive through a complete droplet lifetime and many attempts were required before a reasonably reliable test could be obtained

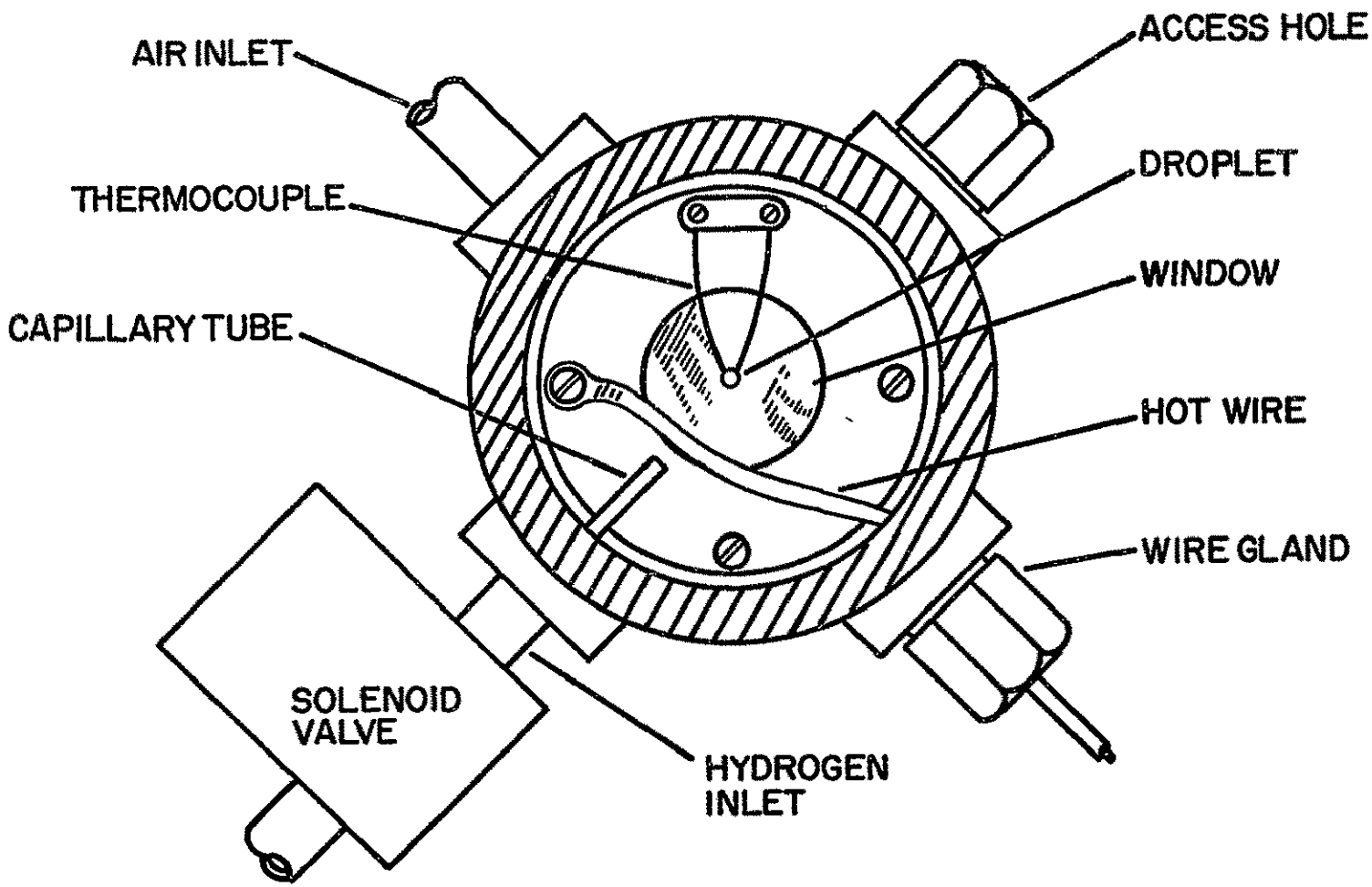

FIGURE 18 SKETCH OF THE DROPLET CHAMBER

The signal from the thermocouple was fed through a D.C. amplifier to a recording oscillograph employing a fluid damped galvanometer. The galvanometer had a flat, 5 percent frequency response to 2200 cps. An internal flash timing unit provided for time sequencing of the temperature chart record

A high speed motion picture camera, mounted in the apparatus as shown in Figure 17, was employed to photograph the combustion process The camera was operated at speeds of approximately 150 pictures per second An internal light, powered by a 100 cps pulse generator, provided a time correlation of the film. Synchronization of the photograph and temperature records was accomplished with a second internal camera light by feeding the signal to a second galvanometer in the recording oscillograph. The light, which was initially on, was turned off during the test providing a simultaneous indication on both the camera film and the temperature record.

A stroboscopic light source which was actuated by a photoelectric pickup was employed as a background light. The pickup was sensitized by small strips of reflecting tape attached to the camera drive. An adjustable electronic delay in the pickup circuit provided a method of synchronizing the light with the rotating camera prism. The flashing of the background light was set to give alternate shadowgraphs and dark field photographs of the droplet. However, in the experiments, accurate measurements of droplet diameters could not be made from the shadowgraphs at high pressures due to combustion luminosity and refractive effects

Three different methods for igniting the droplet were employed in the experiments. These were a spark igniter, a flame igniter and a hot wire igniter. The spark igniter system, consisting of an oil burner ignition transformer and electrodes, provided a satisfactory method of igniting the droplet at atmospheric pressure. However, attempts to test at higher pressures were unsuccessful The impedance of the gap between the electrodes at higher pressures was greater than that at other points in the electrical circuit and arcing at these points resulted. Physical constraints on the apparatus prevented adequate insulation to eliminate this problem

The flame igniter is illustrated in Figure 18. Hydrogen was introduced into the droplet chamber through a capillary tube and directed toward the droplet. An electrically heated wire ignited the entering hydrogen, which in turn ignited the droplet. The hydrogen diffusion flame was extinguished as soon as possible after the droplet ignited, since the presence of gas flow caused a disturbance to the droplet, especially at high pressures.

The hydrogen was stored in a small cylinder mounted inside the free fall apparatus as illustrated in Figure 17. The cylinder was of sufficient capacity to maintain a uniform flow when the pressure was kept slightly higher than that of the droplet chamber. The hydrogen flow was controlled by a solenoid valve which was automatically actuated during a test.

The flame igniter did not operate well at pressures above 100 psia. The hydrogen solenoid became difficult to control and the hydrogen flow caused excessive disturbances to the droplet

The hot wire igniter, which provided a satisfactory method of ignition at pressures above 100 psia, consisted of an electrically heated wire located close to the droplet. At the beginning of the free fall period, electrical power was momentarily supplied to the wire, causing it to heat up and ignite the droplet.

The high pressure gases required for the hydrogen igniter and droplet chamber were supplied from commercially pure gas cylinders

Two timing devices were used to automatically control the operation of the apparatus A falling weight switch was used for functions which required accurate time sequencing, such as the release of the free fall chamber and operation of the igniter The falling weight was held in its uppermost position by an electromagnet which could be released automatically. A cycling timer was used to control less critical functions such as the camera, electromagnet and temperature recorder

5.2 Operation of the Apparatus

The preliminary steps in the operation of the apparatus involved focussing the camera, pressurizing the air supply to the release mechanism and calibration of the thermocouple output with a millivolt potentiometer The thermocouple-amplifier-galvanometer circuit was also checked ossacionally with a boiling water bath as a reference. In tests with the hydrogen igniter, the hydrogen storage tank was charged at this time The droplet was then mounted on the thermocouple junction and the droplet chamber was closed and pressurized. For environments other than air, the chamber was

first evacuated with a vacuum pump and then pressurized with the desired gas environment The gas lines were removed by means of quick-disconnect fittings at the top of the free fall chamber. The falling weight switch, cycling timer and panel switches were then set to their proper positions, completing the preliminary operations.

The actual test was conducted automatically upon actuation of the cycling timer. The sequence of events in the test was as follows·

1. Camera and recording oscillograph on
2 Electromagnet de-energized-weight falls
3. Weight trips release solenoid switch and free fall of chamber begins
4 Weight trips switch to activate igniter.
5 Internal camera light turned off providing simultaneous indication on temperature trace and camera film
6. Droplet ignites.
7. Weight trips switch to deactivate igniter
8. All components off at the end of the free fall period.

The data consisted of the motion picture film and the oscillograph record of the droplet temperature The films were analyzed in the same manner discussed in Chapter III.

CHAPTER VI

THEORETICAL AND EXPERIMENTAL RESULTS

6.1 Low Pressure Burning Rates

Experimental measurements of steady droplet burning rates were obtained from the zero gravity apparatus described in the preceding chapter for n octane and n decane droplets These measurements were restricted to low pressures since combustion luminosity and refractive effects at high pressures prevented the measurement of droplet diameters The test droplets were suspended from a quartz filament and ignited at atmospheric pressure under zero gravity conditions Most of the burning rate tests employed the spark igniter system although a few experiments were also conducted with the flame igniter system. The ambient oxygen concentration was varied from 20 to 100% by volume The measured burning rates were compared with values predicted by the Goldsmith and Penner (8) theory using the low pressure phase equilibrium approximations Corrections to the theory for convection effects were not necessary in this case due to the absence of gravitational effects and forced flow in the zero gravity apparatus.

The burning rate constant, defined by Equation (4.3), was used to represent the data. The measured burning rate constant was obtained from the experimental variation of diameter squared with time in the same manner as that discussed in Chapter IV. The burning rate constants reported here are average values obtained from

five or more separate tests The values from the individual tests were within 5% of the average.

The results of the burning rate tests obtained in the zero gravity apparatus are shown in Figure 19 for n octane and n decane For n decane, the experimental burning rates obtained when the hydrogen flame igniter was used were consistently higher than the values obtained when the spark igniter was employed This behavior was attributed to convection effects induced by the hydrogen jet since the photographs revealed a slight distortion of the flame zone in the direction of the hydrogen flow

The experimental results are compared with the low pressure theory for the two methods of computing the heat of reaction, which were discussed in Chapter IV The two methods illustrate the increased influence of dissociation effects at the higher oxygen concentrations due to the higher flame temperature The agreement between the measured and computed results at low ambient oxygen concentrations is comparable to that obtained in the baseline study on the flat flame burner apparatus. The agreement improves considerably at the higher oxygen concentrations for the theory employing the corrected heat of reaction. The theory employing the standard heat of reaction overestimated the measured burning rate by roughly a factor of two over the entire range of ambient oxygen concentrations. The results also indicate the molecular weight effect found in the baseline study with the heavier fuel, n decane, showing the largest errors.

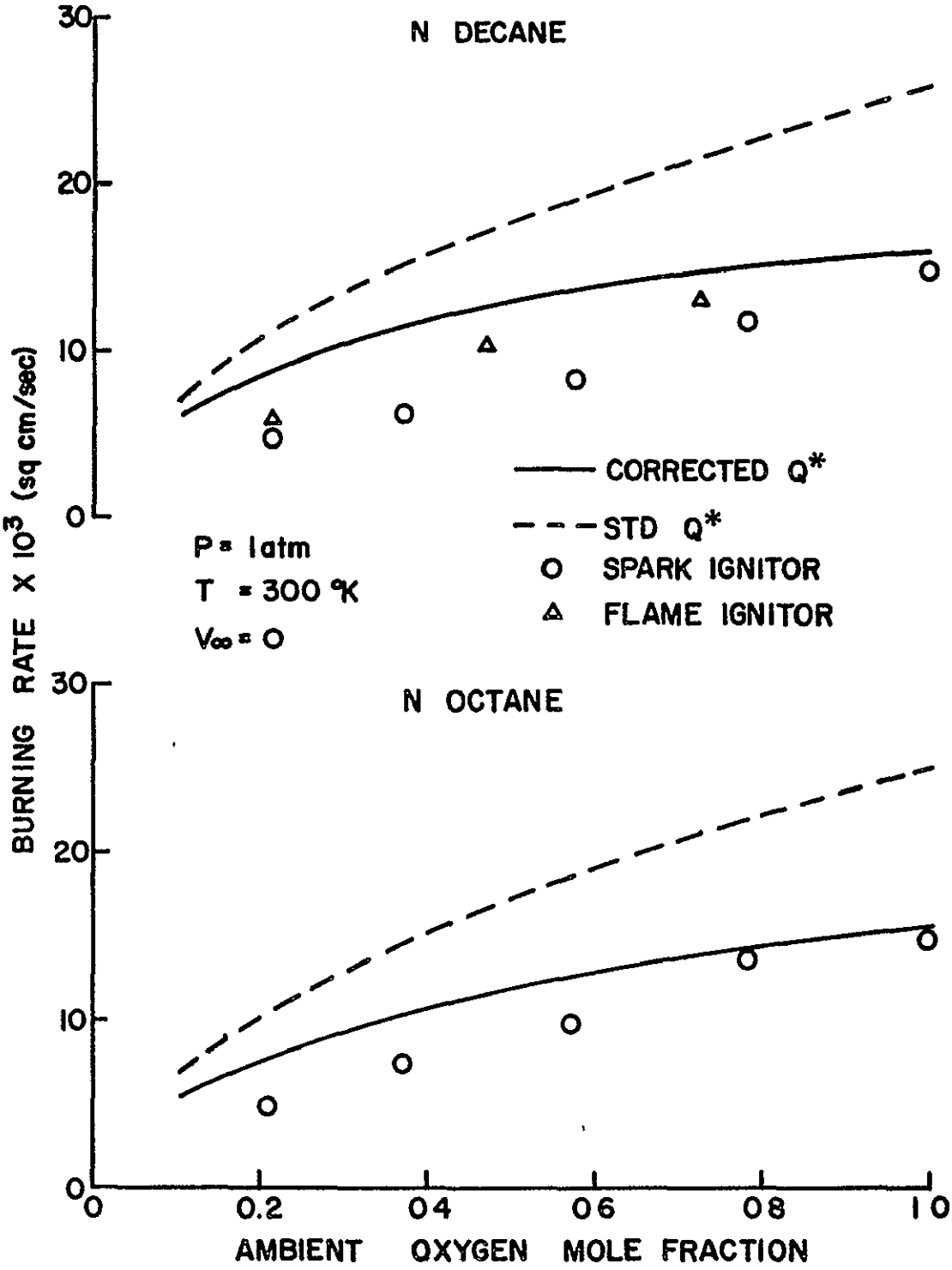

FIGURE 19 N OCTANE AND N DECANE BURNING RATES AT VARIOUS AMBIENT OXYGEN CONCENTRATIONS UNDER ZERO GRAVITY CONDITIONS, $d_{\ell\ avg} = 1100\mu$

6 2 Temperature Measurements

The principle measurement in the high pressure experiments was the droplet steady burning temperature. For these measurements, the droplets were suspended from a thermocouple junction, ignited with the hot wire igniter, and the temperature variation during combustion was recorded on an oscillograph

A typical temperature record is shown in Figure 20 for an n decane droplet burning in air at a pressure of one atmosphere The origin of the time axis is arbitrary and was taken as the time when the hot wire began glowing The series of peaks at the beginning of the trace were due to the noise signal sent to the thermocouple when power was first supplied to the hot wire

Following ignition, the droplet temperature increases during the heat up period until the steady burning period is reached The temperature remains relatively constant during the steady burning period until the droplet has completely gasified and then begins rising again until combustion is completed

Figure 21 shows temperature traces at various pressures for n octane droplets burning in air The time of ignition was taken to be the origin of time. The liquid temperature at the time of ignition, the steady burning temperature and the rate of liquid temperature rise during the heat up period increased with increasing ambient pressure Also, a progressively shorter period of time was spent at the steady burning condition as the pressure increased The temperature trace for a pressure of 40 8 atm shows an approach to the steady burning state as indicated by the small inflection of

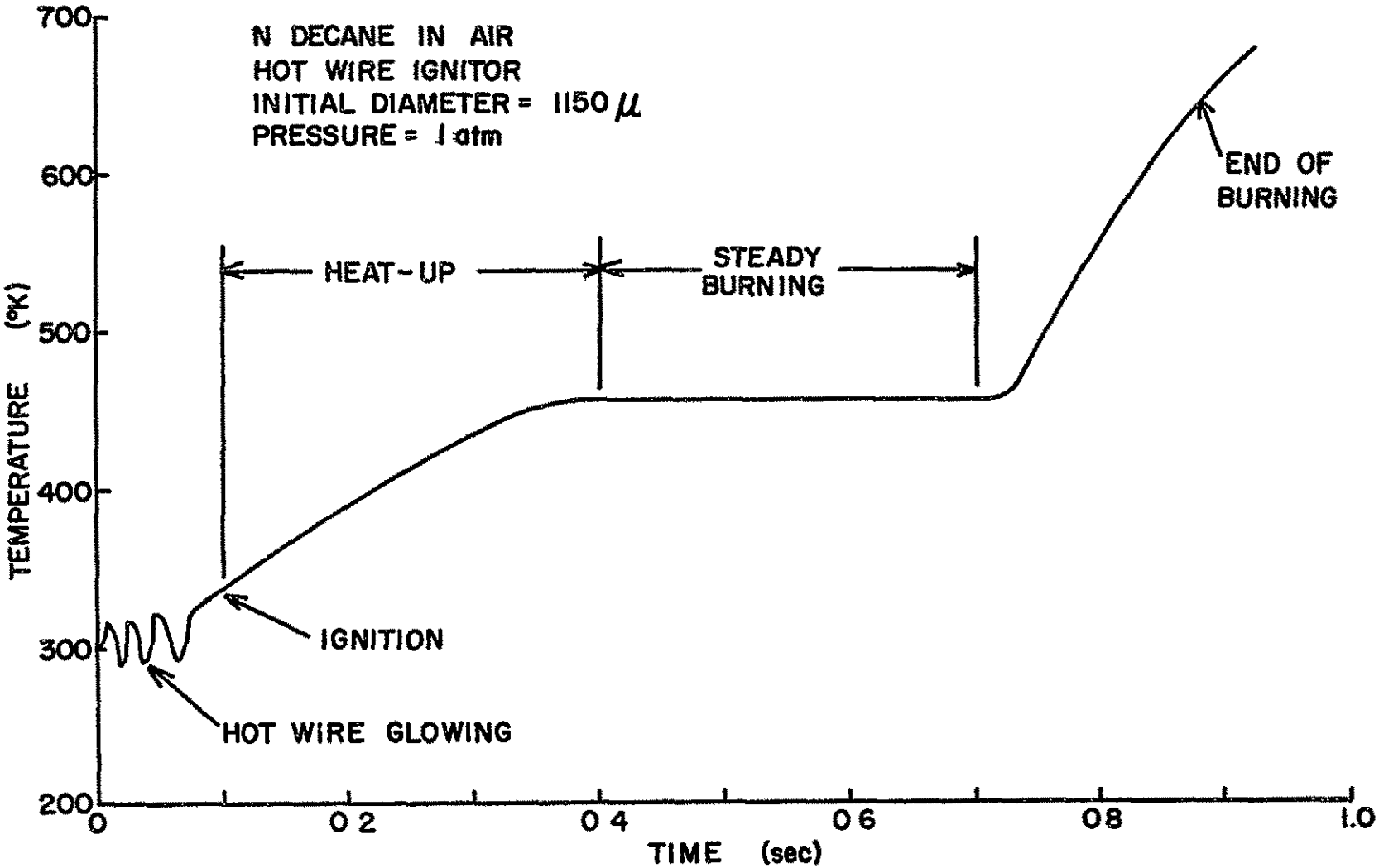

FIGURE 20 TYPICAL DROPLET TEMPERATURE RECORD

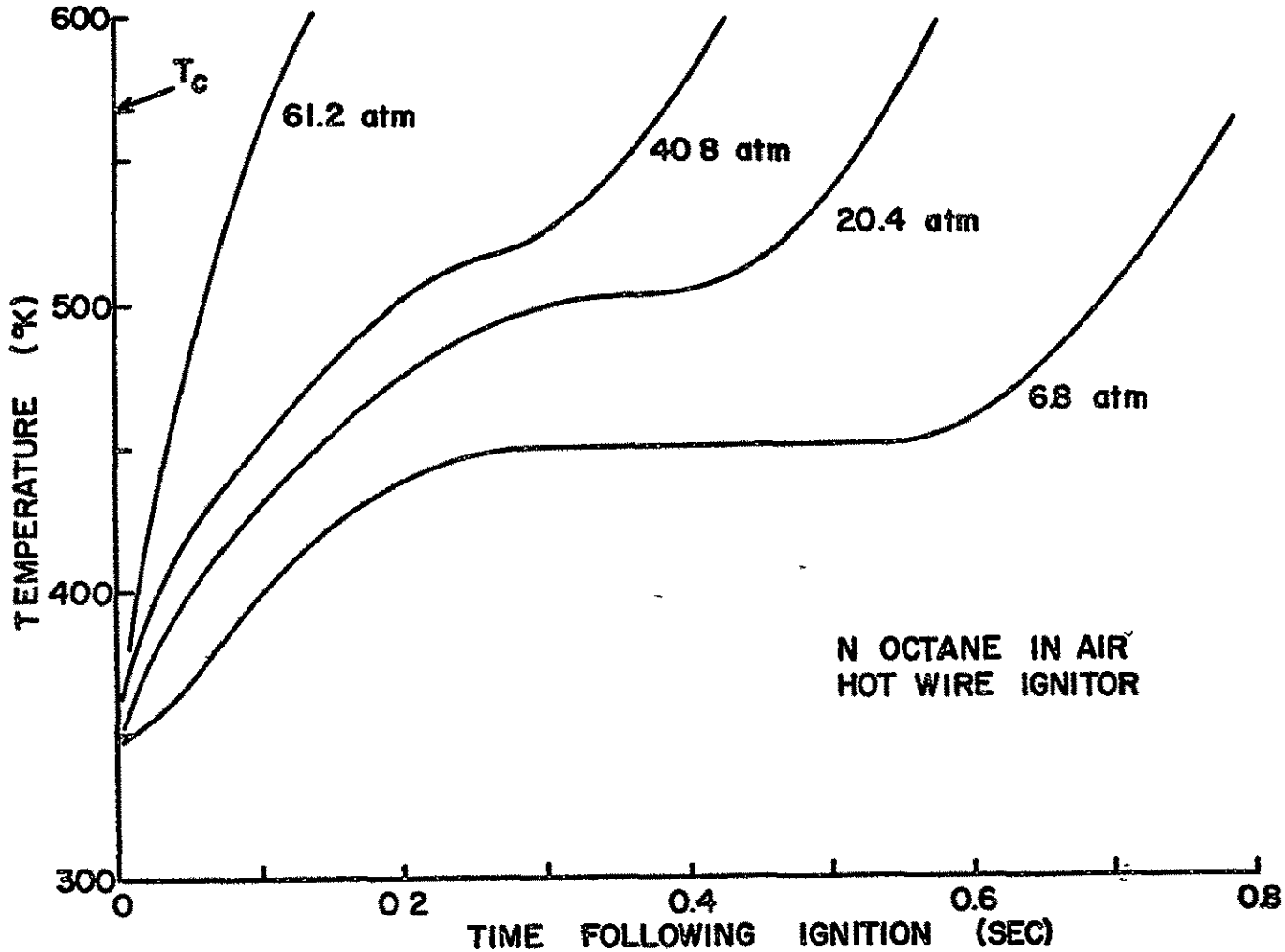

FIGURE 21 DROPLET TEMPERATURE MEASUREMENTS AT VARIOUS PRESSURES

the temperature trace. At sufficiently high pressures, as shown at 61.2 atm , the droplet temperature rises continuously with no tendency to level out The onset of this condition was taken to be the upper pressure limit for steady droplet burning (or the onset of supercritical burning)

6 3 High Pressure Results

Steady burning temperatures for n octane and n decane droplets burning in air were obtained on the zero gravity apparatus Tests were conducted at ambient pressures ranging from one atmosphere to the upper limit for steady droplet burning. The experimental results were compared with both the low pressure and high pressure theories presented in Chapter II

The solution for $B_1 = 0$ in the outer region was used in the calculations since this quantity was small for the species considered, as shown in the physical property tables of Appendix D. Computational efforts were reduced further by taking the flame temperature to be 3000°K for the bulk of the calculations. This assumption eliminates the necessity of solving Equation (2.51) for the flame cemperature simultaneously with Equations (2 28) to (2.35) for steady burning temperatures In practice, it was found that the results were not strongly influenced by this assumption.

The measured steady burning temperatures for the combustion of n decane and n octane droplets in air are shown in Figures 22 and 23 respectively The data shown represent averages of two or more separate tests Typically, the values from the individual tests

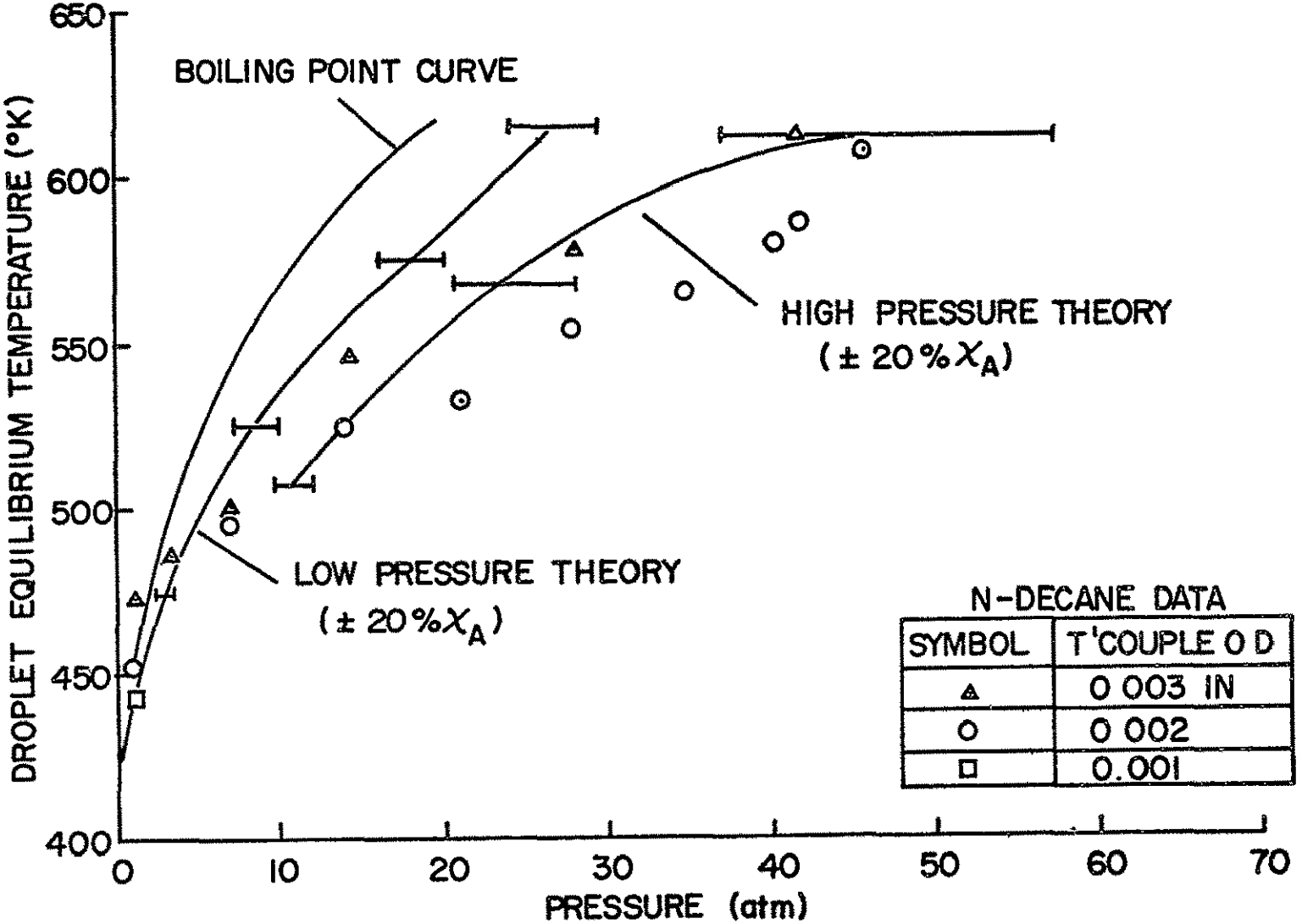

FIGURE 22 THEORETICAL AND EXPERIMENTAL STEADY BURNING TEMPERATURES FOR N DECANE DROPLETS BURNING IN AIR UNDER ZERO GRAVITY CONDITIONS

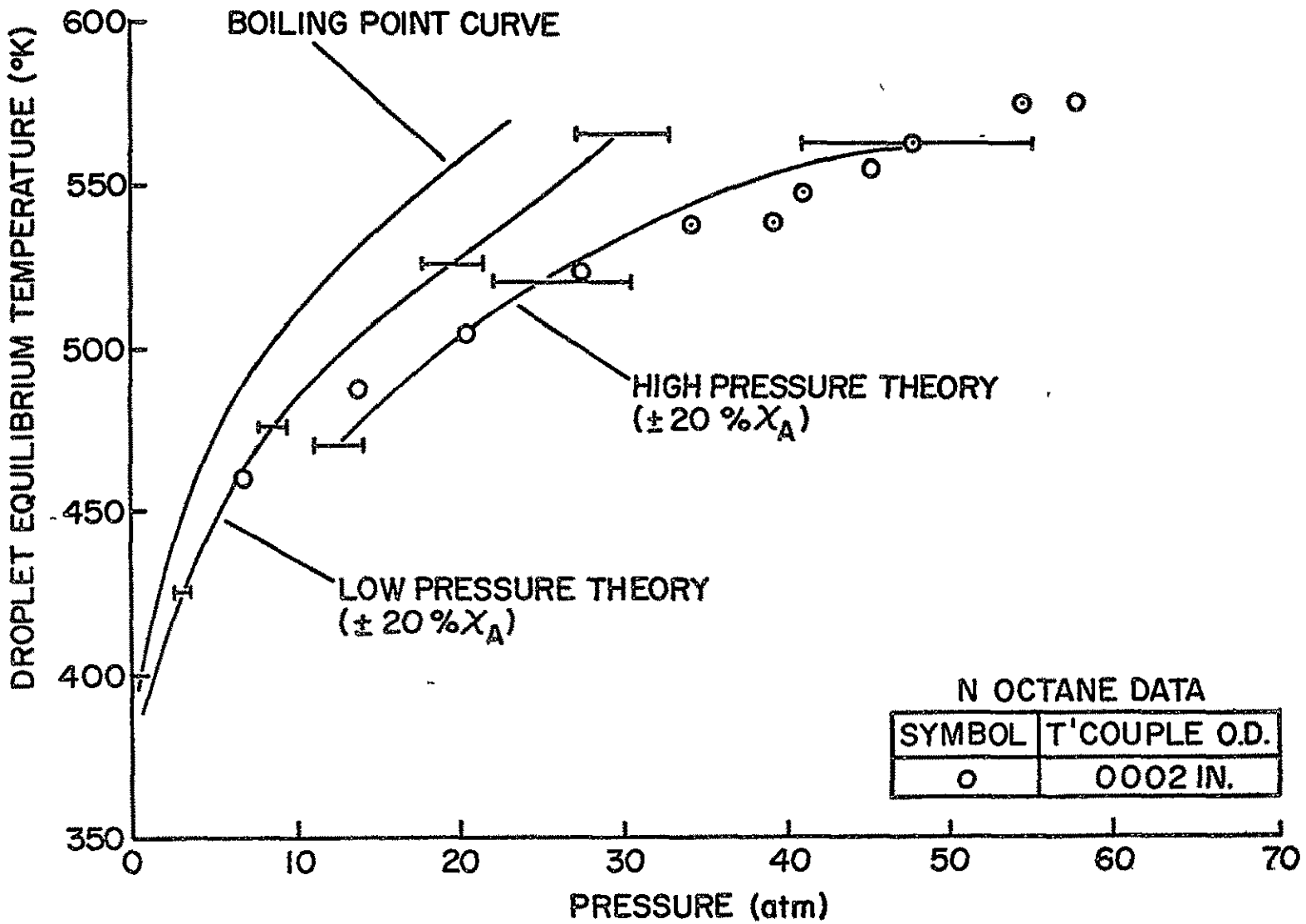

FIGURE 23 THEORETICAL AND EXPERIMENTAL STEADY BURNING TEMPERATURES FOR N OCTANE DROPLETS BURNING IN AIR UNDER ZERO GRAVITY CONDITIONS

were within 6% of the average. Data are shown for .003, .002 and .001 inch O.D. thermocouple wires for n decane (Figure 22) in order to illustrate conduction errors for the thermocouples The bulk of the measurements were made with .002 inch wires since this size was the smallest which could be used reliably over the entire pressure range, as discussed in Chapter V. However, the measurements made at atmospheric pressure with the three different wire sizes indicated that the conduction errors for the .002 inch wires were small relative to the measurements with the .001 inch wires The data is terminated at the highest pressure where a steady burning temperature was observed The onset of supercritical combustion was determined within the pressure ranges listed in Table 4.

The theoretical predictions of steady droplet burning temperatures, as well as the boiling temperatures of the pure fuels are also shown on Figures 22 and 23 The theoretical curves are terminated where steady burning solutions no longer exist Along with the low pressure theory, two versions of the high pressure theory were considered. Since the concentration of nitrogen at the droplet surface is much greater than either carbon dioxide or water, for combustion in air, the simplest high pressure model assumed that the combustion products were equivalent to nitrogen. Under this assumption, only the binary system, fuel-nitrogen, must be considered in the phase equilibria calculations The second high pressure model considered the complete quarternary system, fuel-nitrogen-carbon dioxide-water at the droplet surface.

TABLE 4

MEASURED AND PREDICTED PRESSURES REQUIRED FOR SUPERCRITICAL COMBUSTION IN AIR

FUEL	N PENTANE	N OCTANE	N DECANE
MEASURED CRITICAL BURNING PRESSURE, ATMOSPHERES	---------	58- 61	44- 47
MEASURED CRITICAL P_r	---------	2.35-2.49	2.13-2.30
PREDICTED CRITICAL P_r LOW PRESSURE THEORY	1.08-1 26	1.18-1 43	1.23-1.50
PREDICTED CRITICAL P_r *HIGH PRESSURE THEORY	1.20-1 70	1.65-2 25	1.75-2.75

*Results for complete quarternary system and combustion products taken equivalent to nitrogen essentially the same

The two high pressure theories gave essentially identical results and are in reasonable agreement with the data, both with respect to steady burning temperatures and the pressures required for the onset of supercritical combustion. This suggests that the approximations made with respect to water in the phase equilibria calculations may not exert a large influence on the results due to the predominance of nitrogen in the system for combustion in air.

The low pressure theory underestimates the pressure required for supercritical combustion by roughly a factor of two This is in contrast to Wieber's (13) earlier low pressure calculations for n heptane, which yielded reduced pressures for supercritical burning in the same range as the present measurements. This agreement appears to be fortuitous, however, due to an anomalously low value of the fuel thermal conductivity, when compared with reported values (58), employed in the calculations of Reference (13)

The sensitivity of the calculated results to errors in properties was examined by parametrically varying χ_A($\pm$20%), T_f (2000 to 4000°K) and the k_{ij}($\pm$20%). Variation of the latter two parameters caused only slight changes in the results The influence of χ_A variations was much larger and the limiting curves shown on Figures 22 and 23 (as well as the ranges for the predicted critical pressure ratio for supercritical burning shown in Table 4) are due to the variation of this parameter.

The χ_A parameter is proportional to the Lewis number in Region A. Since this parameter is frequently assumed to have a constant value of unity, in low pressure droplet combustion models (10, 39, 48),

its influence was examined further. For simplicity, the constant property, droplet combustion model presented in Appendix B was employed. Calculations of steady equilibrium temperatures as a function of pressure were examined for evaporating n heptane droplets for various values of the Lewis number. The results are presented in Figure 24. The influence of the Lewis number on the equilibrium temperatures, as well as on the pressures required for supercritical burning, increases greatly as the Lewis number is decreased. The pressures required for supercritical burning approach the critical pressure of the pure fuel as the Lewis number approaches unity This behavior explains the agreement of Wieber's (13) calculations with the present data, since the low fuel thermal conductivity employed by Wieber resulted in a Lewis number of approximately 0.25.

Calculated critical burning pressures for n pentane are also given in Table 4. Comparison of the results for the three fuels indicates that the pressure required for supercritical burning approaches the critical pressure of the fuel as the molecular weight of the paraffin decreases. This behavior is also a consequence of the influence of the Lewis number. On the basis of the physical properties tabulated in Appendix D, the Lewis number, computed at a given temperature, increases with the decreasing molecular weight for the paraffins. Therefore, from the trend established by Figure 24, the larger Lewis numbers for the lighter paraffins result in a lower critical burning pressure.

The influence of thermal radiation on the computed results for n decane are examined in Appendix E. The results indicate that

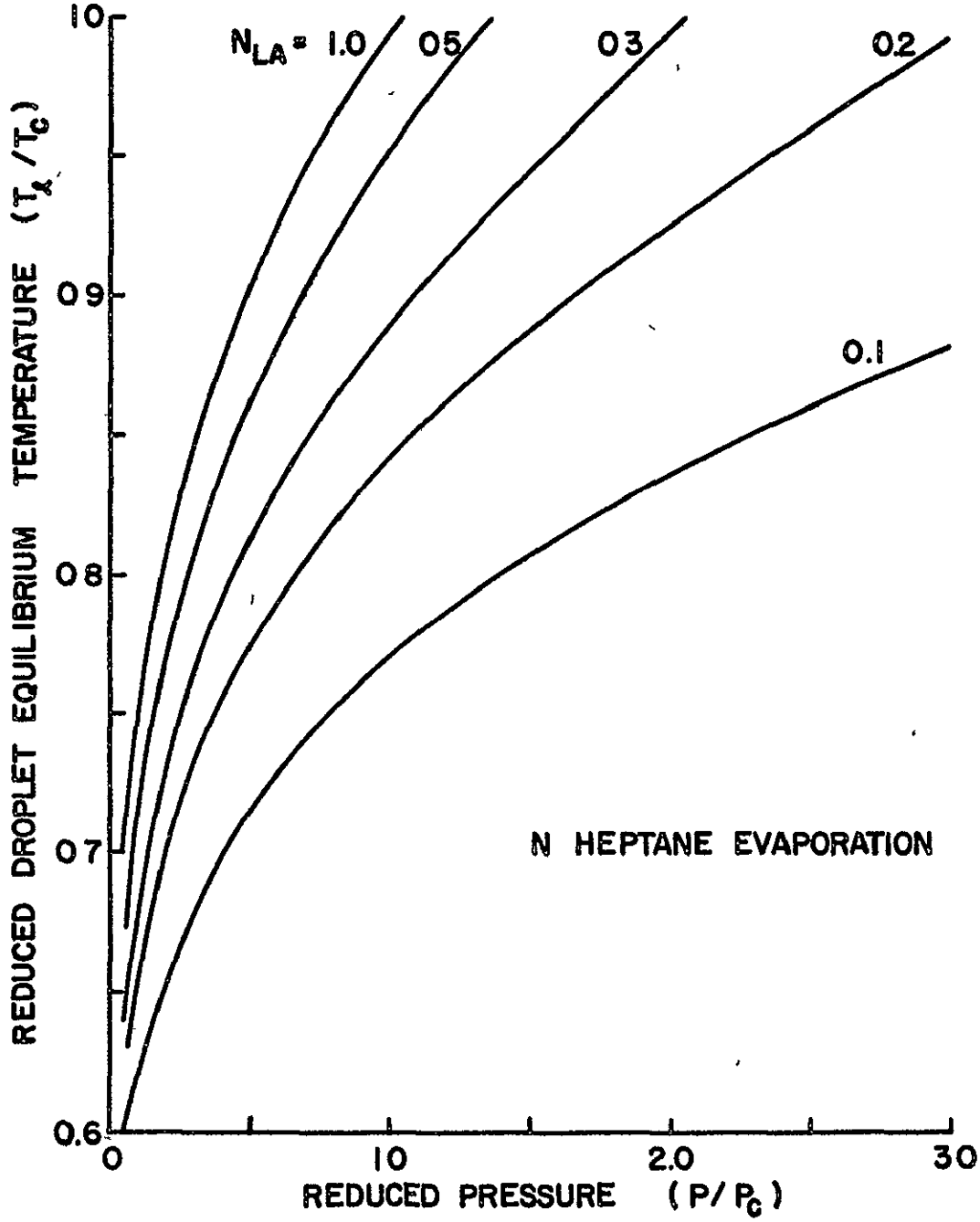

FIGURE 24 EFFECT OF THE LEWIS NUMBER ON COMPUTED STEADY BURNING TEMPERATURES FOR EVAPORATING N HEPTANE DROPLETS, T_∞ = 2780°K

steady burning temperatures are not very sensitive to radiation effects. Even when 75% of the total heat transferred to the droplet is due to radiation, increases in the steady burning temperatures were less than 3%. For the same conditions, increases in the droplet surface fuel mole fraction were on the order of 15% Since these variations are on the order of those due to errors in the physical properties, the neglect of thermal radiation in the analysis appears justified for the conditions of the present study.

6.4 Discussion

The general characteristics of droplet combustion in the vicinity of the critical point are best illustrated with plots of droplet surface mole fraction as a function of liquid temperature. Figure 25 shows this plot for the combustion of n pentane, with droplet phase equilibria based on the low pressure theory.

With the heat of vaporization given as a function of liquid temperature from the low pressure theory, Equations (2.28) to (2 30) yield the locus of steady burning states shown on the figure. The locus of phase equilibrium states was obtained by dividing the vapor pressure of the fuel,at a given liquid temperature, by the total pressure. With the low pressure theory, the droplet surface follows the locus of phase equilibrium states, at a given pressure, during its heat up process. The liquid temperature increases until the locus of steady burning states is reached The intersection between the locus of phase equilibrium states and the locus of steady burning states yields the steady burning droplet conditions for a given total pressure.

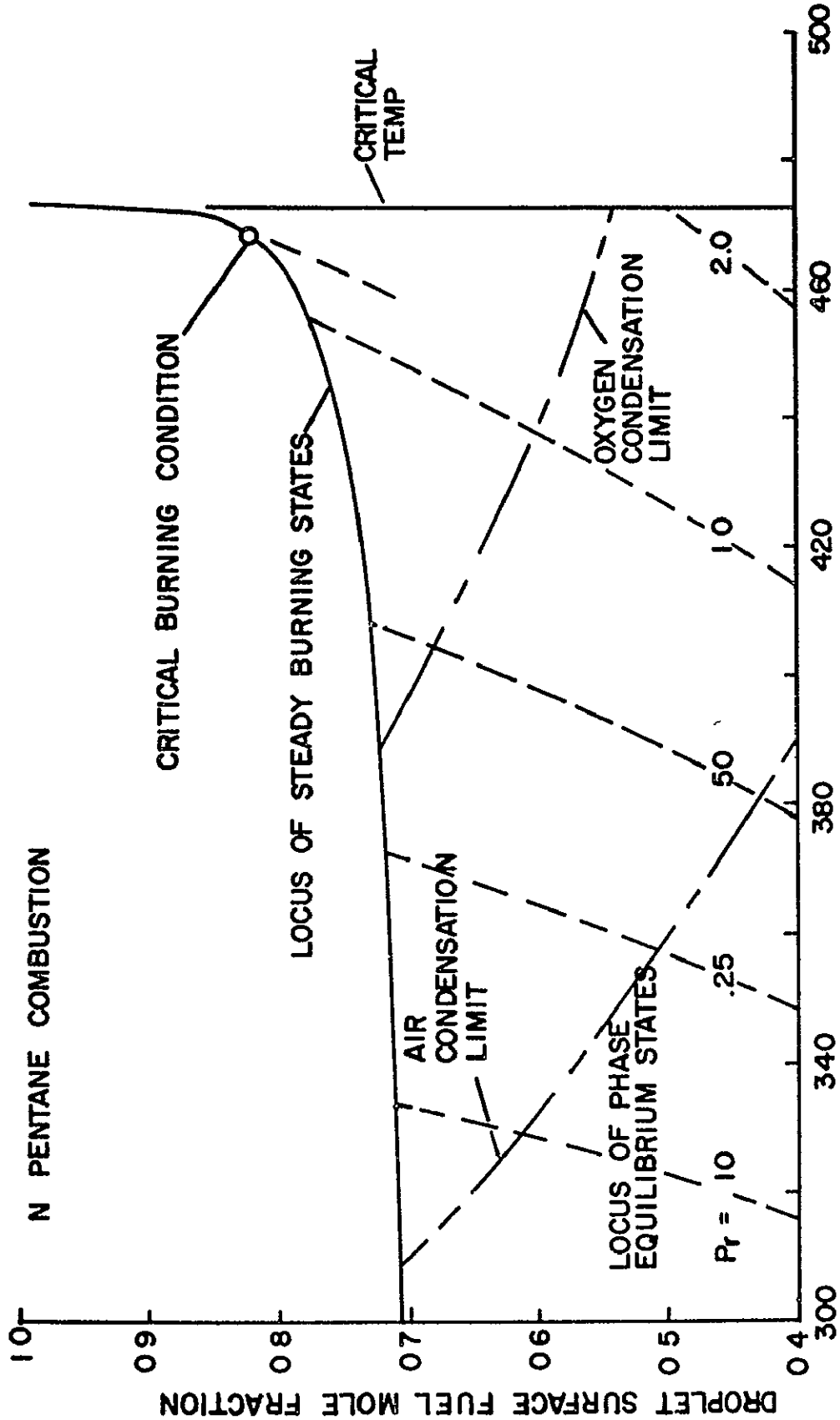

FIGURE 25 LOW PRESSURE THEORY PREDICTIONS OF DROPLET SURFACE FUEL MOLE FRACTION AS A FUNCTION OF LIQUID TEMPERATURE FOR N PENTANE, T_f = 3000°K

As the total pressure increases, a condition is reached where the two loci are just tangent to each other This is the highest pressure where steady burning is possible and is denoted as the critical burning condition on Figure 25. At pressures higher than the critical burning pressure, the droplet temperature continues to rise until the critical temperature of the fuel is exceeded. By default of definition, with the low pressure model, several investigators (12, 13, 59) assume that the droplet gasifies when the critical temperature of the fuel is reached.

For burning hydrocarbon droplets, conditions were found along the locus of both phase equilibrium states and steady burning states where water can condense at the droplet surface. The upper liquid temperature limit for condensation is shown in Figure 25, for n pentane burning in air and oxygen. The limit occurs at lower liquid temperatures for combustion in air since the presence of nitrogen at the droplet surface, in this case, reduces the concentration of water. Since the present analysis does not consider water condensation, its results are invalid below the condensation limit.

For normal paraffins lighter than n pentane, the calculations indicated that water can condense throughout the steady burning region. For paraffins heavier than n pentane water condensation is not a problem during steady burning at pressures greater than one atmosphere. However, even for these materials, condensation may still be a complicating factor in computing the heat up of heavier hydrocarbons at high pressures.

The general characteristics of the high pressure theory are illustrated in Figure 26, where the assumption has been made that the combustion products are equivalent to nitrogen. This case is formally identical to the evaporation of a fuel droplet in a nitrogen environment at 3000°K. The locus of steady evaporation states was computed for constant liquid phase composition, i.e finite nitrogen flux at the droplet surface, in order to correspond to an evaporating droplet.

As before, the droplet conditions for steady evaporation are determined by the intersection of the locus of phase equilibrium states with the locus of steady evaporation states and the upper limit for steady evaporation is located where the two loci become tangent. As was the case for the low pressure theory, where the upper limit is not the critical point of the fuel, the upper limit for the high pressure theory is not a critical mixing point. At pressures higher than the critical evaporation condition, the droplet temperature increases continuously and the droplet material becomes gaseous when the critical mixing temperature is reached (along the locus of critical mixing states in Figure 26). Unlike a pure liquid-vapor critical temperature, a critical mixing temperature is a function of pressure. For the n decane-nitrogen system shown in Figure 26, the liquid temperature where droplet gasification occurs, decreases with increasing pressure in the supercritical evaporation regime.

The solubility of the ambient gas in the liquid fuel droplet becomes quite large at high pressures For the conditions shown on Figure 26, the nitrogen mole fraction in the liquid phase was

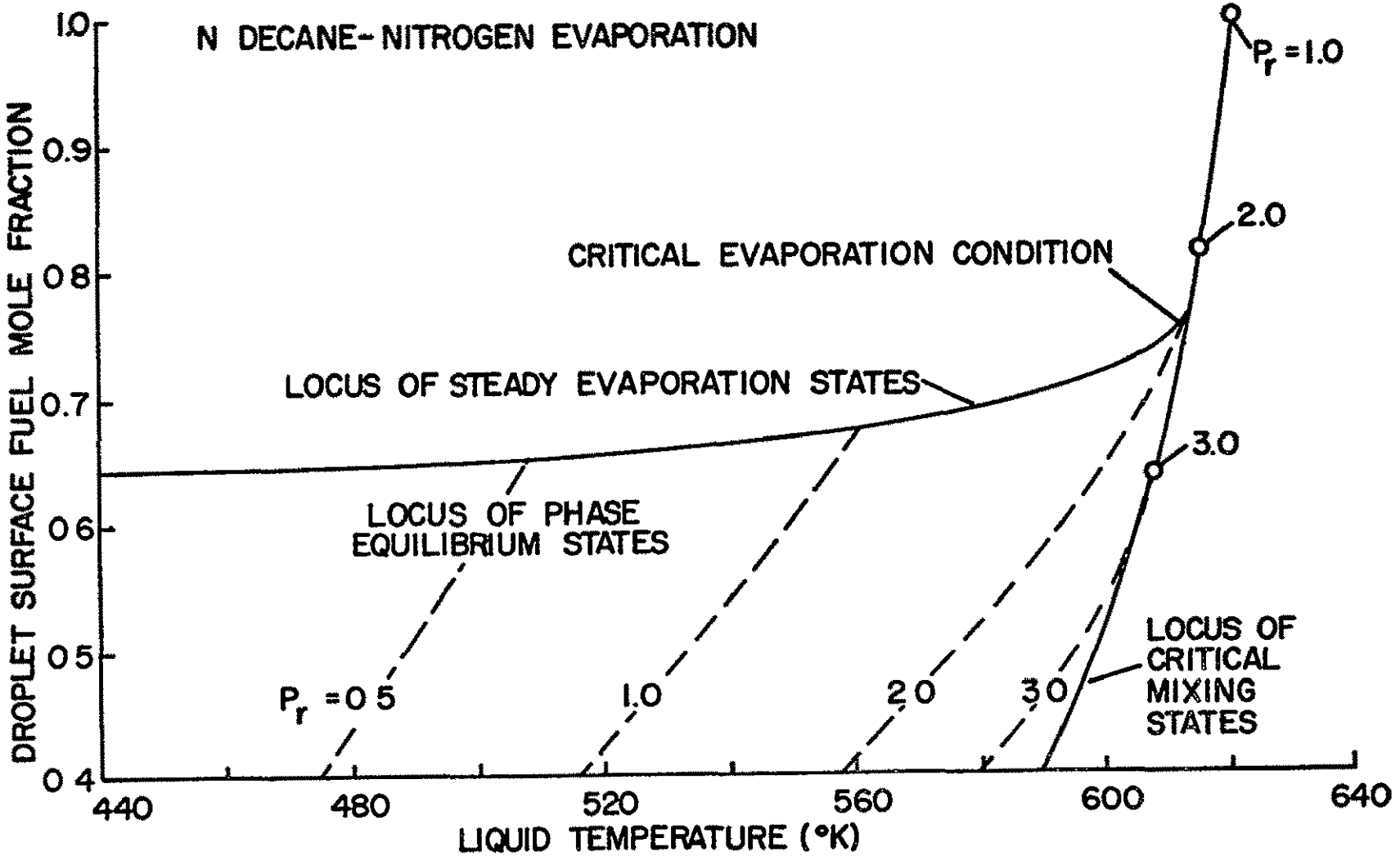

FIGURE 26 HIGH PRESSURE THEORY PREDICTIONS OF DROPLET SURFACE FUEL MOLE FRACTION AS A FUNCTION OF LIQUID TEMPERATURE FOR N DECANE EVAPORATING IN NITROGEN, T_∞ = 3000°K

0 175 at the critical evaporation condition. For all of the cases considered in the present study, the concentrations of the ambient gases in the liquid phase increased with the liquid temperature for fixed total pressures greater than the critical pressure of the pure fuel. This behavior was shown for the n decane-nitrogen system in Figure 5, presented in Chapter II. Dissolved gas concentrations along the critical mixing line were found to be appreciable (20-40% for hydrocarbons heavier than n octane) for the fuels considered in the present calculations.

For the quarternary system fuel-nitrogen-carbon dioxide-water considered in the complete high pressure model, phase equilibrium depends on the proportions of nitrogen, carbon dioxide and water in the non fuel portion of the gas at the droplet surface. Since these proportions depend upon the mole flux of each component at the droplet surface, they can only be specified, a priori, at a steady evaporation state where the assumption of a constant liquid phase composition provides a fixed relationship for the fluxes. In this case, the locus of phase equilibrium states during heat up will depend on the actual history of the heat up process, and diagrams analogous to Figures 25 and 26 cannot be constructed to cover all cases.

CHAPTER VII

SUMMARY AND CONCLUSIONS

7.1 Summary

The overall objective of the present investigation was to study the characteristics of bipropellant droplet combustion in the vicinity of the critical point.

A theoretical model for the prediction of steady droplet burning conditions at high pressures was developed by extending the variable property, steady droplet burning theory of Goldsmith and Penner (8). The extensions included the effects of dissolved gas evaporation, separate determination of the concentrations of the various gas phase species and allowance for variable specific heats of all species.

Ambient gas solubility and high pressure effects were considered in the determination of phase equilibrium conditions at the droplet interface. The calculations for these conditions employed the Redlich and Kwong equation of state along with suitable mixing rules for application to multicomponent mixtures. Confidence in the calculations was established by comparing the computed phase equilibrium behavior with the experimental data in the literature.

Due to the limited experimental verification of the Goldsmith and Penner theory, a series of experiments were conducted on a flat flame burner apparatus to provide a more stringent test of the theory. Test droplets of various alcohols and normal paraffin

hydrocarbons were burned in the combustion products of a flat flame burner at atmospheric pressure. The burner provided ambient temperatures in the range of 1660 to 2530°K and ambient oxygen concentrations in the range of 0 to 40% volume at the droplet location. The measured steady droplet burning rates were compared with values predicted by the Goldsmith and Penner theory for the conditions of the experiments.

The results of the baseline study indicated that the model, when corrected for dissociation effects at the flame zone, provides a reasonable prediction of the trends of the burning rate with respect to ambient temperature and oxygen concentration. However, the model progressively overestimates the burning rate as the molecular weight of the fuel is increased. On the basis of a qualitative evaluation, this failure was attributed to fuel decomposition in the region between the droplet surface and the oxidation zone.

Additional burning rate measurements at atmospheric pressure were obtained on a zero gravity apparatus for the combustion of n octane and n decane droplets. The ambient oxygen concentration for these experiments was varied from 20 to 100% by volume. The agreement between the measured and computed results at low ambient oxygen concentrations was comparable to that obtained on the flat flame burner apparatus. Agreement between the measured values and those predicted by the low pressure theory, corrected for dissociation, improved considerably with increasing ambient oxygen concentration

Measurements were made of steady burning temperatures and the pressures required for the supercritical combustion of n octane and n decane droplets burning in air in the zero gravity apparatus Theoretical results were obtained with the conventional low pressure treatment of phase equilibrium at the droplet surface as well as high pressure models which allowed for high pressure effects and finite ambient gas solubility. The high pressure models were in reasonable agreement with the data, both with respect to steady burning temperatures and the pressures required for the onset of supercritical combustion The low pressure model underestimated the pressures required for supercritical combustion by roughly a factor of two.

The calculations also indicated conditions where water should condense on the droplet surface, both during heat up and steady burning, for the normal paraffin hydrocarbons

7.2 Conclusions

The major conclusions of the study are as follows

1. The variable property steady droplet burning model of Goldsmith and Penner (8), when corrected for dissociation effects at the flame zone, provides a reasonable estimate of the trends of the burning rate with respect to ambient temperature and oxygen concentration at low ambient pressures.
2. The model fails to predict the observed trend of the burning rate with respect to molecular weight. The absolute errors between the measured and computed burning rates were greatest for materials heavier than n decane. For lighter materials,

the model provides a reasonable estimate of the burning rate This failure is attributed to fuel decomposition in the region between the droplet surface and the oxidation zone

3. High pressure corrections and solubility effects should be considered in estimating droplet conditions at high pressures as well as the pressures required for supercritical combustion For combustion in air, a good approximation can be obtained by assuming that the gas at the droplet surface is a binary mixture of fuel and nitrogen due to the predominance of nitrogen in the system

4. The theoretical results showed the greatest sensitivity with respect to the value of χ_A. Since this parameter is proportional to the Lewis number, the common unity Lewis number assumption will not yield useful predictions of droplet conditions at high pressures

5 Conditions were found where water should condense on burning droplets for the normal paraffins. This occurred for steady burning at pressures greater than one atmosphere for paraffins up to n pentane. Condensation can also occur for the heavier hydrocarbons during heat up, at sufficiently low droplet temperatures.

6. The results of the baseline study indicate that decomposition of the fuel molecule in the region between the droplet surface and the oxidation zone may occur. Since decomposition was neglected in the theoretical analysis, the computed results may be in error for cases where significant decomposition is

involved. A quantitive evaluation of decomposition effects is not possible at present and this question deserves further study.

7. Thermal radiation can contribute a significant portion of the total heat transferred to the droplet at the high pressure levels required for supercritical combustion. While this has relatively little effect on steady burning temperatures, droplet burning rates will be affected to a greater extent and radiation should be considered, particularly when convection is small, as in the present experiment.

BIBLIOGRAPHY

1. Priem, R. J , "Propellant Vaporization as a Criterion for Rocket Engine Design Calculations of Chamber Length to Vaporize a Single n-Heptane Drop," NACA TN 3985, July 1957.

2 Priem, R J , and M. F Heidmann, "Propellant Vaporization as a Design Criterion for Rocket Engine Combustion Chambers," NASA Technical Report R-67, 1960

3. Spalding, D. B , "The Combustion of Liquid Fuels," Fourth Symposium (International) on Combustion, Williams and Wilkins, Baltimore, 1953, pp. 847-864.

4 Godsave, G. A. E., "Studies of the Combustion of Drops in a Fuel Spray - The Burning of Single Drops of Fuel," Fourth Symposium (International) on Combustion, Williams and Wilkins, Baltimore, 1953, pp 818-830.

5 Hottell, H. C., G. C. Williams and H C Simpson, "Combustion of Droplets of Heavy Liquid Fuels," Fifth Symposium (International) on Combustion, Reinhold, New York, 1954, pp. 101-129.

6. Kobayasi, K., "An Experimental Study of the Combustion of a Fuel Droplet," Fifth Symposium (International) on Combustion, Reinhold, New York, 1954, pp 141-148.

7 Bolt, J A. and M A. Saad, "Combustion Rates of Freely Falling Drops in a Hot Atmosphere," Sixth Symposium (International) on combustion, Reinhold, New York,1956, pp. 717-725.

8. Goldsmith, M. and S. S. Penner, "On the Burning of Single Drops of Fuel in an Oxidizing Atmosphere," Jet Propulsion, Vol 24, 1954, pp. 245-251.

9 Goldsmith, M , "Experiments on the Burning of Single Drops of Fuel," Jet Propulsion, Vol. 26, 1956, pp 172-178.

10. Williams, F A , "On the Assumptions Underlying Droplet Vaporization and Combustion Theories," Journal of Chemical Physics, Vol. 33, July 1960, pp. 131-144.

11 Brzustowski, T A , "Chemical and Physical Limits on Vapor-Phase Diffusion Flames of Droplets," Canadian Journal of Chemical Engineering, Vol. 43, February 1965, pp 30-35.

12. Spalding, D. B , "Theory of Particle Combustion at High Pressures," ARS Journal, Vol. 29, November 1959, pp 828-835

13 Wieber, P. R., "Calculated Temperature Histories of Vaporizing Droplets to the Critical Point," AIAA Journal, Vol. 1, No. 12, December 1963, pp. 2764-2770

14. Rosner, D. E., "On Liquid Droplet Combustion at High Pressures," AIAA Journal, Vol. 5, No. 1, January 1967, pp. 163-166

15. Manrique, J A., "Theory of Droplet Vaporization in the Region of the Thermodynamic Critical Point," NASA CR-72574, 1969.

16. Savery, W and G L Borman, "Experiments on Droplet Vaporization at Supercritical Pressures," AIAA Paper No. 70-6, January 1970.

17 Feath, G. M., "On the Prediction of Pure Monopropellant Droplet Life Histories," AIAA Paper No. 69-563, June 1969

18. Dominicis, D. P., "An Experimental Investigation of Near Critical and Supercritical Burning of Bipropellant Droplets," NASA CR-72399, April 1968.

19 Williams, F. A , Combustion Theory, Addison Wesley, Reading, Massachusetts, 1965.

20. Eisenklam, P., S. A. Arunachalam and J. A. Weston, "Evaporation Rates and Drag Resistance of Burning Drops," Eleventh Symposium (International) on Combustion, The Combustion Institute, Pittsburgh, 1967, pp. 715-728.

21 Frössling, N , "Uber die Verdunstung Fallender Tropfen," Beitrag. Geophysics, Vol. 52, 1938, pp. 170-216.

22. Fendell, F. E., M. L. Sprankle and D. S. Dodson, "Thin-Flame Theory for a Fuel Droplet in Slow Viscous Flow," Journal of Fluid Mechanics, Vol. 126, Part 2, 1966, pp. 267-280.

23 Fendell, F. E., "Decompositional Burning of a Droplet in a Small Peclet Number Flow," AIAA Journal, Vol. 6, No. 10, 1968, pp. 1946-1953.

24. Rosner, D. E., Personal Communication, 1968.

25. Wolfhard, H. G. and W. G. Parker, "Evaporation Processes in a Burning Kerosine Spray," Journal of the Institute of Petroleum, Vol. 35, 1949, pp. 818-830

26. Brzustowski, T. A. and R Natarajan, "Combustion of Aniline Droplets at High Pressures," Canadian Journal of Chemical Engineering, Vol. 44, August 1966, pp 194-201.

27. Penner, S. S., Chemistry Problems in Jet Propulsion, Macmillan, New York, 1957.

28. Faeth, G. M., "The Kinetics of Droplet Ignition in a Quiescent Air Environment," Ph D. Thesis, The Pennsylvania State University, 1964.

29. Sengers, J V , "Behavior of Viscosity and Thermal Conductivity of Fluids Near the Critical Point," Critical Phenomena, National Bureau of Standards, Misc. Publ. No. 273, 1966, pp. 165-178.

30. Bird, R. B., N E Stewart and E N. Lightfoot, Transport Phenomena, Wiley, New York, 1960

31 Reid, R C. and T. K Sherwood, The Properties of Gases and Liquids, McGraw-Hill, New York, 1966

32. Redlich, O. and J. N S. Kwong, "On the Thermodynamics of Solutions," Chemical Reviews, Vol 44, 1949, pp. 233-244.

33. Prausnitz, J. M. and P. L Chueh, Computer Calculations for High Pressure Vapor-Liquid Equilibria, Prentice Hall, New Jersey, 1968.

34. Poettmann, F. H and D L. Katz, "Phase Behavior of Binary Carbon Dioxide-Paraffin Systems," Industrial and Engineering Chemistry, Vol. 37, No. 9, September, 1945, pp 847-853.

35. Poston, R S. and S. S McKetta, "Vapor-Liquid Equilibrium in the n Hexane-Nitrogen System," Journal of Chemical Engineering Data, Vol. 11, No. 3, July 1966, pp. 364-365.

36. Akers, W. W , D. M. Kehn and C. H. Kilgore," Volumetric and Phase Behavior of Nitrogen-Hydrocarbon Systems; Nitrogen-n Heptane System," Industrial and Engineering Chemistry, Vol. 46, No. 12, December, 1954, pp. 2536-2540.

37. Azarnoosh, A. and S. S. McKetta, "Nitrogen-n Decane System in the Two Phase Region," Journal of Chemical Engineering Data, Vol. 8, 1963, pp 494-496.

38. Prausnitz, J M., C. A. Eckert, R V Orye and J P. O'Connell, Computer Calculations for Multicomponent Vapor-Liquid Equilibria, Prentice Hall, New Jersey, 1967, p 18.

39. Reamer, H. H , R H. Olds, B. H Sage and W. Lacey, "Compositions of the Coexisting Phases of the n Butane-Water System in the Three Phase Region," Industrial and Engineering Chemistry, Vol. 36, No. 4, April 1944, pp. 381-383.

40. Griswold, J. and J E. Kasch, "Hydrocarbon-water Solubilities at Elevated Temperatures and Pressures," Industrial and Engineering Chemistry, Vol. 34, No. 7, July 1942, pp. 804-806.

41. Lewis, G N. and M. Randall, Thermodynamics, 2nd Ed , Revised by K. S. Pitzer and L Brewer, McGraw-Hill, New York, 1961.

42. Friedman, R. and A. Macek, "Ignition and Combustion of Aluminum Particles in Hot Gases," Combustion and Flame, Vol. 6, No. 1, March 1962, pp. 9-19

43. Jones, W. H. (Chairman), JANAF Thermochemical Tables, Dow Chemical Company, Midland, Michigan.

44. Yuge, T., "Experiments on Heat Transfer from Spheres Including Combined Natural and Forced Convection," ASME Transactions, Vol. 82, Series C, 1960, pp. 214-220.

45. Allender, C., "Untersuchung des Absorptions - Vorganges in Absorbentenshichten mit Linearer Absorptionsistherme," Transactions of the Royal Institute of Technology, Stockholm, No. 70, 1953.

46. Acrivos, A. and T. D. Taylor, "Heat and Mass Transfer from Single Spheres in Stokes Flow," Physics of Fluids, Vol 5, No. 4, 1962, pp 287-394.

47. Combs, R L., Discussion of Reference 20, Eleventh Symposium (International) on Combustion, The Combustion Institute, Pittsburgh, 1967, p. 728.

48 Aldred, J. W. and A. Williams, "The Burning Rates of Drops of n-Alkanes," Combustion and Flame, Vol. 10, 1966, pp 396-398.

49. Sioui, R H. and L. H. S. Roblee, Jr., "The Prediction of the Burning Rate Constants of Suspended Hydrocarbon Fuel Droplets," Combustion and Flame, Vol. 13, 1969, pp 447-454.

50. Hall, A. R., "Experimental Temperature Gradients in Burning Drops," Seventh Symposium (International) on Combustion, Butterworths, London, 1959, pp. 399-407.

51. Wise, H. and C. M. Ablow, "Burning of a Liquid Droplet-III. Conductive Heat Transfer Within the Condensed Phase During Combustion," Journal of Chemical Physics, Vol. 27, No. 2, August 1957, pp. 389-393

52. Griswold, J., Fuels Combustion and Furnaces, McGraw-Hill, New York, 1946, pp. 163-165.

53 Benson, S W , The Foundations of Chemical Kinetics, McGraw-Hill, New York, 1960, pp 504-506.

54 Palmer, H. B and C F. Cullis, "The Formation of Carbon from Gases," The Chemistry and Physics of Carbon, P L. Walker (Ed.), Vol. 1, Marcel Dekker, Inc., 1965, pp 265-325

55. Gordon, A. S , "A Review of the Kinetics and Mechanism of the Pyrolysis of Hydrocarbons," Fifth AGARD Combustion Colloquium, MacMillan, New York, 1963, pp. 111-134.

56. Gordon, A. S., S. R Smith and J. R. McNesby, Jr., "Study of the Chemistry of Diffusion Flames," Seventh Symposium (International) on Combustion, Butterworths, London, 1958, pp. 317-324.

57. Tsuji, H. and Y. Ichiro, "The Structure of Counterflow Diffusion Flames in the Forward Stagnation Region of a Porous Cylinder," Twelfth Symposium (International) on Combustion, The Combustion Institute, Pittsburgh, 1969, pp 997-1005.

58. Maxwell, J. D., Data Book on Hydrocarbons, Van Nostrand, New York, 1950.

59. Faeth, G. M , D. P. Dominicis, J. F. Tulpinsky and D R Olson, "Supercritical Bipropellant Droplet Combustion," Twelfth Symposium (International) on Combustion, The Combustion Institute, Pittsburgh, 1969.

60. Hottel, H. C. and A. F. Sarofim, Radiative Transfer, McGraw-Hill, New York, 1967.

61. Rossini, F. D., Selected Values of the Physical and Thermodynamical Properties of Hydrocarbons and Related Compounds, American Petroleum Institute, Carnegia, 1953.

62. International Critical Tables, McGraw-Hill, New York, 1926-1930.

63. Stull, D. R., "Vapor Pressure of Pure Substances, Organic Compounds," Industrial and Engineering Chemistry, Vol. 39, No. 4, April 1947, pp. 517-540

64. Svehla, R. A., "EStimated Viscosities and Thermal Conductivities of Gases at High Temperatures," NASA Technical Report R-132, 1962.

65. Wilke, C. R., "Diffusional Properties of Multicomponent Gases," Chemical Engineering Progress, Vol. 46, No. 2, 1950, pp. 95-104.

APPENDIX A

CHECK OF ASSUMPTIONS OF THE ANALYSIS

A 1 Constant Total Pressure Assumption

Reference (28) gives the following approximate expression for the estimation of pressure changes across the boundary layer surrounding a spherically symmetric droplet.

$$\frac{P_\ell - P_\infty}{P} = - \frac{W}{2R\ T} \left[\frac{DX_{1\ell}}{r_\ell (1 - X_{1\ell})} \right]^2 \qquad (A.1)$$

Equation (A.1) was obtained by integrating the momentum equation for the flow field resulting from the binary diffusion of fuel vapor from the droplet. Constant fluid properties and equal molecular weights of both species were assumed

Substitution of some typical values into Equation (A.1) indicates that there is less than 5% change in pressure across the boundary layer for droplets as small as 10μ in diameter at a pressure of one atmosphere, providing $X_{1\ell} \leq 0.9$. For larger droplets or pressure levels, the variation of pressure is much smaller. Therefore, the assumption of a constant total pressure in the boundary layer appears to be valid for the conditions of the present study

A.2 Radiation Assumption

A simplified model was used to estimate the contribution of radiant energy to the droplet from the flame. Following Godsave (4), the system is considered as a hot radiating surface (the flame front)

surrounding a cooler body (the droplet). In view of the sharp temperature gradient between the droplet and the flame, the radiation and absorption of the gases in the region between the flame zone and the droplet were neglected. Since the flame surrounding the droplet is relatively transparent, the reflection of radiation from the flame back to the droplet is neglected Under these assumptions, the system is equivalent to a thin transmitting and non-reflecting spherical shell at the temperature T_f surrounding the droplet. If the radiation loss by the droplet is neglected, due to its relatively low temperature, the radiant energy flux absorbed by the liquid droplet is

$$Q_R = 4\pi r_\ell^2 e_f a_d s T_f^4 \qquad (A.2)$$

where e_f is the emissivity of the thin zone of radiating gases, a_d is the absorptivity of the droplet and s is the Stefan-Boltzmann constant.

Assuming that the ambient gases are insoluble in the liquid phase, the total heat flux to the droplet for steady burning is,

$$\dot{Q}_T = \dot{n}L \qquad (A.3)$$

The ratio of the radiant energy flux, $\dot{Q}_R$, to the total energy flux, $\dot{Q}_T$, was evaluated for n decane combustion at a flame temperature of 3000°K for various pressures and droplet diameters. The molar burning rate, $\dot{n}$, was calculated with the constant property solution given in Appendix B. The physical properties were obtained with the

equations and methods of Appendix D. Measured droplet temperatures were employed in the calculations, and high pressure effects were considered in the evaluation of the heat of vaporization, L

Absorptivities for paraffin droplets are given by Hottel, et al. (5) as a function of droplet size. For droplet diameters of 100μ and 1000μ, the absorptivities are 0.132 and 0.546 respectively.

The radiating gases were assumed to be carbon dioxide and water vapor. Hottel and Sarofim (60) present charts for the estimation of emissivities for mixtures of these two gases as a function of total pressure, gas temperature, mean beam length and the partial pressures For the present calculations, the mean beam length was taken to be that for infinite parallel plates as given in Reference (60). The actual temperature and concentration gradients in the radiating zone were approximated by a constant temperature and concentration zone having a thickness of 100μ. The temperature of the zone was taken as 3000°K. The partial pressures of the carbon dioxide and water vapor were based on the average concentrations of these species at the flame zone. The calculated mole fractions were 0.126 and 0.139 for carbon dioxide and water vapor respectively.

With the above assumptions, the emissivity, e_f, was found to vary between 5×10^{-4} and 5×10^{-3} as the pressure was varied up to 50 atmospheres. Since some of the conditions were outside of the range given on the charts of Reference (60), extrapolation was necessary and the values must be considered provisional.

The results of the calculations are presented in Table 5 as the ratio of the radiant energy flux to the total energy flux

TABLE 5

RADIATION CONTRIBUTIONS, $\dot{Q}_R/\dot{Q}_T$

P (atm.)	d_ℓ = 100μ	d_ℓ = 1000μ
1	4.5×10^{-4}	1.9×10^{-2}
10	1.2×10^{-3}	5.1×10^{-2}
50	1.1×10^{-2}	4.7×10^{-1}

These results indicate that radiant energy absorbed by the droplet represents a small fraction of the energy required to vaporize the droplet at moderate pressures However, this effect increases rapidly with increasing pressure and can become quite significant at pressures of 50 atmospheres.

APPENDIX B

ADDITIONAL THEORETICAL CONSIDERATIONS

B.1 Goldsmith and Penner (8) Analysis

For convenience, the equations of Chapter II are reformulated for the conditions presented in Reference (8). In their analysis, Goldsmith and Penner assumed that the ambient gases were insoluble in the liquid phase. Under this assumption, the mole flux fractions in the inner field become

$$\varepsilon_1 = 1, \qquad \varepsilon_i = 0, \qquad (i=2, \ldots, N) \tag{B.1}$$

The combustion products and inert gases were treated as a single species. Thus, the problem reduces to the consideration of a binary mixture of fuel and products in the inner region and a binary mixture of oxygen and products in the outer region. Consistent with the notation of Chapter II, the fuel, products and oxygen are designated as species 1, 2 and 3 respectively.

With regard to specific heats, Goldsmith and Penner used constant average values for all of the non-fuel species. Thus, for the three species considered, the specific heats are

$$C_{p1} = A_1 + B_1 T, \qquad C_{p2} = C_{pp}, \qquad C_{p3} = C_{po} \tag{B.2}$$

where C_{pp} and C_{po} designate the constant average specific heats of the products and oxygen components respectively.

Under these assumptions, the equations presented in Chapter II are easily reduced to given expressions for the mole fractions at the droplet surface, combustion temperature, flame radius and burning rate which correspond to the conditions of Goldsmith and Penner. Where the outer region is concerned, the solutions derived for zero B_1 (Chapter II, Section 2.4), must be used.

The surface mole fractions at the droplet surface are

$$X_{1\ell} = 1 - \exp\left\{\frac{2\chi A}{\phi}\left[\tan^{-1}\left(\frac{A_1 + B_1 T_\ell}{\phi}\right) - \tan\left(\frac{A_1 + B_1 T_f}{\phi}\right)\right]\right\} , \qquad \phi^2 > 0 \tag{B.3}$$

or

$$X_{1\ell} = 1 - \left[\frac{(A_1 + B_1 T_f + \zeta)(A_1 + B_1 T_\ell - \zeta)}{(A_1 + B_1 T_f - \zeta)(A_1 + B_1 T_\ell + \zeta)}\right]^{\chi_A/\zeta} , \qquad \zeta^2 > 0 \tag{B 4}$$

or

$$X_{1\ell} = 1 - \exp\left[\frac{2\chi_A B_1 (T_\ell - T_f)}{(A_1 + B_1 T_\ell)(A_1 + B_1 T_f)}\right] , \qquad \zeta^2 = 0 \tag{B.5}$$

and

$$X_{2\ell} = 1 - X_{1\ell} \tag{B 6}$$

where

$$\zeta^2 = -\phi^2 = A_1^2 - 2B_1\left(L_1 - A_1 T_\ell - \frac{B_1}{2} T_\ell^2\right) \tag{B.7}$$

The combustion temperature becomes

$$T_f = -\frac{\mu}{\nu} + \left(\frac{\mu}{\nu} + T_\infty\right)\Big/\left(1 - \frac{X_{3\infty}}{\delta_3}\right)^{\nu C_{po}/\chi_B} \tag{B.8}$$

where

$$\nu = \left(\alpha_2 \frac{C_{pp}}{C_{po}} + \alpha_3 \right) \Big/ (\alpha_2 + \alpha_3) \tag{B.9}$$

$$\mu = - \frac{Q_R / C_{po}}{\alpha_2 + \alpha_3} - \nu T^* \tag{B 10}$$

and

$$Q_R = Q^* - L_1 + A_1 \, (T_\ell - T^*) + \frac{B_1}{2} \, (T_\ell^2 - T^{*2}) \tag{B 11}$$

The quantity Q^* represents the standard heat of combustion for gaseous products and reactants at the reference temperature T^*. The quantity δ_3, represents the mole flux fraction of oxygen in the outer field and is given by Equation (2.16) of Chapter II. For the conditions considered here, these mole flux fractions are:

$$\delta_2 = \frac{\alpha_2}{\alpha_2 + \alpha_3} \quad ; \quad \delta_3 = \frac{\alpha_3}{\alpha_2 + \alpha_3} \tag{B.12}$$

The flame radius for these conditions is

$$\frac{1}{r_f} = \frac{4\pi \, \lambda_{B\ell}}{n_f \, C_{po} \, \nu \, T_\ell} \left\{ (T_\infty - T_f) - \frac{\mu}{\nu} \ln \left[\frac{\mu + \nu \, T_\infty}{\mu + \nu \, T_f} \right] \right\} \tag{B 13}$$

Finally, the expression for the molar burning rate becomes

$$\frac{\dot{n} T_\ell B_1}{4\pi r_\ell \, \lambda_{A\ell}} \left(1 - \frac{r_\ell}{r_f} \right) = \ln \left\{ 1 + (T_f - T_\ell) \left[A_1 + \frac{B_1}{2} \, (T_f + T_\ell) \right] \Big/ L_1 \right\} + \psi \tag{B.14}$$

where

$$\psi = -\frac{2A_1}{\phi}\left\{\tan^{-1}\left(\frac{A_1 + B_1T_f}{\phi}\right) - \tan^{-1}\left(\frac{A_1 + B_1T_\ell}{\phi}\right)\right\}, \quad \phi^2 > 0 \tag{B 15}$$

or

$$\psi = \ln\left[\frac{(A_1 + B_1T_f + \zeta)(A_1 + B_1T_\ell - \zeta)}{(A_1 + B_1T_f - \zeta)(A_1 + B_1T_\ell + \zeta)}\right]^{A_1/\zeta}, \quad \zeta^2 > 0 \tag{B 16}$$

or

$$\psi = -\frac{2A_1B_1\ (T_f - T_\ell)}{(A_1 + B_1T_f)(A_1 + B_1T_\ell)}, \quad \zeta^2 = 0 \tag{B 17}$$

B.2 Constant Property Analysis

If the assumptions that the fuel thermal conductivity and specific heat are independent of temperature are made along with the assumptions of the preceding section, the analysis will correspond essentially to the one presented by Godsave (4) With the exception of the combustion temperature, the expressions of the preceding section must be rederived from the steady burning conservation equations presented in Section 2.2 of Chapter II. For convenience, the constant average specific heat of each species is designated as

$$C_{p1} = C_{pF}, \quad C_{p2} = C_{pp}, \quad C_{p3} = C_{po} \tag{B.18}$$

Omitting the details of the derivation, which are similar to those presented in Chapter II, the results are as follows

$$X_{1\ell} = 1 - \left[1 + \frac{C_{pF}}{L_1}(T_f - T_\ell)\right]^{-N_{LA}} \tag{B 19}$$

$$X_{2\ell} = 1 - X_{1\ell} \tag{B.20}$$

$$T_f = -\frac{\mu}{\nu} + \frac{(\mu/\nu + T_\infty)}{\left(1 - \frac{X_{3\infty}}{\delta_3}\right)^{\nu/N_{LB}}} \tag{B.21}$$

$$\frac{1}{r_f} = \frac{4\pi\ \lambda_B}{\dot{n}_f\ C_{po}\ \nu}\ \ln\left(\frac{\mu + \nu\ T_\infty}{\mu + \nu\ T_f}\right) \tag{B.22}$$

and

$$\frac{n}{4\pi r_\ell\ \lambda_A}\left(1 - \frac{r_\ell}{r_f}\right) = \frac{1}{C_{pF}}\ \ln\left[1 + \frac{C_{pF}}{L_1}\ (T_f - T_\ell)\right] \tag{B 23}$$

where ν and μ are given in Equations (B.9) and (B 10) respectively. The quantity Q_R which appears in the expression for μ is

$$Q_R = Q^* - L_1 + C_{pF}\ (T_\ell - T^*) \tag{B.24}$$

The quantities N_{LA} and N_{LB} represent the Lewis Numbers for regions A and B respectively. They have the form

$$N_{LA} = \frac{\lambda_A}{C_{pF}(CD)_A} \tag{B.25}$$

and

$$N_{LB} = \frac{\lambda_B}{C_{po}(CD)_B} \tag{B.26}$$

APPENDIX C

PHASE EQUILIBRIUM RELATIONS

C.1 Component Fugacities

The expression for the fugacity of a component in a mixture was obtained by substituting the equation of state and mixing rules of Chapter II into Equation (2 54) and integrating. The result, for a component i in a mixture of N components is given by the following expression

$$\ln (f_i/X_i P) = \ln\left(\frac{v}{v - b^\circ}\right) + \frac{b_i^\circ}{v - b^\circ} - \frac{2\sum_{j=1}^{N} X_j a_{ji}^\circ}{RT^{3/2} b^\circ}\left(\ln\frac{v + b^\circ}{v}\right)$$

$$+ \frac{a^\circ b_i^\circ}{RT^{3/2} b^{\circ 2}}\left[\ln\left(\frac{v + b^\circ}{v}\right) - \frac{b^\circ}{v + b^\circ}\right] - \ln\frac{Pv}{RT} \qquad (C\ 1)$$

The molar volume, v, is determined from the equation of state, which is cubic in v

C.2 Heat of Vaporization

The heat of vaporization of a component i in a mixture, L_i, is the difference between the partial molar enthalpy in the vapor and liquid phases, i.e ,

$$L_i = \bar{h}_i^V - \bar{h}_i^L \qquad (C.2)$$

The partial molar enthalpy of component i in a mixture is determined by the following thermodynamic relation.

$$\frac{\bar{h}_i^\circ - \bar{h}_i}{RT^2} = \frac{\partial}{\partial T}\left(\ln \frac{f_i}{X_i P}\right) \qquad (C\ 3)$$

where $\bar{h}_i^\circ$ represents the partial molar enthalpy in the ideal state. Differentiating Equation (C 1) and substituting into Equation (C 3) results in the following

$$\frac{\bar{h}_i^\circ - \bar{h}_i}{RT^2} = (\bar{A} - 1)\frac{\bar{C}}{Z} + \frac{\bar{A}}{T} + \bar{B} \qquad (C\ 4)$$

where

$$\bar{A} = -\frac{b^\circ}{v - b^\circ} - \frac{b_i^\circ v}{(V - b^\circ)^2} + \frac{2\sum_{j=1}^{N} a_{ji}^c X_j}{RT^{1.5}(v + b^\circ)} - \frac{a^\circ b_i^\circ}{RT^{1.5}(v + b^\circ)^2} \qquad (C\ 5)$$

$$\bar{B} = \frac{3}{2RT^{2.5} b^\circ}\left\{2\left(\sum_{j=1}^{N} X_j a_{ji}^\circ\right)\ln\left(\frac{v + b^\circ}{v}\right) - \frac{a^\circ b_i^\circ}{b^\circ}\ln\left(\frac{v + b^\circ}{v}\right) + \frac{a^\circ b_i^\circ}{v + b^\circ}\right\} \qquad (C\ 6)$$

$$\bar{C} = \frac{\frac{2\bar{D}Z}{T} + \frac{PZ}{(RT)^2}\left[\frac{a^\circ}{2T^{3/2}} + b^\circ R\right] - \frac{3.5\, a^\circ b^\circ P^2}{R^3 T^{4.5}}}{3Z^2 - 2Z + \bar{D}} \qquad (C\ 7)$$

$$\bar{D} = \left(\frac{a^\circ}{T^{1/2}} - b^\circ RT - b^{\circ 2}P\right)\frac{P}{(RT)^2} \qquad (C.8)$$

and

$$Z = \frac{Pv}{RT} \qquad (C\ 9)$$

is the mixture compressibility factor.

By solving Equation (C.4) in each phase, and substituting the results into Equation (C 2), the heat of vaporization for each component in the mixture is determined

C 3 Physical Constants

The pure component constants, P_c, T_c, v_c and ω employed in the calculations are given in Table 6

TABLE 6

PURE COMPONENT CONSTANTS

COMPONENT	P_c (atm)	T_c (°K)	$v_c \left(\frac{cc}{g\text{-mole}}\right)$	ω
N DECANE	20.8	617 6	603 0	0 479
N OCTANE	24.6	568 6	486 0	0 398
N HEPTANE	27 1	540 3	426.0	0 349
N HEXANE	29.9	507.3	368 0	0 298
N PENTANE	33 3	469.5	311.0	0.252
CARBON DIOXIDE	72.9	304 2	94 3	0 225
NITROGEN	33.5	126.2	90.1	0.040
WATER	218.3	647 0	56 0	0.344

The binary interaction parameters, k_{ij}, used in the investigation are presented in Table 7.

TABLE 7

BINARY INTERACTION PARAMETERS

COMPONENT	N_2	CO_2	H_2O
N DECANE	50	.43	.55
N OCTANE	.40	34	45
N HEPTANE	.35	29	40
H HEXANE	30	.25	.35
N PENTANE	.25	20	30
NITROGEN	00	00	.00
CARBON DIOXIDE	00	.00	00

APPENDIX D

PHYSICAL PROPERTIES

D 1 References for Physical Properties

The physical properties employed in the calculations were obtained from the references listed in Table 8 The specific correlations are given in the following sections.

The combustion products were treated as a single species for the low pressure calculations The properties for this effective species were obtained by averaging the properties for an equimolar mixture of carbon dioxide, nitrogen and water vapor.

The constant average property values, required in some of the calculations, were evaluated at an average temperature for the region of interest. The average temperatures employed for Regions A and B were calculated as·

$$T_A = (T_\ell + T_f)/2 \qquad \text{(D 1)}$$

and

$$T_B = (T_f + T_\ell)/2 \qquad \text{(D.2)}$$

D.2 Liquid Phase Properties

The liquid phase molar density, vapor pressure and heat of vaporization employed in the low pressure calculations were correlated with the following equations·

$$C_\ell = (C_1 + C_2 T_\ell)/W \qquad \text{(g-mole/cc)} \qquad \text{(D 3)}$$

TABLE 8

REFERENCES FOR PHYSICAL PROPERTIES

PROPERTY	REFERENCES		
	PARAFFINS	ALCOHOLS	AMBIENT GAS
C_ℓ	61	62	--
P_v	61	62, 63	--
L	31[a]	31[a]	--
λ	58	64[b]	64
C_p	61	31[c]	64
D	31[d]	31[d]	31[d]
Q*	61	62	--
σ	--	--	64
T_c	31	31	31

[a] Watson Correlation, Reference (31)
[b] Computed, Method of Reference (64)
[c] Computed, Rihani and Doraiswamy Method, Reference (31)
[d] Slattery and Bird Correlation, Reference (31)

$$P_v = C_3 \exp\left(\frac{-1}{T_\ell/C_4 - C_5}\right) \qquad \text{(atm)} \qquad \text{(D 4)}$$

$$L = C_6 W\,(1 - T_\ell/T_c) \qquad \text{(cal/g-mole)} \qquad \text{(D 5)}$$

The constants C_1 to C_6 are tabulated in Table 9 along with the molecular weight, W, and critical temperature, T_c, for each of the components considered in the calculations The liquid temperature, T_ℓ, used in the equations is in degrees Kelvin.

D.3 Gas Phase Properties

The specific heat of each species in the gas phase was represented by the equation

$$C_p = A + BT \qquad \text{(cal/g-mole °K)} \qquad \text{(D 6)}$$

The specific heat constants, A and B, are tabulated in Table 10 for all species considered

The thermal conductivity correlations employed for Regions A and B are as follows·

$$\lambda_A = \lambda_{A\ell}\,(T/T_\ell) \qquad \text{(D 7)}$$

and

$$\lambda_B = \lambda_{B\ell}\,(T/T_\ell) \qquad \text{(D.8)}$$

The constants $\lambda_{A\ell}$ and $\lambda_{B\ell}$ represent the thermal conductivities of the gas mixture, evaluated at the temperature T_ℓ, for Regions A and B respectively These constants were evaluated by averaging the thermal conductivities of the fuel (λ_F), oxygen (λ_O) and combustion

TABLE 9

CONSTANTS IN THE LIQUID PHASE PROPERTY EQUATIONS

COMPONENT	C_1	C_2 x 10^3	C_3	C_4	C_5 x 10^3	C_6	W	T_c
METHANE	0.578	1.395	1667.	896.	7.83	156 0	16 04	190.7
PROPANE	0.846	1.152	8650	1870.	13 39	169.4	44.09	369.9
N PENTANE	0.903	0.945	9130.	2450	16.78	128.3	72.15	469.5
N HEPTANE	0 941	0.879	10531.	2925.	19 30	117.8	100.20	540.3
N OCTANE	0 974	0.879	11080.	3120	20.45	113 8	114 22	568.6
ISO OCTANE	0.942	0 856	8536	2900	18.16	98.5	114.22	543.6
N DECANE	0.962	0.792	11780.	3455.	22.80	106.6	142.28	617.6
N TRIDECANE	1.005	0.818	12300.	3850	25.95	100.0	184.36	677.0
N HEXADECANE	1.025	0.810	14100	4220	28 20	95 3	226.44	717.0
METHANOL	1.085	1.008	0.78 x 10^6	4600.	00 00	397.0	32 04	513 2
ETHANOL	1.050	0.893	1.73 x 10^6	5060.	00.00	316 5	46 07	516.3
BUTANOL	0.997	0.648	1.83 x 10^6	5610	00.00	222.0	74.12	563 0
HEPTANOL	1.014	0.662	3.16 x 10^6	6670.	00.00	167.2	116 20	638.5
DECANOL	1.030	0.677	1.28 x 10^6	7070	00.00	155 0	158.28	655.0

TABLE 10

SPECIFIC HEAT AND THERMAL CONDUCTIVITY CONSTANTS

COMPONENT	A	B $\times 10^3$	C_7 $\times 10^3$
METHANE	6.42	9 63	4 12
PROPANE	19 38	17.63	2 90
N PENTANE	31.75	28.86	1 97
N HEPTANE	44.10	40.00	1.76
N OCTANE	50.30	45 80	1 76
ISO OCTANE	50.30	45 80	1 76
N DECANE	62 70	56.90	1.76
N TRIDECANE	81.10	73.80	1 76
N HEXADECANE	99 60	90.70	1.76
METHANOL	14 40	9 27	2.95
ETHANOL	20 70	13.38	3.35
BUTANOL	33.35	21.50	3.35
HEPTANOL	52.30	33 75	3 35
DECANOL	71.25	45.90	2.80
WATER VAPOR	10 48	00.95	----
CARBON DIOXIDE	13.12	00.60	----
NITROGEN	7.88	00.34	----
OXYGEN	7.22	1.10	1.54
COMBUSTION PRODUCTS	8.35	2 48	1.96

products (λ_p) in Regions A and B as follows.

$$\lambda_{A\ell} = \frac{X_{1\ell}}{2} \lambda_F (T_\ell) + \left(1 - \frac{X_{1\ell}}{2}\right) \lambda_p (T_\ell) \tag{D.9}$$

$$\lambda_{B\ell} = [\lambda_o(T_\ell) + \lambda_p (T_\ell)]/2 \tag{D.10}$$

The species thermal conductivities, λ_F, λ_P and λ_O, were computed as

$$\lambda = C_7 T \qquad \text{(cal/cm sec °K)} \tag{D.11}$$

The constants, C_7, are tabulated in Table 10 for all of the fuels considered as well as the values for oxygen and the combustion products.

The gas phase molar density was computed from the ideal gas equation of state, i e.,

$$C = P/RT \tag{D.12}$$

Effective diffusion coefficients for Regions A and B were computed according to a method derived by Wilke (65) for fuel diffusing through the combustion products in Region A and oxygen diffusing through combustion products in Region B Binary diffusion coefficients for each of the species required by this method were computed with the Slattery-Bird correlation as given in Reference (31) Since the molar density, given by Equation (D.12), and the effective diffusion coefficient, D, always appear as a product in the analysis, they were combined into a single correlation for each region. The resulting correlations are.

$$(CD)_A = \frac{10^{-7}\ T_A^{1.334}}{C_8 + C_9\ T_A^{0.511}} \qquad \text{(g-mole/cm sec)} \qquad \text{(D 13)}$$

and

$$(CD)_B = \frac{10^{-7}\ T_B^{1.334}}{C_{10} + C_{11}\ T_B^{0.511}} \qquad \text{(g-mole/cm sec)} \qquad \text{(D.14)}$$

The constants, C_8 to C_{11}, are tabulated in Table 11.

D.4 Heat of Reaction

The standard heat of reaction of the fuels, at a reference temperature of 298°K, is tabulated in Table 12

The corrected heat of reaction was calculated as the chemical energy release, allowing for dissociation, for combustion of a stoichiometric mixture of fuel and oxygen at various temperatures. The thermochemical properties for these calculations were taken from Reference (43), with the exception of the heat of formation of the fuel which was calculated from the standard heat of reaction given in Table 12 and the heats of formation of the combustion products. The results of these calculations were correlated with temperature by a least squares polynomial of the following form

$$Q^* = 10^6 \left[C_{12} + C_{13}\ T_{fR} + C_{14}\ T_{fR}^{\ 2} + C_{15}\ T_{fR}^{\ 3} + C_{16}\ T_{fR}^{\ 4} \right]$$

(cal/g-mole) (D 15)

where

$$T_{fR} = T_f/1000 \quad , \ (°K) \qquad \text{(D 16)}$$

The constants in Equation (D.15) are tabulated in Table 12.

TABLE 11

MOLAR DENSITY AND DIFFUSION COEFFICIENT CONSTANTS

COMPONENT	C_8	C_9	C_{10}	C_{11}
METHANE	6.70	0.872	6.47	0 935
PROPANE	11.94	1 790	5.54	1.015
N PENTANE	15.62	2 440	5.28	1 040
N HEPTANE	18.71	2.965	5.17	1 050
N OCTANE	20.10	3.190	5.14	1.052
ISO OCTANE	19.21	3.095	5.14	1 052
N DECANE	22.70	3.620	5.08	1.058
N TRIDECANE	26.10	4.170	5 04	1.062
N HEXADECANE	29.10	4.650	5.01	1.065
METHANOL	13.69	1 455	6.47	0 935
ETHANOL	14.10	1.815	5.83	0.993
BUTANOL	16.64	2.430	6.35	1.030
HEPTANOL	20.80	3 190	5.17	1.050
DECANOL	23.30	3 690	5.08	1.058

TABLE 12

HEATS OF REACTIONS

COMPONENT	STANDARD HEAT OF REACTION (kcal/g-mole)	C_{12}	C_{13}	C_{14}	C_{15}	C_{16}
METHANE	191.76	3.1483	- 4 4647	2.4671	-0.5837	0.0483
PROPANE	488.53	6.6930	- 9 4950	5.3261	-1.2806	0.1077
N PENTANE	782.04	10.2349	-14.5267	8.1853	-1.9775	0.1670
N HEPTANE	1075.85	13 7765	-19.5572	11 0442	-2.6743	0.2264
N OCTANE	1222.77	15.5467	-22.0729	12 4738	-3 0228	0.2561
ISO OCTANE	1219.01	15.5439	-22 0729	12.4738	-3.0228	0.2561
N DECANE	1516 63	19.0899	-27.1036	15.3327	-3 7196	0.3154
N TRIDECANE	1957.40	24.4019	-34.6493	19 6208	-4.7648	0.4045
N HEXADECANE	2398.17	29.7142	-42.1949	23.9089	-5.8099	0 4935
METHANOL	161.69	3.1182	- 4.4647	2.4671	-0.5837	0.0483
ETHANOL	305.48	4.8857	- 6.9769	3 8963	-0.9321	0.0780
BUTANOL	597.40	8 4261	-12.0111	6.7557	-1.6290	0.1374
HEPTANOL	1039.39	13.7398	-19 5570	11.0440	-2.6743	0 2264
DECANOL	1479.96	19 0527	-27.1036	15.3330	-3.7196	0.3154

D.5 Ambient Gas Properties

The Reynolds number and Prandtl number appearing in the convection correction, Equation (4.2), were evaluated for the ambient gas mixture. The properties appearing in these two dimensionless numbers were determined for a gas mixture of N components as follows.

Specific Heat

$$C_p = \sum_{i=1}^{N} X_i W_i C_{pi} \Big/ \sum_{i=1}^{N} X_i W_i \qquad \text{(D 17)}$$

where

$$C_{pi} = C_{17} + C_{18}\, T_\infty \qquad \text{(cal/gm °K)} \qquad \text{(D 18)}$$

Viscosity

$$\sigma = \sum_{i=1}^{N} X_i \sigma_i \qquad \text{(D.19)}$$

where

$$\sigma_i = C_{19} + C_{20}\, T_\infty \qquad \text{(gm/cm sec)} \qquad \text{(D.20)}$$

Thermal Conductivity

$$\lambda = \sum_{i=1}^{N} X_i \lambda_i \qquad \text{(D.21)}$$

where

$$\lambda_i = C_{21} + C_{22}\, T_\infty \qquad \text{(cal/cm sec °K)} \qquad \text{(D.22)}$$

Density

$$\rho = P \sum_{i=1}^{N} X_i W_i / R\, T_\infty \qquad \text{(gm/cc)} \qquad \text{(D 23)}$$

The constants, C_{17} to C_{22}, are tabulated in Table 13 for all of the species present in the ambient gas mixture.

TABLE 13

CONSTANTS IN THE AMBIENT GAS PROPERTY EQUATIONS

COMPONENT	C_{17}	C_{18} x 10^3	C_{19} x 10^5	C_{20} x 10^8	C_{21} x 10^5	C_{22} x 10^8
O_2	0.248	0 0167	20 2	27.3	4 55	13 22
O	0.282	0 0167	18 5	25 0	7.18	12 82
N_2	0 282	0 0121	15.2	23.5	3 18	12 32
NO	0 277	0.0072	19 5	25 5	3.70	13 21
CO_2	0.298	0.0135	15.2	23.5	1.19	13 97
CO	0.292	0 0085	16 3	23.5	3 20	12 82
H_2O	0.583	0.0530	13 6	26 0	-4 74	33 25
H_2	3.610	0.2580	10 7	18.2	31.00	74 30

APPENDIX E

RADIATION EFFECTS

The effect of thermal radiation on the computed steady burning temperature was examined by comparing results allowing for a finite radiant energy flux with those obtained when radiation was neglected. For a finite radiant energy flux, Q_R, the energy balance at the droplet surface during steady burning is,

$$4\pi r_\ell^2 \lambda \left.\frac{dT}{dr}\right|_{\ell+} + \dot{Q}_R = \dot{n}H \quad , \tag{E.1}$$

where H is the weighted heat of vaporization defined by Equation (2.21) and the product nH represents the total heat flux, Q_T, required to vaporize the evaporating material from the droplet

Letting

$$H' = H - \dot{Q}_R/n \quad , \tag{E.2}$$

the energy balance, Equation (E.1), can be written as

$$4\pi r_\ell^2 \lambda \left.\frac{dT}{dr}\right|_{\ell+} = nH' \tag{E 3}$$

Noting the similarity between Equation (E.3) and Equation (2 7), it is observed that the equations derived in Chapter II, neglecting radiation, can be employed for the case of a finite radiant energy flux by replacing H by H'. The quantity, H', can be written in terms of the ratio of the radiant energy flux to the total energy flux as follows

$$H' = (1 - Q_R/\dot{Q}_T)\ H \qquad (E.4)$$

Steady droplet burning temperatures were computed for n decane evaporating in nitrogen at a temperature of 3000°K and various pressures for different values of the heat flux ratio, Q_R/Q_T The results are shown in Table 14 along with the computed values of the droplet surface fuel mole fraction, $X_{1\ell}$. The results show that the steady burning temperature is not very sensitive to radiation effects. Even when 75% of the total heat transferred to the droplet is due to radiation, the steady burning temperature increased by less than 3% over the range of pressures considered. The droplet surface fuel mole fraction is somewhat more sensitive, showing increases on the order of 8% when the heat flux ratio is 0 5 and of 15% when the heat flux ratio is 0.75.

TABLE 14

RADIATION EFFECTS ON STEADY BURNING TEMPERATURES

P (atm)	$\dot{Q}_R/\dot{Q}_T$	T_ℓ (°K)	$X_{1\ell}$
	0	507	660
10 3	0 5	512	725
	0.75	518	.775
	0	559	.680
20 7	0.5	569	740
	0.75	576	.786
	0	592	710
31.2	0 5	600	765
	0 75	606	.806
	0	609,5	.755
41 4	0.5	612	800
	0.75	---*	---

*Critical temperature exceeded

VITA

Robert Stephen Lazar [redacted] He attended Rogers High School in Newport, Rhode Island, graduating in June 1960 From July, 1960 to June, 1965, he was engaged in a cooperative work-study program with the U.S. Naval Underwater Weapons Research and Engineering Station in Newport, Rhode Island, and the University of Rhode Island. He received the degree of Bachelor of Science in Mechanical Engineering in June, 1965 and the degree of Master of Science in Mechanical Engineering in October, 1966 from The University of Rhode Island

He attended The Pennsylvania State University from September, 1966 to January, 1969 under a National Aeronautics and Space Administration Predoctoral Traineeship From January, 1969 to July, 1970, he was employed as a Research Assistant in Mechanical Engineering at The Pennsylvania State University

He has co-authored three publications on the subject of droplet combustion. He holds memberships in the American Society of Mechanical Engineers, American Institute of Aeronautics and Astornautics, The Combustion Institute, Tau Beta Pi, Phi Kappa Phi and Sigma Xi